
Doctoral Dissertations

Student Theses and Dissertations

Fall 2020

Process intensification of fuel synthesis and electrolysis

Jeremy Lee Hartvigsen

Follow this and additional works at: https://scholarsmine.mst.edu/doctoral_dissertations



Part of the [Chemical Engineering Commons](#)

Department: Chemical and Biochemical Engineering

Recommended Citation

Hartvigsen, Jeremy Lee, "Process intensification of fuel synthesis and electrolysis" (2020). *Doctoral Dissertations*. 2951.

https://scholarsmine.mst.edu/doctoral_dissertations/2951

This thesis is brought to you by Scholars' Mine, a service of the Missouri S&T Library and Learning Resources. This work is protected by U. S. Copyright Law. Unauthorized use including reproduction for redistribution requires the permission of the copyright holder. For more information, please contact scholarsmine@mst.edu.

PROCESS INTENSIFICATION OF FUEL SYNTHESIS AND ELECTROLYSIS

By

JEREMY LEE HARTVIGSEN

A DISSERTATION

Presented to the Graduate Faculty of the

MISSOURI UNIVERSITY OF SCIENCE AND TECHNOLOGY

In Partial Fulfillment of the Requirements for the Degree

DOCTOR OF PHILOSOPHY

in

CHEMICAL ENGINEERING

2020

Approved by:

Joseph Smith, Advisor

Fatih Dogan

Xinhua Liang

Douglas Ludlow

Ali Rownaghi

© 2020

Jeremy Lee Hartvigsen

All Rights Reserved

ABSTRACT

As more renewable energy is added to the electric grid, energy storage becomes a high priority. Suggestions have been made for energy storage in the form of fuel and chemicals. Currently, Solid Oxide Electrolysis systems can operate in endothermic mode and reduce the electrical requirement by supplying heat. Fuel synthesis from syngas is exothermic and can supply heat. However, the temperature mismatch in the normal operation of the electrolysis step and fuel synthesis step makes the direct utilization of this heat impossible. This work explores possibilities of alternate arrangements of coupling electrochemical systems and chemical synthesis. This work also explores potential for heat integration between the electrolysis and synthesis steps. This is done through exploring higher temperature fuel synthesis systems, and a new intermediate temperature electrolysis system.

The successful use of a Mo₂C/HZSM-5 catalyst for ethylene production is shown. Analysis of potential benefits and limitations of each technological approach are examined. The breakeven carbon pricing for the hybrid energy system production of chemicals to be competitive with fossil-fuel based chemical production is calculated.

ACKNOWLEDGMENTS

I first must thank my advisor. Dr. Smith provided me with the opportunity, support, and encouragement to pursue and finish my PhD. Without his support and direction, this work would never have been completed.

A special thanks to Dr. Dogan for the usage of his lab, and support for the work on intermediate temperature alkaline electrolysis.

Also, a big thanks for the rest of my committee for the time to review and provide feedback on my dissertation and research.

I cannot acknowledge enough the role of my father in my education. My formal education in science and engineering started long after I started learning as a child on his lap. He's been a veritable fountain of science and engineering knowledge and has always been able to provide insightful discussion on challenges encountered on any topic.

Beyond all others, I must thank my wife for unrelenting support and encouragement. Her willingness to bear the load of caring for three young and rambunctious boys enabled me to focus on completing this work.

Lastly, my boys, for being a motivation beyond anything I could have done for myself.

TABLE OF CONTENTS

	Page
ABSTRACT	iii
ACKNOWLEDGMENT	iv
LIST OF ILLUSTRATIONS	ix
LIST OF TABLES	xii
NOMENCLATURE	xiii
SECTION	
1. INTRODUCTION	1
1.1. PREVIOUS WORK	1
1.2. BACKGROUND	2
1.2.1. Major Components of the Proposed Hybrid Energy System	4
1.2.1.1. Carbon dioxide source.....	4
1.2.1.2. Renewable energy from wind turbines.....	5
1.2.1.3. Carbon-emission-free baseload-type generator.....	5
1.2.1.4. Solid oxide electrolyzer.....	6
1.2.2. Components Of The Hybrid System That Will Not Be Studied	6
1.3. ELECTROCHEMICAL REDUCTION OF CO₂	7
1.3.1. Current State of the Art.....	8
1.3.2. Low-Temperature CO ₂ Electrochemical Reduction.	9
1.3.3. High-Temperature CO ₂ Electrochemical Reduction.....	10
2. RESEARCH OUTLINE	12
2.1. RESEARCH OBJECTIVES	12

2.2. RESEARCH QUESTIONS	12
2.3. RESEARCH APPROACH	12
3. THERMODYNAMICS.....	14
3.1. WATER SPLITTING	14
3.2. IN-SITU FUEL SYNTHESIS.....	18
3.3. COKING.....	19
4. CATALYSIS	21
4.1. SYN-GAS TO OLEFIN APPROACH	22
4.2. METHANE COUPLING CATALYST SYSTEM APPROACH.....	29
5. SOEC ELECTROCHEMISTRY.....	34
5.1. COKING RESISTANT ELECTRODES	35
5.2. ELECTROLYTE CONDUCTIVITY	36
6. ECONOMIC PRODUCT SCREENING.....	40
6.1. PRODUCT ECONOMICS OVERVIEW	40
6.2. MARKETS	42
6.2.1. Paraffins	45
6.2.2. Oxygenates.....	45
6.2.3. Olefins.....	46
6.2.4. Benzene, Toulene, Xylene	48
6.2.5. Ammonia.....	49
7. INTERMEDIATE TEMPERATURE ALKALINE ELECTROLYZER SYSTEM	50
7.1. INTEGRATED ALKALINE AND FT SYSTEM ANALYSIS	50
7.2. EXPERIMENT	51
7.3. ECONOMICS	53

8. INTEGRATED FUEL SYNTHESIS AND SOLID OXIDE ELECTROLYSIS	54
8.1. METHODS	54
8.1.1. Catalyst Preparation	54
8.1.2. Cell Description	55
8.2. TEST STAND.....	55
8.2.1. Test Stand Operating Constraints	56
8.2.2. Sampling Method.....	57
8.3. TEST PROCEDURE	58
8.3.1. Baseline Nickel Cell	58
8.3.2. Cobalt Electrolysis Cell	59
8.3.3. Nickel Cell with Mo-HZSM5 Layer.....	59
8.4. RESULTS	59
8.4.1. Electrochemical Performance.....	60
8.4.1.1. Baseline nickel cell.....	60
8.4.1.2. Cobalt cell.....	60
8.4.2. Nickel Cell with Mo-HZSM5 Layer.....	62
8.4.3. Chemical Products	63
8.4.3.1. Cobalt cell products.....	64
8.4.3.2. Low temperature products.....	65
8.4.3.3. High temperature products	68
8.4.4. Experimental Uncertainty.....	72
9. ECONOMIC EVALUATION.....	74
9.1. INTEGRATED ELECTROLYSIS AND SYNTHESIS REACTOR COSTS	75
9.1.1. System Costs.....	75

9.1.2. System Lifetime	76
9.1.3. Catalyst	77
9.2. ELECTRICITY COSTS	77
9.2.1. ERCOT Pricing Data	77
9.2.2. Hybrid Energy System Analysis	80
9.2.2.1. Nuclear co-generation	81
9.2.2.2. Wind turbine.....	81
9.3. ECONOMIC CASES.....	81
9.3.1. Hydrogen Production.....	82
9.3.2. Fischer-Tropsch and Solid Oxide	83
9.3.3. Non-OCM-SOEC Ethylene	84
9.3.4. Non-OCM-SOEC Benzene	86
9.4. CARBON PRICING	87
9.5. ECONOMIC SUMMARY.....	88
9.6. SCALING AND APPLICABILITY	89
10. CONCLUSIONS	90
10.1. DISSERTATION SUMMARY	90
10.2. RESEARCH CONTRIBUTIONS	91
10.3. LIMITATIONS.....	92
10.4. FUTURE WORK.....	92
APPENDIX.....	93
BIBLIOGRAPHY.....	94
VITA.....	103

LIST OF ILLUSTRATIONS

	Page
Figure 1.1 Typical Hybrid Energy System To Produce Liquid Fuels From CO ₂ [6].....	2
Figure 1.2 Modified Pathway Focus From DOE's H2@Scale Program.....	3
Figure 1.3 Integrated Fuel Synthesis And Co-Electrolysis Reactor Scheme	8
Figure 1.4 In-Situ Direct Methanation SOEC Experiment Vs Theory At 1 Bar And 800 °C [36].....	11
Figure 3.1 Water Splitting Thermodynamics And Typical Operating Temperatures And Voltages For PEM, Alkaline, And SOEC.....	15
Figure 3.2 Net Heat Flux For A Theoretical Water Electrolysis Cell.....	17
Figure 3.3 Net Heat Flux For A Theoretical Combined FT And Electrolysis Cell.	19
Figure 3.4 Coking And Non-Coking Region For Different C:H Ratios For The Synthesis Of Hydrocarbons In-Situ. Conditions Are At 1 Bar And 650 °C. HSC Chemistry 6.0	20
Figure 4.1 Product Weight Distribution By Carbon Number Of Fischer-Tropsch Polymerization Reaction.....	23
Figure 4.2 Weight Fraction Of C ₂ And C ₃ Hydrocarbons As A Function Of Alpha.....	24
Figure 4.3 Fischer-Tropsch Mechanism Pathways [41][47].....	25
Figure 4.4 Fe-Co-Ce Catalyst Alpha Vs Temperature With Alpha Fit To Eqn 6.....	27
Figure 4.5 Ru Catalyst Alpha Vs Temperature With Alpha Fit To Eqn 6.....	28
Figure 4.6 Electro-Reduction Of Steam And Carbon Dioxide At 650 C And 1 Bar	31
Figure 4.7 Electro-Reduction Of Steam And Carbon Dioxide At 725 C And 1 Bar	31
Figure 4.8 Electro-Reduction Of Steam And Carbon Dioxide At 800 C And 1 Bar	32
Figure 5.1 Ohmic Losses Vs Electrolyte Thickness. Typical Electrolyte Supported Cells And Electrode Cell Electrolyte Thickness Shown Operated At 650 C.....	38

Figure 6.1	Electrochemical Production Of Chemicals Pricing. Prices Based On-- March 2016 [64] [65] [66] [67]	41
Figure 6.2	Electrochemical Production Of Chemicals Pricing. Prices Based On June 2020 [67][68].....	42
Figure 6.3	Chemicals And Fuel Use Pathways Of Methanol.....	46
Figure 6.4	Major Chemical Products Derived From Ethylene [75] [76]	47
Figure 6.5	Hydrocarbon Gas Liquid Pipelines And Ethylene Cracker Map [78]	48
Figure 6.6	Benzene Product Pathways	49
Figure 6.7	Equilibrium Ammonia Concentration As A Function Of Temperature And Pressure	49
Figure 7.1	I-V Curves Of High Temperature Alkaline Electrolysis Compared With Previous Literature Experiments And Traditional Technologies [83].....	52
Figure 7.2	Nyquist Plot Of High Temperature Alkaline Electrolyzer.	52
Figure 8.1	Fresh And Spent Mo HZSM5 Catalyst.....	55
Figure 8.2	Test Stand Diagram For High Temperature FT-SOEC	56
Figure 8.3	Baseline Nickel Cell IV Curve At A Temperature Of 800 °C	61
Figure 8.4	Baseline Nickel Cell Nyquist Plot At 800 °C	61
Figure 8.5	Cobalt Cell Nyquist Plot At 600 °C	62
Figure 8.6	Voltage-Current Curve For Nickel Cell At 800 C.....	63
Figure 8.7	Nyquist Plots Of Cell At 800 °C	63
Figure 8.8	Ultimate Composition Of Outlet Vs Current	66
Figure 8.9	Mole Percent Of Products Vs Current.	67
Figure 8.10	Ultimate Composition At Exit At 800 °C	69
Figure 8.11	Mole Percent Composition At Exit At 800 °C. Minor Products C ₂ H ₄ , C ₂ H ₆ , CO Are Plotted On The Secondary Axis.....	70
Figure 8.12	Products Compared To Theoretical. Experimental Results Are Dotted Lines Of The Same Color As The Theoretical Prediction.....	71

Figure 8.13 Ethylene Measurement Vs Theoretical	71
Figure 9.1 Electrolysis Stack Learning Curve Based On A Single Production Site	75
Figure 9.2 Real Time ERCOT Pricing Data Fraction Of Hours In A Year [63].....	78
Figure 9.3 ERCOT 2018 Wind Production Capacity Factor As A Fraction Of The Year.[87]	79
Figure 9.4 Wind Capacity Vs Pricing And Wind Percent Of Load Vs Pricing For ERCOT 2018.	80
Figure 9.5 ERCOT Wholesale Grid Priced Electricity To Hydrogen.....	83
Figure 9.6 Fischer-Tropsch And SOEC Cost For Olefin Production.....	84
Figure 9.7 Tornado Chart For FT-SOEC Production Of Ethylene. (\$/Kg).....	85
Figure 9.8 Tornado Chart For FT-SOEC Production Of Benzene (\$/Kg)	86

LIST OF TABLES

	Page
Table 1.1 Survey Of Existing Single-Unit Electrochemical Synthesis Of Hydrocarbons	9
Table 4.1 Weight Fraction of C ₂ + Hydrocarbons Via Non-Oxidative Coupling Methane as a Function of Temperature (Celsius)	30
Table 8.1 Current Needed For Full Reduction Of Incoming Steam And Carbon Dioxide Stream For A Given Gas Flow Rate.....	57
Table 8.2 Cobalt Cell Products At 600 °C. (Mole Percent)	64
Table 8.3 Cobalt Cell with Syn-Gas Feed. (Mole Percent)	64
Table 9.1 Carbon Emissions of Studied Chemicals By Pathway [92].....	87
Table 9.2 Chemical Costs Via Different Pathways. Breakeven CO ₂ Costs In Current And Historical Markets.....	88

NOMENCLATURE

Symbol	Description
α	Chain Propagation Probability
A	Amps
E	Electrochemical Potential
F	Faraday's Constant
G	Gibbs Energy
H	Enthalpy
R	Gas Constant
R	Electrical Resistance
T	Absolute Temperature
V	Volts
z	Electron Transference number

1. INTRODUCTION

1.1. PREVIOUS WORK

Until fossil-based fuels no longer dominate U.S. and global energy portfolios, there is a need to continue to explore innovative and cost-effective approaches to reduce carbon dioxide emissions. Hybrid-energy systems (HES) are an increasingly active area of research. Hybrid systems are the cooperation of various energy systems all together to produce an optimum economic and technical output [1, 2, 3]. These systems produce a synergy in further reducing carbon emissions by utilizing all the energy streams [4]. A single-unit direct electrochemical system for the production of fuel and chemicals is proposed for integration into hybrid energy systems. This work includes a techno-economic evaluation of the proposed single unit direct electrochemical systems as part of a hybrid energy system. Results from this techno-economic study will guide the development of an environmentally sustainable and economically attractive conversion methodology. The goal will be to establish a process that uses CO₂ to generate a value-added product instead of focusing on ways to sequester it in the ground.

Previous work has focused on a proposed sustainable hybrid energy system that combines an oxy-fired Pressurized Circulating Fluid Bed (PCFB) reactor with a solid oxide electrolysis (SOE) unit. [1] Steam from the PCFB and captured carbon dioxide, together with renewable electric power generated via wind turbines is fed to the SOE unit to generate oxygen and hydrogen [5].

Using the same main components of the previous hybrid energy system, this work focuses on the development of an integrated Fischer Tropsch and solid oxide electrolysis

cell (FT-SOEC) for the hydrocarbon synthesis steps. The FT-SOEC replaces the typical separate unit operations of a SOEC system with water gas shift (WGS) reactors and Fischer Tropsch (FT) reactors. This work also shifts the product focus based on the economics. Instead of focusing primarily on the production fuels, this work focuses on the green production of petrochemical feedstocks. A sample hybrid energy system with the major components examined in this work is shown in (Figure 1.1).

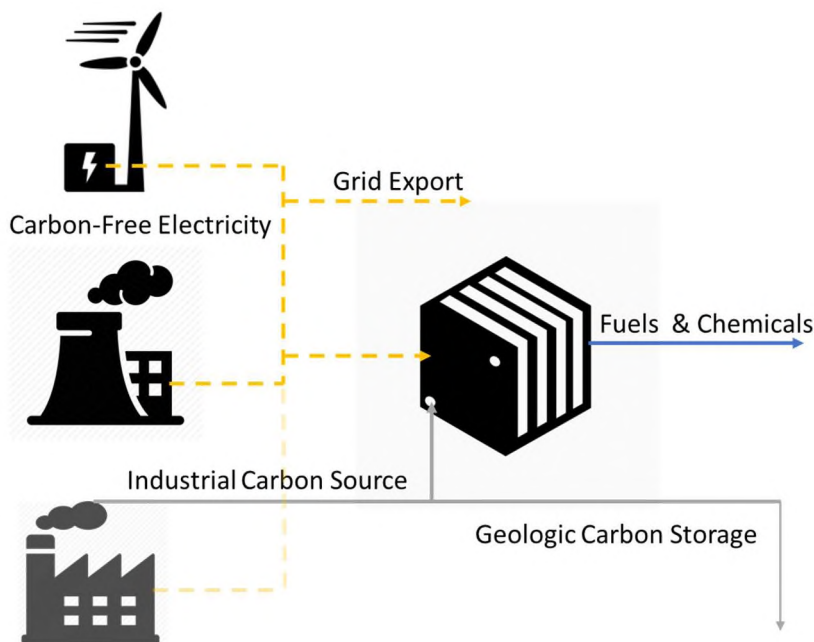


Figure 1.1 Typical Hybrid Energy System To Produce Liquid Fuels From CO₂ [6]

1.2. BACKGROUND

The modern energy sector is increasingly moving away from pure fossil fuel systems and moving towards renewable energy production. These renewable generation systems are more environmentally friendly and sustainable, and they reduce greenhouse gas emissions. A major challenge for these systems is that they are non-dispatchable.

Additionally, the scope and scale of the energy transition incurs debate as to whether or not existing assets in the energy system can be replaced quickly enough to address climate change concerns, or if they need to be repurposed or modified to reduce the most severe impacts of fossil based energy systems. Addressing these challenges through hybrid systems provides greater flexibility and economic output than simple single unit and storage systems.

A proposed major link in the sector-coupling of energy systems is hydrogen. The US Department of Energy's H2@scale initiative focuses on the ways that hydrogen can be used to reduce carbon emissions (Figure 1.2). This work focuses primarily on using

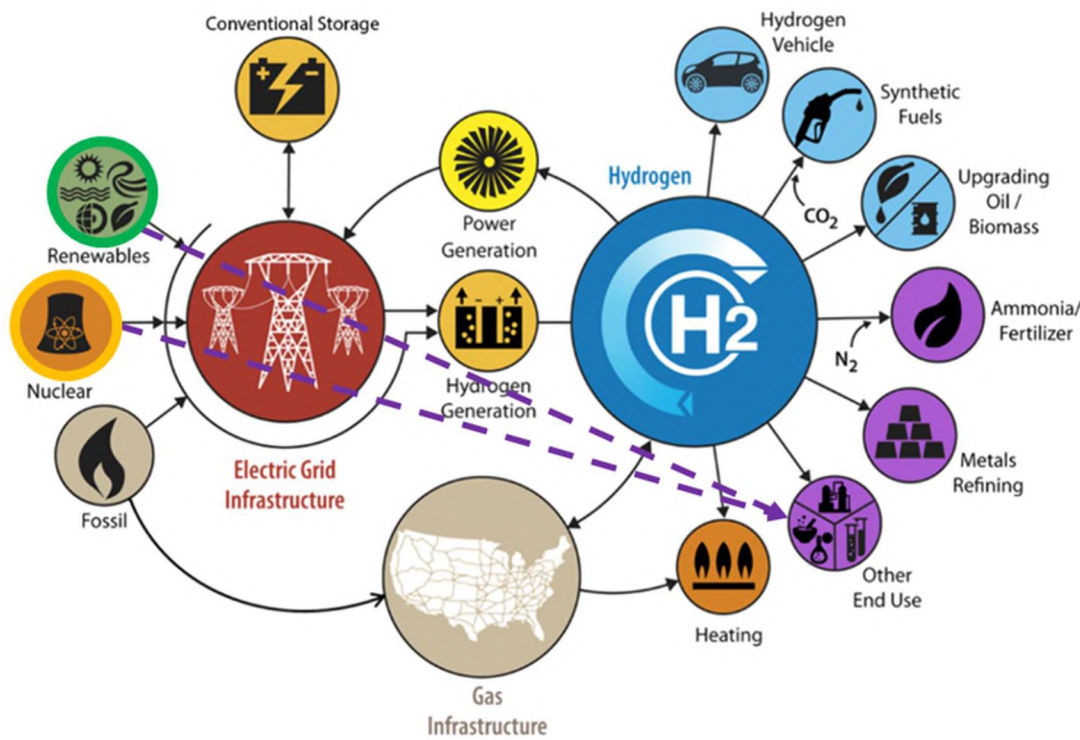


Figure 1.2 Modified Pathway Focus From DOE's H2@Scale Program

electricity from renewable sources and baseload nuclear to bypass many of the intermediate processes and products for direct production of other end-use chemicals.

1.2.1. Major Components of the Proposed Hybrid Energy System. To better understand the proposed hybrid energy system, the major individual components will now be discussed. Some of these components are interchangeable with other similar components, however, for the scope of this work only the following will be included in the economic analysis of the system. A baseline comparison between an integrated SOEC and fuel synthesis system will be compared with a system that includes separate electrolysis and fuel synthesis operational units. This will clarify the advantages and disadvantages of the proposed system compared to the established technological baseline.

1.2.1.1. Carbon dioxide source. An industrial carbon dioxide source will be part of the system. The carbon dioxide will be used to produce chemicals. This results in the system being a carbon beneficiation system rather than simple sequestration. For a variety of end-use chemicals, the long-term stability of the finished products will result in a non-geologic sequestration. Most plastics and chemicals end up as products and any decay to atmospheric carbon emissions is very slow. Sample carbon dioxide sources include, stream methane reformers, cement plants, bioethanol, and traditional fossil fuel electric generating stations. For the purposes of the economic analysis, it assumes that carbon dioxide can be obtained for \$40/ton. This represents a lower bound estimate of commonly expected costs for the capture of CO₂ from point source emissions [7]. This generalizes the result from a single specific carbon dioxide source to a broadly applicable starting point for the analysis of any hybrid energy system.

1.2.1.2. Renewable energy from wind turbines. Effective use of intermittent renewable wind energy in the HES requires some combination of effective storage, dispatchable generation or dispatchable loads. The proposed system operates a dispatchable load by using a SOE unit that operates at variable rates without efficiency loss. This configuration allows a wind turbine to produce at full rated capacity during periods of acceptable wind supply and convert all generated electricity immediately into a chemical based product.

1.2.1.3. Carbon-emission-free baseload-type generator. The baseload generation unit is either a fossil plant, such as the PCFB coal plant with Carbon Capture and Sequestration (CCS) in the previous work by Buchheit et al. or an existing light water reactor nuclear power generator [5]. Existing nuclear power units typically have typically fully depreciated capital assets and have difficulty ramping output up and down. In the case of nuclear, the operating cost of light water reactors in the United States is approximately \$30/MWh. Since there are many times the market electricity costs go below that, the nuclear plant would be able to operate more profitably by selling the electricity at a fixed cost for hydrogen production.

Coal plants have a similar paradigm to nuclear plants. A coal plant with CCS would provide an ideal source for the carbon dioxide needed to produce the hydrocarbon chemicals necessary for displacement of traditional petroleum-based chemicals. Additionally, most chemicals would act as a form of carbon sequestration as they are not intended to be burned and re-release the carbon to the atmosphere.

For the purposes of the HES, the only significant difference between the nuclear plant and the coal plant are the availability of CO₂, either directly from the power plant or

indirectly. The nuclear plant can use the electricity without the need for carbon capture, but in context of the HES, it is assumed that any coal-based electricity also includes CCS.

1.2.1.4. Solid oxide electrolyzer. Solid Oxide Electrolysis (SOE) is an emerging technology that provides flexibility and opportunities for use in a hybrid energy system. Historically, research focus has generally been on solid oxide fuel cells; however, the research emphasis is now shifting toward solid oxide electrolytes in electrolyzers [8]. This is changing as several commercial electrolyzers companies have grown over the past several years. The minimum electrical input to a solid oxide electrolyzer is substantially lower than either alkaline or PEM electrolyzers. The lower electrical requirements along with the ability to utilize process heat in the reaction increase the efficiency of the water splitting reaction. [9] In the past longevity and costs have been key issues, as well as the price of carbon-free electricity [10] [11]. These challenges have largely been addressed by the development of better electrolytes, electrodes, and production processes, as well as cost of electricity declines associated with the increase in solar and wind electricity production. [12] [13] [14]

1.2.2. Components Of The Hybrid System That Will Not Be Studied.

Although there are many components of the hybrid energy system, previous work has shown all the major components are capable of operation together. For this work the focus will be solely on the FT-SOEC, and other components will interact with the FT-SOEC through a grid connection or via simple direct electricity production and consumption. This focus results in a system boundary where the primary economic input to the system is the pricing and availability of green electricity.

1.3. ELECTROCHEMICAL REDUCTION OF CO₂

The traditional use of SOEC in the reduction of CO₂ is the co-electrolysis of CO₂ and steam into syngas. This approach is well validated experimentally [9] [15]. The alternative approach for using SOEC to produce fuels is standard high temperature steam electrolysis followed by water-gas shift reactions (WGS). This is the approach used by Sunfire to produce “blue crude” for Audi [16].

In comparison to SOEC co-electrolysis, the direct electrochemical reduction of CO₂ directly to hydrocarbon fuels and chemical feedstocks in a one step process is a very difficult technical challenge. Many different approaches have been tried. The results are typically either low efficiency, or low power density of the device [17] [18] [19]. Additionally, the selectivity to molecules other than methane and carbon monoxide is rare. This work seeks to develop a new strategy to directly employ some of the advantages of existing SOEC technology in a novel way to produce a single-unit operation, multi-step reaction chain to produce fuels and chemicals. The proposed strategy and obstacles will be discussed.

In order to produce valuable chemicals of interest, a catalyst with high selectivity and a reasonably high conversion efficiency is required. The current body of literature on FT catalysis is based on much lower operating temperatures than are compatible with SOEC. The application of existing syngas conversion catalysts to higher operating temperatures is the initial point of exploration for candidate catalysts. Literature examination of known (Fischer-Tropsch) FT catalyst mechanisms provides insight into the possible mechanisms expected at higher temperatures.

For this work, we will approximate the operating characteristics of the subsequent separation processing steps. The rest of the system and the separation train will be simplified (Figure 1.3). The difficulty of the separation will depend on the single-pass yield of the catalyst. The fuel synthesis system's main components are the integrated FT and SOEC system, a separation and product storage train, a recycle loop, and a DC electric power source. Due to the range of product compositions, a simplified separation scenario will be used as a first order estimate for the initial techno-economic analysis.

1.3.1. Current State Of The Art. The current state of the art in electricity to fuel conversion is a multi-step process typically involving high temperature or low

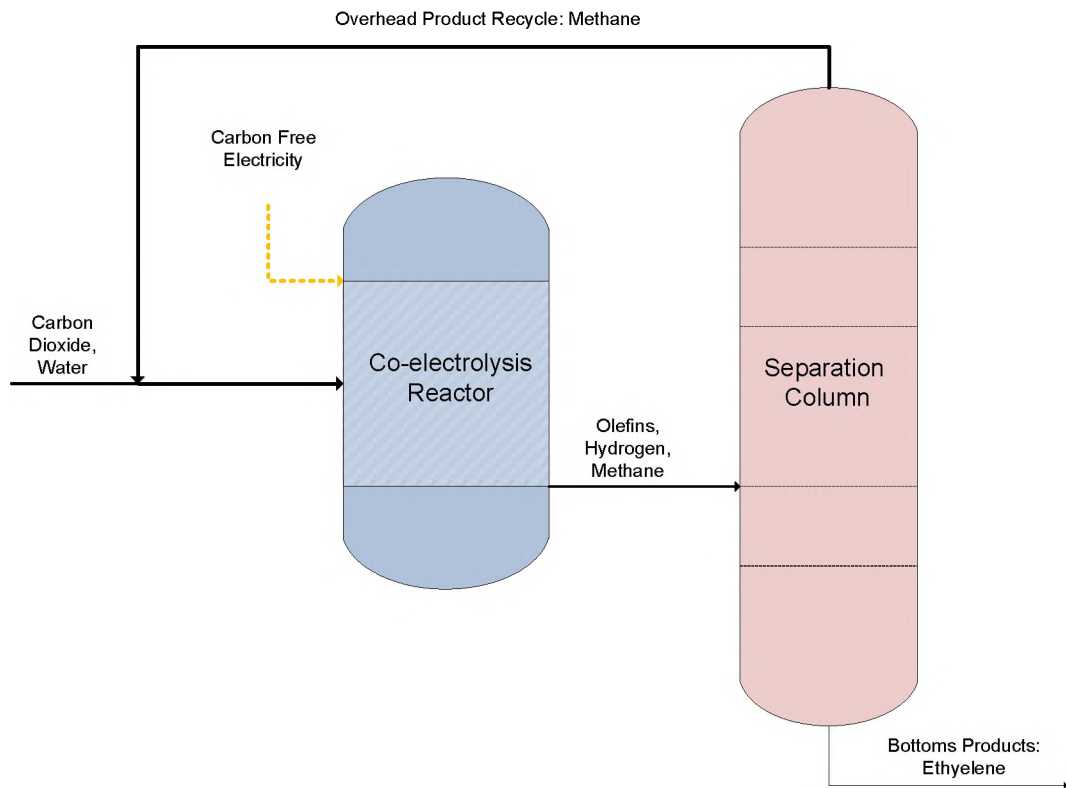


Figure 1.3 Integrated Fuel Synthesis And Co-Electrolysis Reactor Scheme

temperature electrolysis, followed by water-gas shift, and then sent to a syngas conversion reactor [20] [21]. Most syngas conversion reactors are of the Fischer-Tropsch type, although there are other variants that are not typically defined as FT. This work focuses on systems that use a single integrated unit electrolysis and fuel conversion device. The general challenges of these types of devices are low efficiency, low yield and low power density.

1.3.2. Low-Temperature CO₂ Electrochemical Reduction. The majority of the direct CO₂ electrochemical reduction processes have very low current densities. At higher current densities the efficiency and selectivity both drop dramatically [22]. CO is a common product of these reaction systems. Both copper and silver are common catalysts and appear to be close to the ideal for these types of reactions [23]. Gold electrodes are also occasionally used [24]. Examples of the low temperature direction conversions devices are shown in Table 1.1.

Table 1.1 Survey Of Existing Single-Unit Electrochemical Synthesis Of Hydrocarbons

Electrolyte	Catalyst	V	J (mA/cm ²)	Methane	Olefin	Alkane	Hydrogen	Other	Ref
KHCO ₃	Cu	0.99	30	2%	25%	-	60%	CO HCOO-	[16]
KHCO ₃	Cu	1.2	16	present	present	-	present	-	[17]
Ionic Liquid (BMImCl)	Ag	1.55	3.7	none	none	none	trace	CO (99%)	[18]
MeCN	Bi	1.71	3.8	-	none	-	none	CO (95%)	[19]
HClO ₄	Cu	1.7	-	20%	15%	2%	40%	CO (5%)	[20]
NaHCO ₃	RuO ₂ /TiO ₂	0.55	1	-	-	-	-	CH ₃ OH (60%)	[21]
KHCO ₃	Ag-Cu	-1.46	50	-	-	-	-	CO (60%), H ₂ (40%)	[22]
H ₂ SO ₄	Pt-Pd	0.02	5	-	-	-	-	HCOOH	[23]
PO ₄ ³⁻	CuIn	0.7	2	-	-	-	10%	CO (90%), COOH (trace)	[24]
KHCO ₃	CuO	1.7	1.2	-	-	-	-	CH ₃ OH (38%)	[25]

In order to deploy these types of systems economically the current density needs to increase by an order of magnitude or more while maintaining the same overall system efficiency and selectivity [35]. Even the highest currents are still too low to be considered candidates for viable commercial systems.

1.3.3. High-Temperature CO₂ Electrochemical Reduction. For high temperature SOEC-based direct electrochemical reduction to non-syngas products, there is very little in the way of experimental data. Data from Fujiwara et al. is shown in Figure 1.4 and is projected onto a chart of the theoretical products at each stage of reduction [36]. It can be seen that, overall, the data agrees quite well with the thermodynamic equilibrium with an exception of the CO₂ and CO data being shifted more significantly. There is a high likelihood this relates to either the Boudouard reaction, water-gas shift or some other reforming reactions occurring during the quenching of the outflowing gas streams.

Another work with experimental testing of methane production in SOEC co-electrolysis has a similar overall result [37]. The experimental result shows a fully oxidized inlet of steam and carbon dioxide being reduced by 7.5% compared to the fully reduced state (Figure 1.4). A small amount of methane production (.013%) is shown to be achievable at 650 °C. This is much lower than needed for a viable system; however, it is nearly identical to the expected thermodynamic limit of methane formation given the outlet composition. There is some in the literature discussion of whether hydrogenation of carbon is a probable pathway for some of the methane formation in a direct electrochemical reduction system [36]. Based on the experimental results shown in literature, there is some evidence to suggest that carbon hydrogenation is a valid pathway

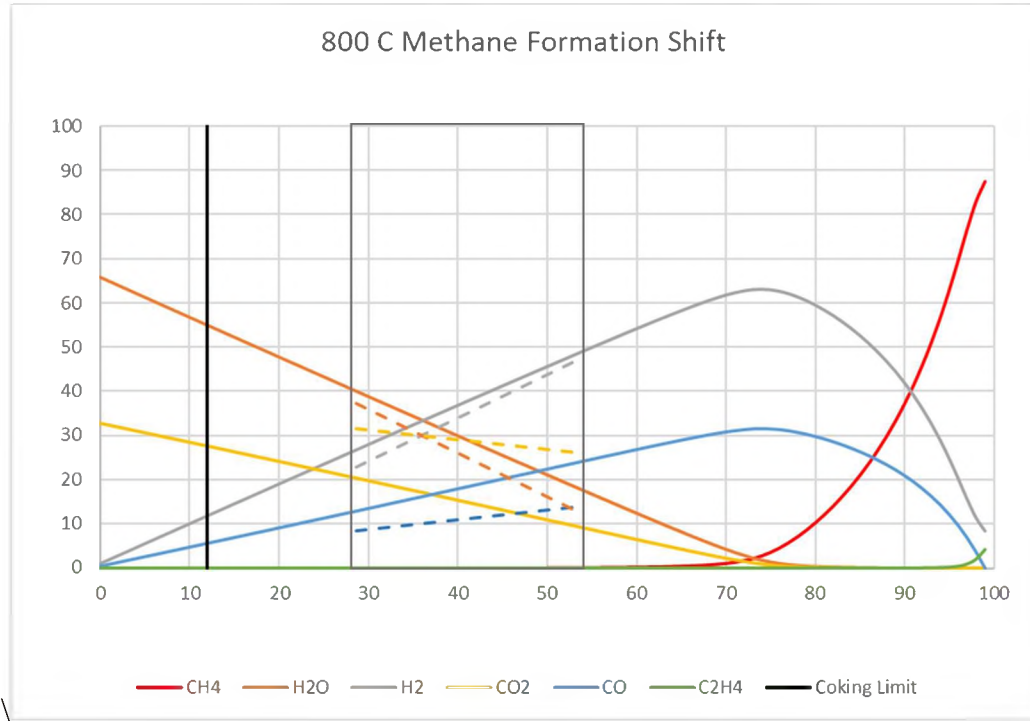


Figure 1.4 In-Situ Direct Methanation SOEC Experiment Vs Theory At 1 Bar And 800 °C [36]

for methane production in a SOEC methanation system. This pathway is significant for the high degree of reduction proposed in this work. The experimental data plotted here and the other experimental results reviewed for this study, also operated at much higher applied voltages than is typically seen in SOEC. These high voltages cause instability in the electrolyte and electrodes. Such high voltages would not be suitable for long-term operation of a commercialized system. Also of note, is that at the conversion achieved, the total quantity of methane is very small. A much higher overall current relative to the flow is needed in order to see significant methane production.

2. RESEARCH OUTLINE

2.1. RESEARCH OBJECTIVES

The primary objective of this work is the production of C₂+ hydrocarbons in a single integrated electrolyzer and FT unit. A Techno-Economic Analysis (TEA) is used to screen the most economical and technically achievable hydrocarbon candidates and compare them with hydrogen production and a traditional syngas and Fischer-Tropsch route to hydrogen production. The comparison between technoeconomic status the proposed systems and the state-of-the-art systems is a secondary objective in the process that supports the primary objective. The technoeconomic evaluation will evaluate the necessary CO₂ cost for the system to breakeven with conventional routes.

2.2. RESEARCH QUESTIONS

The main questions that this work seeks to answer are:

1. What are the optimal economic products for electrochemical production?
2. What are the operating conditions where those products are compatible with thermodynamic and kinetic pathways?
3. What combinations of catalysts and electrolytes work under the conditions identified by the thermodynamics and electrolyzer operating conditions?

2.3. RESEARCH APPROACH

The research approach is to identify catalysts, experimentally test, and economically evaluate the proposed integrated fuel synthesis-SOEC system. A subset of

fuels and chemicals are targeted for production by examining the simple fuels and chemicals that are high value for a given energy input. The literature review and economic analysis will inform which types of catalytic systems and target products are of particular interest. Thermodynamic and kinetic analysis will also be used to screen catalysts for the proposed system. The limitations of test facilities and equipment will also inform the initial systems proposed and test.

Experimental validation tests will be performed after finding catalysts that are compatible with the requirements of the typical SOEC electrolytes. This experimental validation of the literature and theory is a critical advancement. These results will provide the basis for the final techno-economic models.

The techno-economic analysis will evaluate system performance for conversion to hydrocarbons. A modified version of the DOE's H2Analysis tools will be used to estimate the system economics. By comparing results with conventional routes, a breakeven carbon cost for these routes will be calculated.

3. THERMODYNAMICS

A key driver of any energy system is the energy efficiency. A significant attractive feature of SOEC systems are their higher theoretical energy efficiency compared to other hydrogen production systems. This section on thermodynamics will help identify the impact of the integration of the FT and SOEC units into a single FT-SOEC system. It will also identify the operational difficulties associated with coking due to the very high electrochemical reduction of steam and carbon dioxide in the SOEC. The thermodynamic benefits will be used to modify the economic analysis in the DOE's H2Analysis tool. The thermodynamic challenges will be a consideration in the catalyst screening section.

3.1. WATER SPLITTING

The thermodynamics of in-situ generation of fuels and chemicals simultaneous with electrolysis is beneficial for electrolyzer efficiency. The governing equation for the thermodynamics of the system is the Nernst equation. Various reaction products and pathways have different limiting efficiencies.

For a given reaction, the minimum thermodynamic voltages can be found by the following equation:

$$E_{eq} = \Delta G / zF \quad (\text{Eqn. 1})$$

where E_{eq} is voltage, ΔG is the change in free energy, z is moles of electrons transferred in the reaction step, and F is Faraday's constant.

Voltage over the thermal-neutral voltage (eqn 2) results in heat production and loss of system efficiency.

$$E_{tn} = \Delta H/zF \quad (\text{Eqn. 2})$$

Using the heat of formation and the Gibbs energy of formation for water as a function of temperature, along with eqn. 1 and eqn 2, one can easily construct Figure 3.1. The graph of ΔG_f and ΔH_f can then be used to determine the maximum amount of heat that can be used within the reaction at a given temperature. The difference between ΔG_f and ΔH_f increases with increasing temperature. In addition to kinetic limitations, this is part of why high temperature electrolysis is more able to use heat as an input to water or steam electrolysis. Not only are the kinetics improved, but also the maximum driving potential is higher. For a given cell, the current is defined by the operating voltage, the

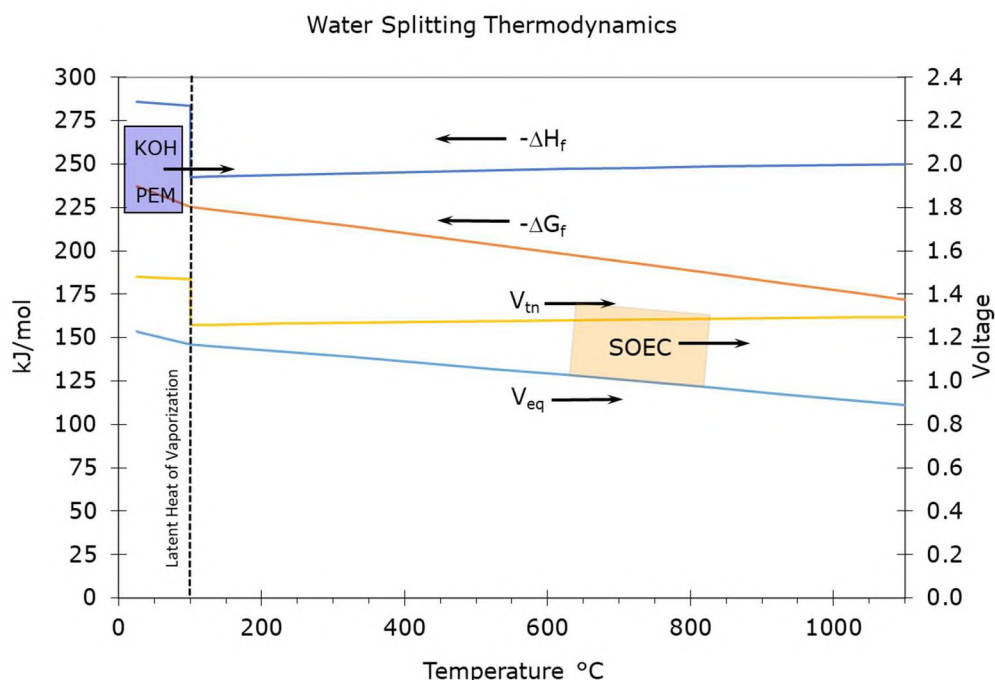


Figure 3.1 Water Splitting Thermodynamics And Typical Operating Temperatures And Voltages For PEM, Alkaline, And SOEC

open circuit potential, and the resistance of the cell. This is just a restating of Ohm's Law applied to an electrochemical cell.

$$V = I \times R \quad (\text{Eqn. 3})$$

Voltage is always a differential property. In this case, the voltage difference is the difference between the applied voltage and the open circuit potential. Restating Ohm's Law specifically for an electrolysis cell yields the following equation.

$$V_{op} - V_{Open\ circuit} = I \times R \quad (\text{Eqn. 4})$$

The open circuit potential at a given temperature is a function of gas composition. The full Nernst equation gives the open circuit potential as a function of temperature and gas composition.

$$E = E^0 - \frac{RT}{zF} \ln \left(\frac{\prod (P_{products})^x}{\prod (P_{reactants})^y} \right) \quad (\text{Eqn. 5})$$

where x and y are the stoichiometric coefficients of the products and reactants. E^0 is the standard potential of the reaction at the given temperature. The other terms R, z, F, and T have been previously defined.

The net heat load for a hypothetical cell is shown in Figure 3.2. It can be seen that for total conversion of the inlet gases the net heat generation of the cell is always greater than zero. A similar analysis by O'Brien et al. has previously been validated experimentally to show heat generation and consumption over the flow path of a SOEC stack [38]. When including the heat needed to convert water to steam, the net heat generation is zero for a much smaller value than the typical electrolysis only system. It is possible that some of this excess higher quality heat could be recovered to further improve the system efficiency, but that is beyond the scope of this work.

The thermal load of the electrolysis stack is zero at the operating voltage of 1.28V. In an ideal system with perfect heat recovery, the thermal load of the whole system is zero at

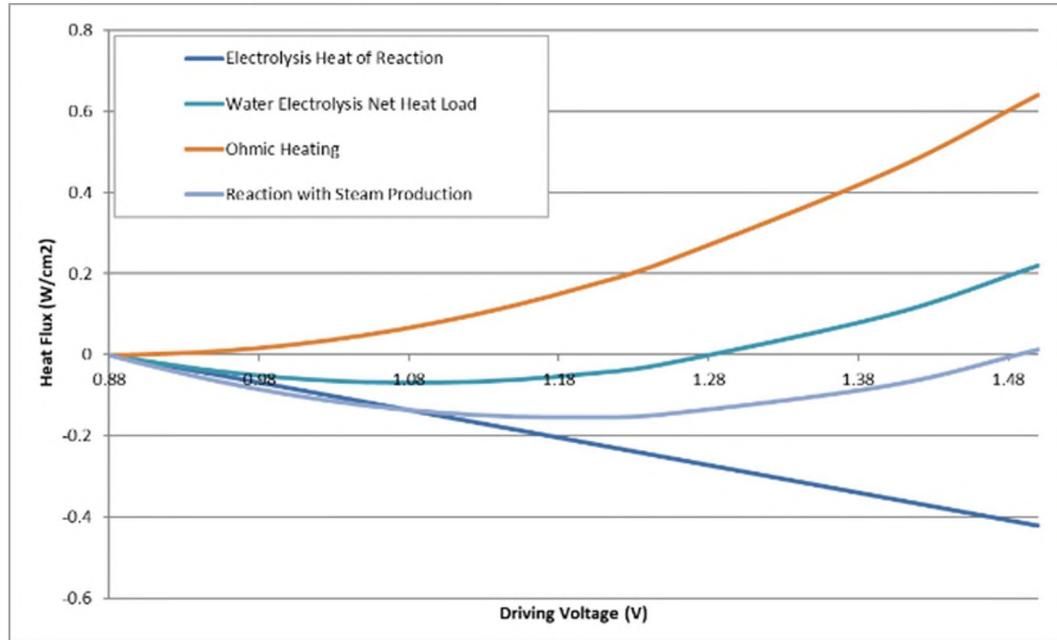


Figure 3.2 Net Heat Flux For A Theoretical Water Electrolysis Cell

1.48V. This corresponds to the higher heating value (HHV) of hydrogen divided by zF
 $E_{eq} = \Delta G / zF$ (Eqn. 1). In this case z is the number of electrons transferred per mole of
hydrogen ($z=2$) and F is Faraday's constant. Actual thermal losses mean that the total
energy would be higher. However, the 39 kWh/kg represents the minimum energy input
to the system. If the system has no other thermal energy inputs, the total electricity
demand required is a minimum of this value.

3.2. IN-SITU FUEL SYNTHESIS

Thermodynamically, the heat release of Fischer-Tropsch can be used to provide heat for the co-electrolysis system. The temperature at which the FT reactions occur, limits the amount of heat that it can provide to the system. The increasing quality of heat provides an increasing availability to provide energy and increase the theoretical efficiency of the hybrid FT-SOEC system. The thermodynamically favorable region for olefin production, the FT operating region and SOEC operating region do not historically overlap. The necessary adjustment is to raise the FT temperature and lower the SOEC temperature. This allows the system to operate where the heat released by the FT reaction can supply the heat needed for the SOEC water splitting reaction. The overall energy input to the system can be viewed from control volume of the electrolysis stack as entirely supplied by electrical energy. Figure 3.3 shows the net heat flux of an integrated FT and electrolysis system. It can be seen that the relevant thermal neutral operating points for the SOEC stack and for the entire system are shifted compared to steam electrolysis only operation. Heat recovery reduces the heat needed to be removed for the FT reaction, and eliminates the heat needing to be supplied for the water splitting reaction. The overall effect from an energy efficiency perspective is to reduce the overall required electrical input energy at the electrolysis stack. However, it should be noted that, from an exergy perspective, the increasing utilization of electricity over various grades of heat, results in a lower exergetic efficiency than from an ideal system. However, since the work anticipates that much of the energy for the electrolysis stack will come from renewable electricity sources, this has a negligible impact from an overall system perspective.

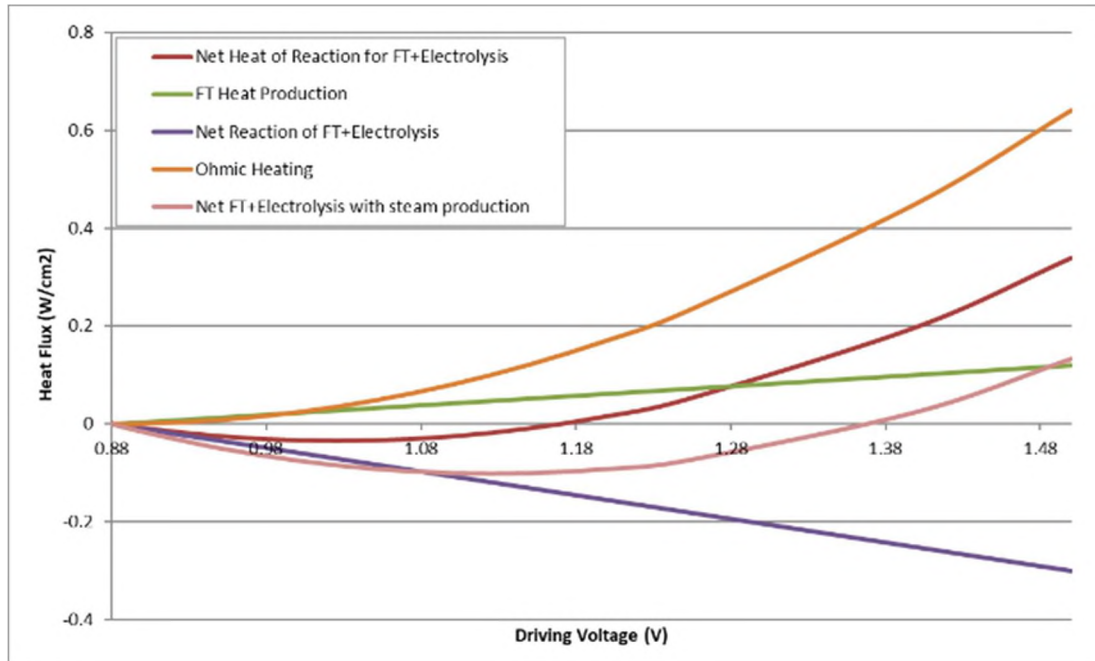


Figure 3.3 Net Heat Flux For A Theoretical Combined FT And Electrolysis Cell

In terms of outlet hydrocarbon composition, increasing the pressure can shift the equilibrium to longer chain hydrocarbons due to Le Chatliers principle. The molar quantity of reactants is higher than the molar quantity of products. This is one reason that FT reactors typically operate at pressures of 10-80 Bar. However, at these temperatures this is only a minor shift compared to the overall thermodynamic favorability of methane production. As will be discussed in a later section, the catalyst kinetics will be a determining factor between the yields of olefins and methane during the in-situ syngas formation and reaction.

3.3. COKING

A key metric of concern will become coking. The coking will depend largely on the operational parameters of the system. Factors such as CO₂/H₂O feed ratio,

temperature, pressure, and catalyst type will all affect the ability for coke formation to occur. The thermodynamic regime where coking cannot occur will be examined as the primary area of operation (Figure 3.4). Similar work done by Jensen et al. [39] shows the coking regime for methane formation. As shown higher hydrogen to carbon ratios reduce the coking rate. Higher hydrogen to carbon ratios unfortunately also encourages methane formation. A variety of different compounds can be added to the system in order to promote coking resistance [40]. These will be discussed further in the relevant catalysis and electrochemistry sections.

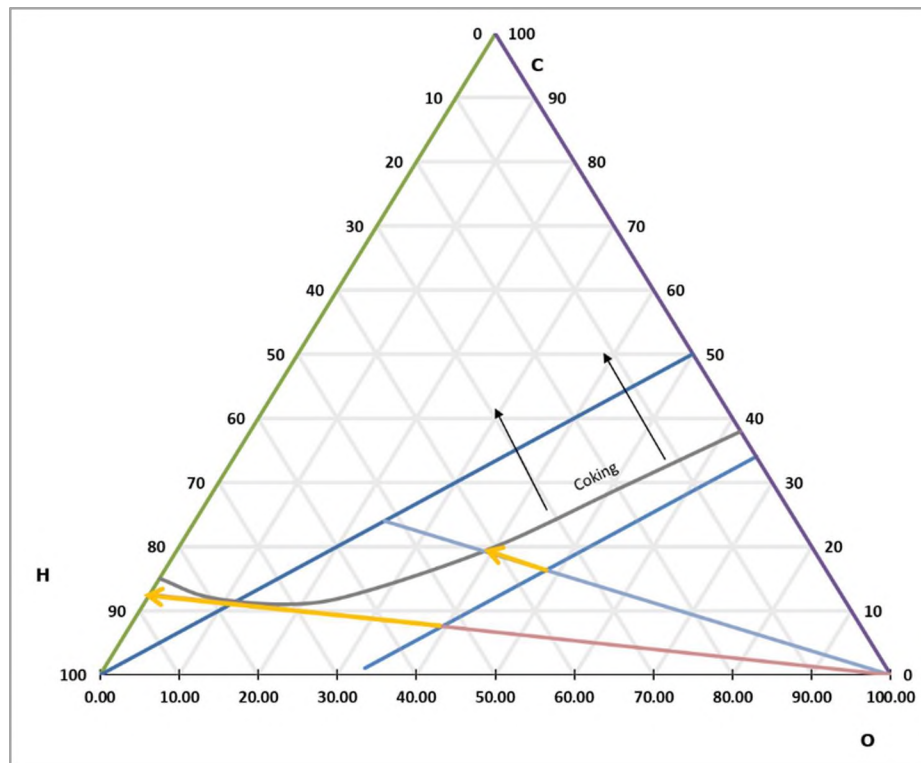


Figure 3.4 Coking And Non-Coking Region For Different C:H Ratios For The Synthesis Of Hydrocarbons In-Situ. Conditions Are At 1 Bar And 650 °C. HSC Chemistry 6.0

4. CATALYSIS

The kinetics of the catalytic system are a key limitation of the system. Compared to normal operating temperatures of 200-400 °C for syngas to olefins, the operating temperature for SOEC systems is much higher. The increased temperature increases the overall catalytic activity of the system. However, keeping the output CH₄ production rate low is still a large priority. The kinetics of methane formation in general grow favorable at increasing temperatures. If the overall kinetics are not supportive of producing C₂₊ hydrocarbons at the required temperatures, then the candidate system is not viable. Therefore, while yield and catalytic activity are of importance, reasonable activity and selectivity towards C₂₊ hydrocarbons production is a key metric in evaluating the potential catalysts and products. A secondary concern for initial screening of potential system is catalyst coking. Catalyst coking is of major importance to system lifetime. While the system will almost certainly thermodynamically favor coke formation, it needs to be kinetically inhibited on the catalyst active surfaces. There are many possibilities for reducing coke formation, and these will be discussed but not evaluated experimentally beyond the basic catalyst systems tested. Analyses and literature screening of synthesis catalysts potentially compatible of higher temperature C₂₊ hydrocarbons synthesis routes and catalysts is a major step in completing the objective of this work.

As a result of literature review and initial experimental screening with non-electrolyzer reactant systems, two different catalyst approaches are explored. The first is a syn-gas to olefin catalyst. The second is a non-oxidative methane coupling catalyst.

4.1. SYN-GAS TO OLEFIN APPROACH

These competing requirements of high hydrogen for non-coking, high per pass conversion, and low hydrogen to carbon ratio for higher olefin yield show the limits of this approach. A highly selective catalyst could potentially produce primarily olefins and hydrogen. At low temperature, hydrocarbons are the thermodynamically favored products. At higher temperature the reaction shifts towards syngas, carbon, and methane. FT is more exothermic than the other undesired reactions, and so increasing temperature shifts away from the conversion towards FT products.

The heat release of the FT reaction results in the overall reaction being net exothermic. The excess heat can be used for various process services, such as producing steam for the electrolyzer. [41] However, because FT is exothermic, the reaction decreases with increasing temperature. This presents a challenge for the high operating temperatures required for SOEC.

In examining some of the lower carbon number products, ethylene and other short olefins are commonly studied for synthesis via FT reactions. Fe, Co, and Ru based catalysts are very common approaches to olefin production from syngas [42]. Based on these being the typical low-temperature (200-300 °C) catalysts for FT to olefins, the potential for their use at high temperatures was examined.

By looking at the chain growth probability in the standard Anderson-Schulz-Flory (ASF) distribution, we can look and see what the fractions of various hydrocarbon ranges by chain propagation probability (Figure 4.1) [43]. This helps to develop a system for chain growth probability to optimize the product distribution.

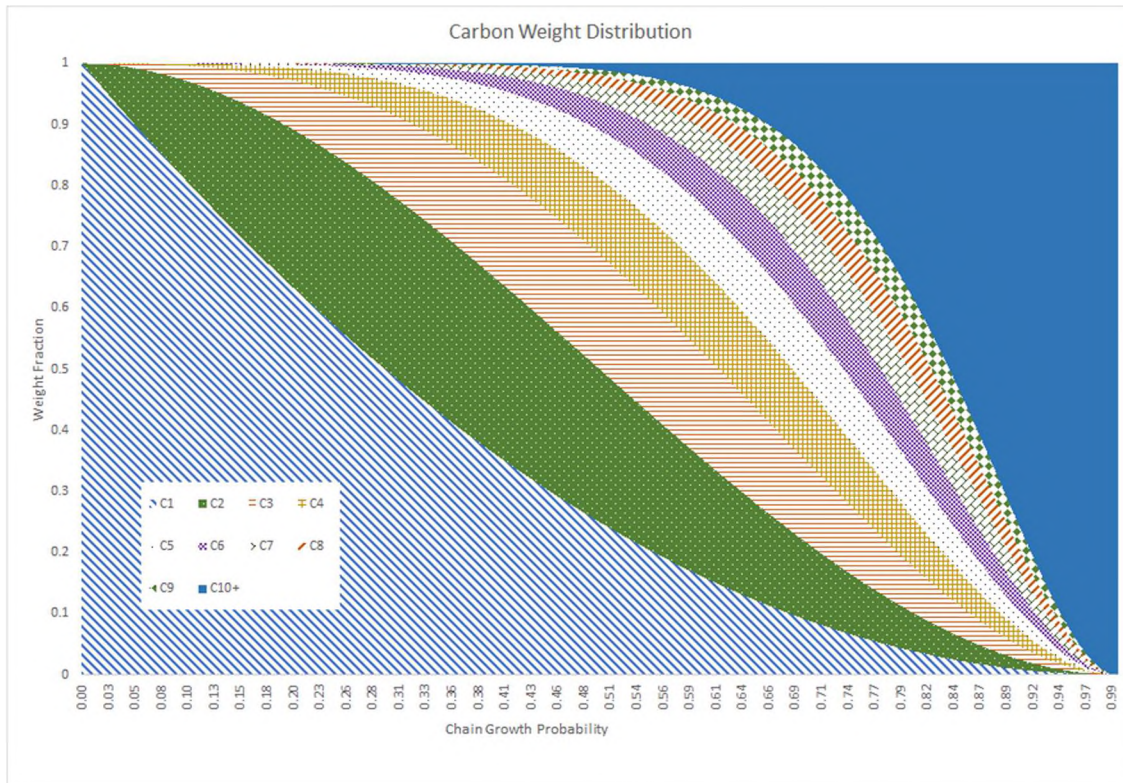


Figure 4.1 Product Weight Distribution By Carbon Number Of Fischer-Tropsch Polymerization Reaction

The product weight distribution determined by the ASF distribution shows the relative importance of a low methane yield. Kinetically restricting the formation of methane is the most substantial improvement to the yield of desired products that can be made. The overall target chain propagation value is based on maximizing the production of C₂-C₃ olefins. As can be seen in Figure 4.2, the maximized total C₂-C₃ olefin production occurs at a chain propagation probability of 0.41.

Additionally, the chain growth probability has an activation energy associated with the change in probability [44]. By determining the chain growth probability as a function of temperature we can find a target for the upper limit temperature for good chain growth to C₂-C₄ hydrocarbons. Research shows that both increasing temperature

and increasing H₂/CO ratio decrease the chain propagation probability. Since it is required that the FT-SOEC will be at a higher temperature than normal FT reactors, and coking probability is decreased with increasing H₂/CO ratio, it is important to evaluate the effect of these changes on the chain propagation probability. Using approximation of the chain growth

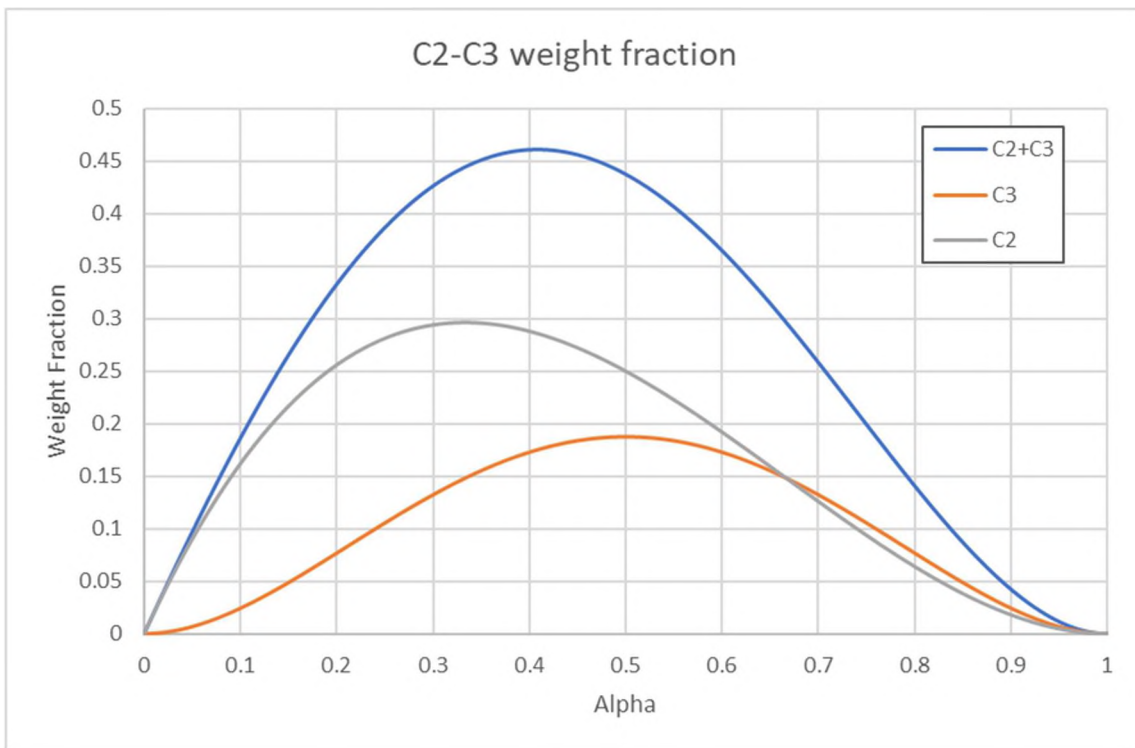


Figure 4.2 Weight Fraction Of C₂ And C₃ Hydrocarbons As A Function Of Alpha

probability as a function of temperature, an estimation of the high temperature chain propagation probability is made in order to estimate high temperature product distribution. [45] [46]

To increase selectivity to C₂+ hydrocarbons, limiting hydrogen active-sites prevents the hydrogen addition to CH₃ groups. The catalyst surface most often achieves

this by reducing the number of adjacent H-M active sites. Without being able to have hydrogen adsorbed to the surface, the CH_3+H group becomes kinetically unfavorable (Figure 4.3). However, this must be tuned in the consideration that CH_2 groups are still necessary for a stable and active pathway to unsaturated bond formation. In the case of higher alcohols this can be achieved through stable OH groups bonding on the surface to OH groups to help the process proceed.

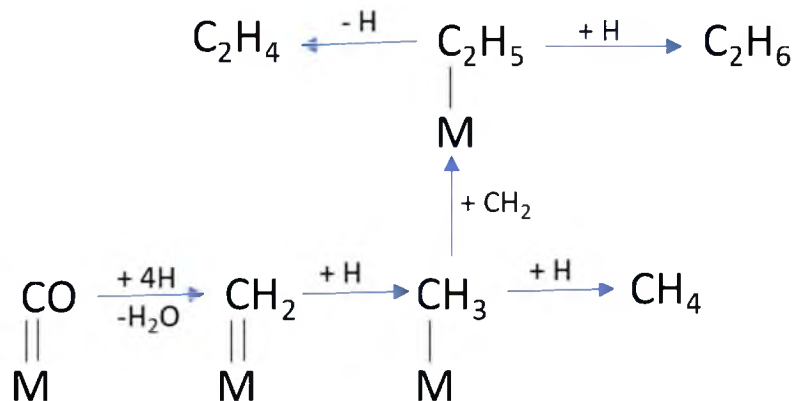


Figure 4.3 Fischer-Tropsch mechanism pathways [41] [47]

The initial screening for catalyst selection was to find catalysts that were selective towards non-methane and non-carbon-dioxide products at elevated temperatures. Additionally, selectivity towards olefins over alkanes was preferred. Low activity was not a serious impediment in the initial catalyst screening. The increased operational temperatures of the catalyst will increase the overall reactivity. The overall system economics are more strongly affected by the SOEC system than the subsequent FT steps. When thermodynamic limitations are taken into consideration, the SOEC electrode area is expected to provide excess catalyst surface area for FT synthesis.

By examining the literature of FT-olefin synthesis, an estimate of the alpha chain propagation factor as a function of temperature was derived. Starting with the following equation from [48]

$$\alpha = \frac{1}{1 + k_\alpha \left(\frac{C_{H_2}}{C_{CO}} \right)^\beta \exp\left(\frac{\Delta E_\alpha}{R} \left(\frac{1}{493.15} - \frac{1}{T} \right)\right)} \quad (\text{Eqn. 6})$$

By calculating and fitting the chain propagation probabilities for various catalyst families to the literature. We can approximate the chain propagation probability activation energy for the various catalysts. For the catalysts examined the syngas ratio is nearly constant, thus turning the entire pre-exponential factor into one unknown.

By fitting the data to the Ruthenium catalyst, it can be seen that the difference in Figure 4.4 that the activation energy for the methanation and olefin synthesis reaction is much smaller than for the Fe-Co-Ce catalyst system. This suggests a Ru based catalyst might be a viable candidate for the production of the olefins at very high temperature (Figure 4.5). Unfortunately, experiments show Ru tends towards methanation at higher temperatures [49]. In contrast to Ru, the Fe-Co-Ce quickly becomes pure methanation reaction at higher temperatures due to the much higher activation energy [50] [51]. This is based on the predicted chain propagation probability.. However, if the hydrogen addition to the methyl group is kinetically restricted then the termination steps may still favor a product higher in ethylene and higher olefin production [52]. Manganese is well characterized and has been shown to promote olefin formation on Fe and Co catalysts [49-54]. The addition of sulfate compounds was shown to promote olefin formation on Fe supported on Alumina to temperatures up to 550 °C.

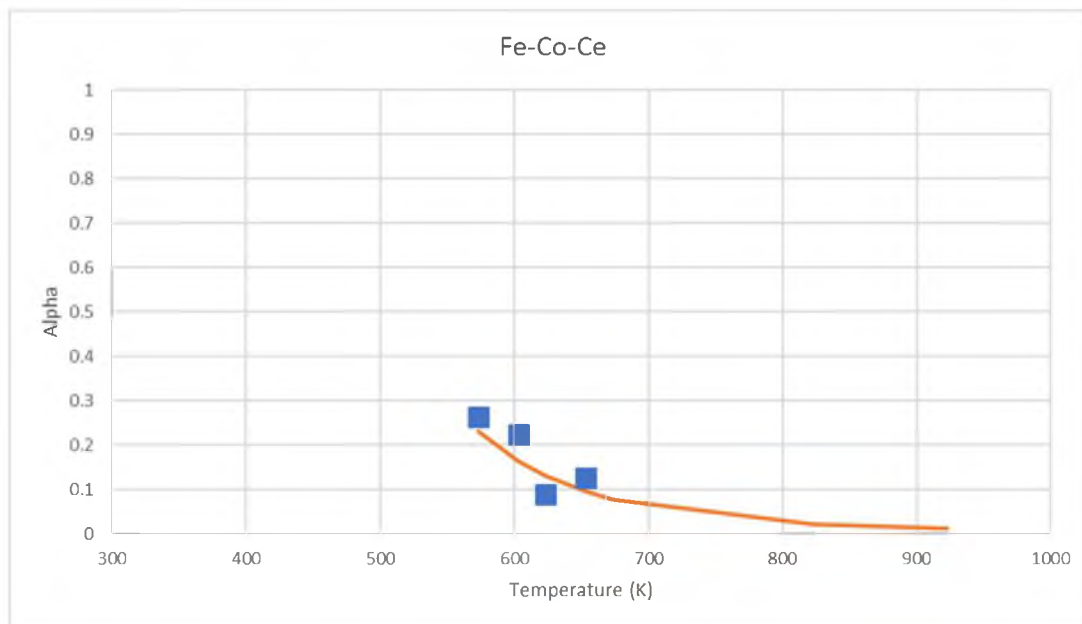


Figure 4.4 Fe-Co-Ce Catalyst Alpha Vs Temperature With Alpha Fit To Eqn 6

Potassium has also been used as a promoter and observed to increase olefin production on Fe-based catalyst [53] [54] [55]. The Co and Fe catalyst system was screened to determine the effectiveness of the cheaper Fe-Co based catalyst. Coking may still present an issue for system lifetime. The variety of supports can also impact the overall composition and catalytic activity of the system. Major types of supports include alumina and carbon-based supports [56] [57]. Potentially compatibility issues with supports is discussed in the SOEC electrochemistry section.

The operating conditions for the system still require that olefin production be thermodynamically favorable, while simultaneously having effective electrolysis steps. These conflicting requirements are partially satisfied by increasing the pressure and operating in the 500–700 °C temperature range. At higher temperature the system has is

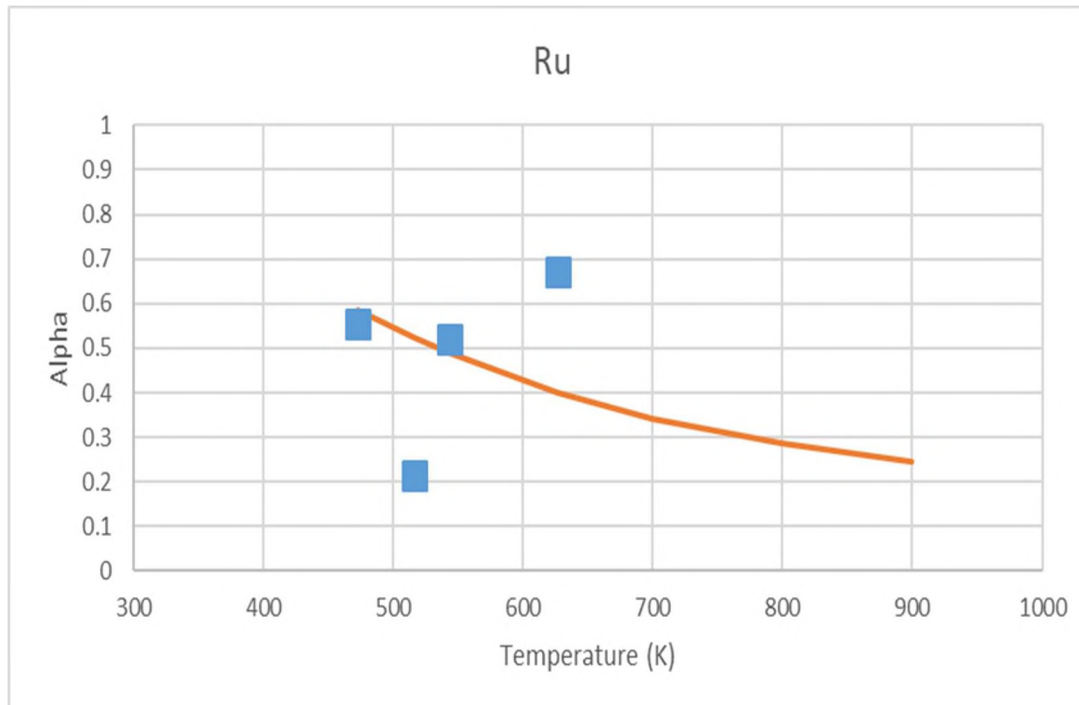


Figure 4.5 Ru Catalyst Alpha Vs Temperature With Alpha Fit To Eqn 6

predicted to have a lower theoretical maximum per pass yield, while at lower temperature, the electrolyzer power density is poor.

Based on the screening results of the catalyst literature and analysis, Co-Fe based catalyst on a ceria support was selected as the initial candidate for the FT-SOEC system. It represents a reasonable compromise between availability, cost, performance, compatibility with SOEC, and similarity to existing SOEC cell composition. This proof of concept catalyst and cell combination will be used to show whether or not within the thermodynamic boundaries that in-situ olefin synthesis in a SOE unit is viable via a syngas intermediate.

4.2. METHANE COUPLING CATALYST SYSTEM APPROACH

An alternate approach was formulated based on the non-oxidative coupling of methane (non-OCM). This approach utilizes the methane formation of the nickel catalyst in the electrode to feed a non-oxidative coupling methane catalyst. Concerns about coking still apply. In this case much more oxygen is removed from the reaction. Since hydrogen is one of the products of methane dehydro-aromatization, any excess hydrogen unreacted in the methanation reactions reduces conversion. This two-step catalytic system has more flexibility in operating temperature, but it still has significant challenges with the potential for carbon deposition. In order to get significant conversion to methane in the electrolysis step carbon deposition will be an even greater concern than a syn-gas route.

Thermodynamic products calculations were performed over a range of oxygen content. These calculations were performed using HSC chemistry 6.0. The decreasing oxygen content corresponds to the electrochemical reduction expected in the SOEC system. Table 4.1 shows the concentration of various expected products of non-oxidative coupling methane. These calculations are compared to calculations from literature and show a very similar result [58].

Changing these calculations to the desired operating temperature and plotting vs oxygen content gives the composition vs percent reduction. The calculations are performed using a 4:1 H:C ratio. For the purposes of the catalyst, coking is considered to be kinetically excluded and is not considered. Based on the method's previous agreement with reported calculations from values, the thermodynamic predictions of these

Table 4.1 Weight Fraction of C₂+ Hydrocarbons Via Non-Oxidative Coupling Methane as a Function of Temperature (Celsius)

	Ethane			Ethylene			Benzene		
	CH4	H2	Ethane	CH4	H2	Ethylene	CH4	H2	Benzene
527	99.0%	0.1%	0.9%	99.4%	0.1%	0.5%	97.5%	0.5%	2.0%
727	CH4	H2	Ethane	CH4(g)	H2(g)	Ethylene	CH4	H2	Benzene
	97.2%	0.2%	2.6%	95.1%	0.0%	4.3%	86.0%	2.6%	11.3%
927	CH4	H2	Ethane	CH4(g)	H2(g)	Ethylene	CH4	H2	Benzene
	94.5%	0.3%	5.2%	80.9%	0.0%	16.7%	60.2%	7.5%	32.3%

calculations are expected to be accurate with an adequate catalyst (Figure 4.6, Figure 4.7, and Figure 4.8).

Examining the product composition at 650 C, ethylene is an almost negligible product, however, methane yield can be almost complete conversion of the incoming products to methane. As shown, at near total reduction of the system the production of ethylene becomes noticeable for the 725 C case. In fact, the limiting case of total reduction is the pure methane feed cases given in the table with comparisons to literature.

At 800 C, the ethylene production is approaching a level that is significant enough that separations might be practical for the recovery of the ethylene from the methane. Further increases in temperature may be beneficial but have a trade-off with SOEC system lifetime and materials. For the proof-of-concept testing, remaining with a more common 800 C operating temperature for stability and better baseline comparison is an appropriate compromise. Future integration of SOEC with non-oxidative coupling methane can potentially benefit from the increasing yield of ethylene with increasing temperature.

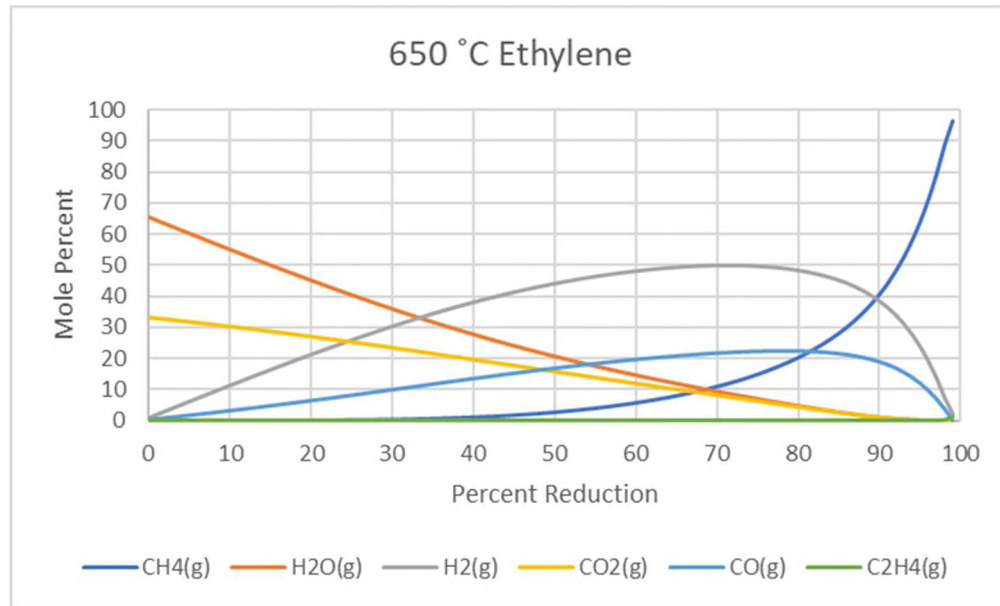


Figure 4.6 Electro-Reduction Of Steam And Carbon Dioxide At 650 C And 1 Bar

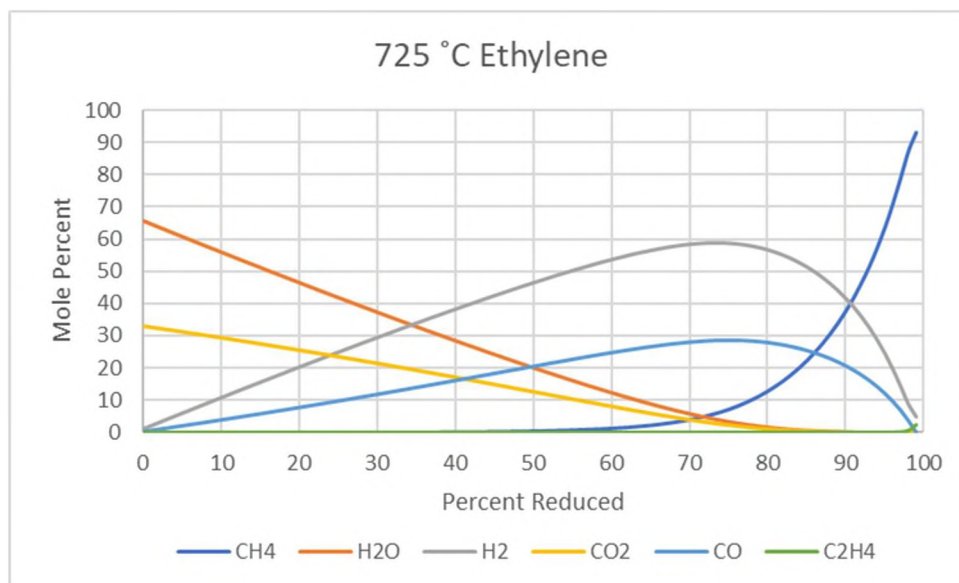


Figure 4.7 Electro-Reduction Of Steam And Carbon Dioxide At 725 C And 1 Bar

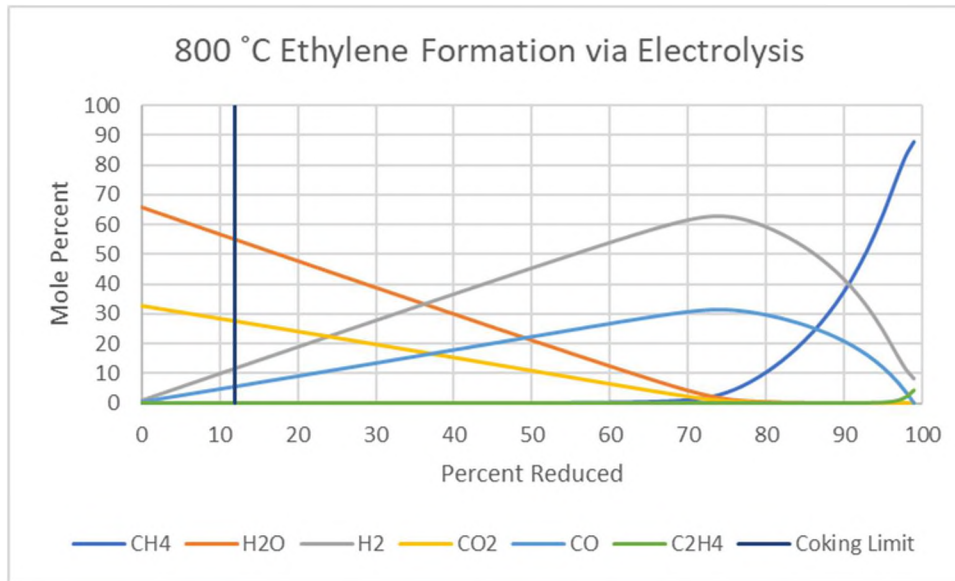


Figure 4.8 Electro-Reduction Of Steam And Carbon Dioxide At 800 C And 1 Bar

There is an extensive body of literature on a variety of non-oxidative coupling methane catalysts. Most of these catalysts are based on zeolites of different varieties. A very common and easy to procure and synthesize catalyst candidate is Mo-HZSM5. The operation of zeolites at high temperature and high steam is a concern for the stability of the catalyst. The catalyst stability is also an area of concern for the electrodes. The zeolites are a compound of silica and alumina, at high temperature and steam, the catalyst is subjected to “steaming” and dealuminification. The removal of alumina from the structure causes an overall coarsening and decrease in surface area. The long-term degradation of the catalyst results from the removal of the alumina from the crystal lattice.

Silica appears to remain stable during the steaming process. This is significant for the system lifetime. Silica is a known poison to SOEC systems. For any long-term system, the stability of silica species in the system is critical. The silica can form silicic

acid and due to the change in pO₂ at the electrolyte and catalyst interface, deposit on the triple phase boundary. This generally results in a near-irreversible poisoning of the system activity. stable in the structure. The long-term operation of an SOEC system with co-located zeolite is a topic of future, but an area of consideration in catalyst selection.

5. SOEC ELECTROCHEMISTRY

This section examines the challenges for a typical SOEC to operate under the conditions expected for the FT-SOEC system. The two major concerns are coking and electrolyte resistance. A coking resistant SOEC system will significantly reduce the challenges of integrating a FT reaction system into the SOEC stack. Coking is also a significant concern for non-OCM-SOEC. In order to have any substantial per pass conversion to non-methane products, coking resistance of the electrolyzer is essential to any of the proposed FT-SOEC systems.

Relatively low temperatures for SOEC needed for the FT-SOEC system create significantly increased ohmic resistance in the electrolyte. The ability of the system to operate at reasonable power density and efficiency requires a low resistance electrolyte. Unlike the FT-SOEC system, non-OCM-SOEC prefers higher operating temperatures and the conductivity of the electrolyte is not a significant challenge for that approach.

In contrast with the difficulties of power density, at the lower temperature desired for the system, many of the durability difficulties associated with SOEC processes can be avoided. The need for non-ferritic materials for the interconnect and other balance of plant components can be reduced or eliminated by the lowering operating temperature requirement of the SOEC system. The major trade-off for operating at a lower temperature is the overall power density of the SOEC. This trade-off is why most current SOEC systems are operated at a temperature much higher than the temperatures necessary for the traditional routes of C_2+ hydrocarbon synthesis.

5.1. COKING RESISTANT ELECTRODES

Coking of the electrode will primarily affect system longevity and is not a primary concern for the initial proof-of-principle testing of this project. However, the potential need for very high oxygen removal makes the coking resistance a necessary consideration important for the initial system. The high rate of oxygen removal may quickly create a situation where a non-coking-resistant electrode will degrade in minutes.

Traditional SOFC and SOEC electrodes are nickel based. Nickel is an excellent promoter of carbon deposition. This presents challenges for the system design. From the catalyst and thermodynamic discussion, we can see that the need for coking resistance in the system will be unavoidable. Normal operation of SOFC systems and SOEC systems avoids coking by having sufficient steam and low enough conversion to avoid coking conditions. Nevertheless, significant research has gone into the production of coking resistant SOFC systems. The ability to feed unreformed hydrocarbons without steam is of significant interest for SOFC systems. Due to interest in co-electrolysis, this type of anti-coking behavior, while not as prevalent, is also an area of research for SOEC systems.

In the past, different electrode compositions have been used in order to reduce the coking of the electrode itself. Platinum has been used for this purpose. This approach would be completely uneconomical for any large scale SOEC system and was not considered for the candidate systems.

Recent work by Skafte et al. has shown the development of a coking resistant electrode that is based on ceria electrodes [59]. Ceria is an oxygen-bearing compound and is able to keep the oxygen available to surface adsorbed species. Changing adsorbed carbon dioxide and carbon monoxide species to carbonates prevents the onset of carbon

formation. At high reducing conditions the system is exposed to in order to produce the extreme deoxygenation of the feed required, the ceria may not be able to supply all of the necessary surface oxygen.

Another approach to reducing coking would be to include some sulfur in the feed. Sulfur-passivated nickel has been shown to greatly reduce the tendency towards coking relative to methanation or methane reforming reactions. This is the basis for the Haldor Topsoe's SPARG process [60]. However, it is observed that the onset of coking under these circumstances, while delayed compared to bare nickel, is still very early relative to the total oxygen removal desired for the high yield of hydrocarbons in the FT-SOEC system.

5.2. ELECTROLYTE CONDUCTIVITY

The conductivity of the electrolyte is one of the more limiting factors in SOEC performance. Exploring the impact of adjusting the operating temperatures of the SOEC electrolyte to meet the needs of an integrated synthesis step is vital in predicting the capabilities and requirements of the combined systems. FT-SOEC has far greater constraints due to the preference towards lower temperature operation for the catalyst kinetics. NOCM -SOEC has no issues and favors even higher temperatures than the typical SOEC operating temperatures. The compromise for optimizing for FT-SOEC is system performance, while the compromise for NOCM -SOEC is system lifetime. Since, system lifetime is only assessed qualitatively for this research, a greater focus is placed on assessing how to optimize the SOEC component performance for lower than normal operating temperatures in order to be compatible with the integrated FT steps.

The objective of integrating FT-based ethylene synthesis with hydrogen production by solid oxide electrolysis places a practical upper limit on device operating temperature of about 650°C in order to achieve a useful equilibrium syngas conversion at a reasonable operating pressure. The standard operating temperature for SOEC operation is around 800°C. While thermodynamics allow a greater use of heat to offset electric energy input as temperatures increase, the reasons for SOEC operation near 800°C are a compromise between performance, and lifetime. Further increases in temperature provide greater performance, but a much shorter useful lifetime.

Lowering the operating temperature to 650°C still enables the high efficiency capabilities of operating below thermal-neutral voltage but may require a new cell design and material set relative to standard electrolyte-supported cells developed for 800°C operation. Although Ceria is known to have a much higher ionic conductivity than zirconia, it has not found wide usage among SOFC developers due to its mixed conductivity when exposed to reducing atmospheres such as hydrogen (low pO₂) which results in an internal shorting current that hurts efficiency and complicates thermal management [61]. However, the pO₂ conditions for electrolysis remain favorable for a ceria electrolyte to be used for combined FT-SOEC.

The 800°C ionic conductivity of YSZ is 0.02-0.03 S/cm and 0.10 S/cm for ScSZ meaning that for an equivalent ionic resistance contribution, a ceria electrolyte operating at 650°C must be a factor of 3 thinner than YSZ and 8 relative to ScSZ [62]. For comparable performance to an 800° electrolyte supported SOEC of YSZ or ScSZ, the target thickness for a ceria electrolyte is in the range of 15- 50µm (Figure 5.1). These electrolyte thicknesses are achievable with commonly available electrode-supported cells.

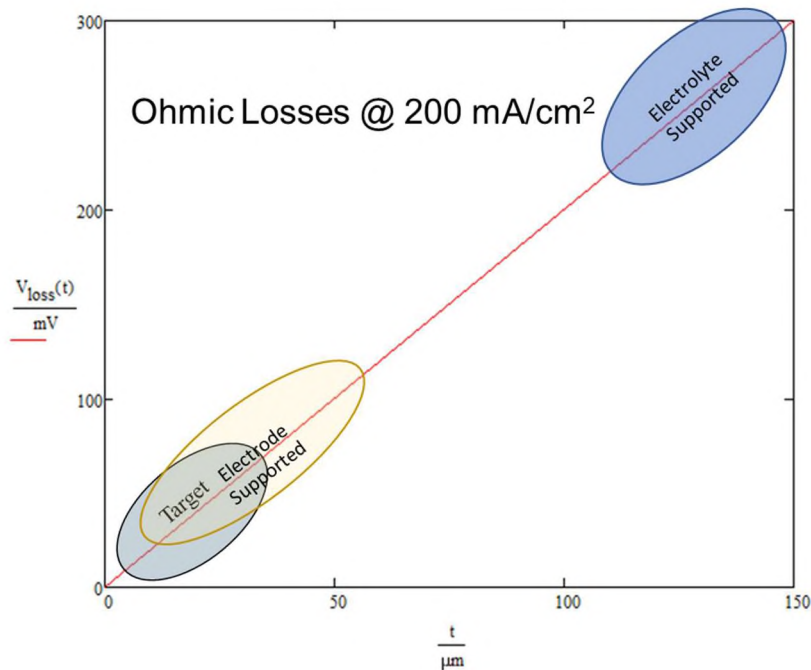


Figure 5.1 Ohmic Losses Vs Electrolyte Thickness. Typical Electrolyte Supported Cells And Electrode Cell Electrolyte Thickness Shown Operated At 650 °C

Where hydrogen electrode-supported SOFCs are preferred, in SOEC mode an oxygen electrode-supported cell design offers performance advantages. At the moment, oxygen electrode-supported cells are a subject of research and not commonly available. Due to the differences in SOFC and SOEC, the fuel side and oxygen side structure, can have different optimal thickness. In SOFC the fuel electrode is a much thicker nickel cermet. This thick, dense nickel cermet structure adds considerable mass transfer resistance while functioning as a cathode in SOEC mode. The SOEC anode (oxygen evolution electrode) offers no mass transfer resistance, as the oxygen mole fraction in the anode pores is 100%, making the pO₂ equal to the local total gas pressure. Evolved oxygen flows out of the porous anode in the Darcy flow regime under a pressure gradient rather than by Fickian diffusion under a concentration gradient. The very small pressure

gradient required to achieve an oxygen flux through a porous anode (oxygen electrode) corresponding to the target 300mA/cm² is negligibly small in contrast to rather pronounced cathode (hydrogen electrode) mass transfer polarizations seen in SOFC hydrogen electrode supported cells operated in SOEC mode.

The resistance of the electrolyte provides ohmic heating. The ohmic heating can also contribute to the heat necessary for the water splitting reaction. Electrode supported cells are commonly available, however, the additional nickel area makes them more likely to catalytically convert the products to equilibrium; this is undesirable.

Due to the ease of which electrolyte-supported cells are able to adapt to custom electrodes, a YSZ thick electrolyte supported cell will be used to validate electrode performance. The use of electrochemical impedance spectroscopy (EIS) can separate the electrolyte effects from the electrode effects. Future work could include an electrode supported cell of a different catalyst composition. Until a proper catalyst is identified formulating a new electrode composition is a substantial effort that may be invalidated by the fuel synthesis pathway catalyst requirements. In the event that a target electrode is developed that needs low-temperature operation in order to be effective in hydrocarbon production, adaptation to an electrode supported cell with thin electrolyte, or a ceria supported cell will need to be developed.

6. ECONOMIC PRODUCT SCREENING

The initial economic screening attempts to identify products that are higher value on an energy input basis. Additionally, products that have large market depths, and market accessibility are also favored. Comparisons are made to hydrogen as the baseline economic case for SOEC in a hybrid energy system. A desirable, but not strictly necessary feature of the product screening is for the product to be economically favorable compared to the hydrogen production baseline.

6.1. PRODUCT ECONOMICS OVERVIEW

Figure 6.1 provides a guideline to the pricing of various hydrocarbon outputs. The vertical axis provides the marginal cost, while the horizontal axis provides a proxy for capital costs. All other factors equal, products higher and to the left are more economical. Factors such as market capacity, transport costs, compression and handling provide other changes that may affect the costs. It can be seen that within the catalyst families, the olefin catalysts have the highest average output.

At the date of the initial data (2016), the olefin catalyst could produce olefins economically at an electricity input price of \$80/MWh (Figure 6.2). An updated version with 2020 market prices is shown in Figure 6.1 for comparison. However, the market and delivery to market of hydrogen is much more complicated. Efforts to optimize the olefin catalyst to a much higher mix of low carbon olefins would improve product value and therefore improve the overall system economics. Additionally, the available market

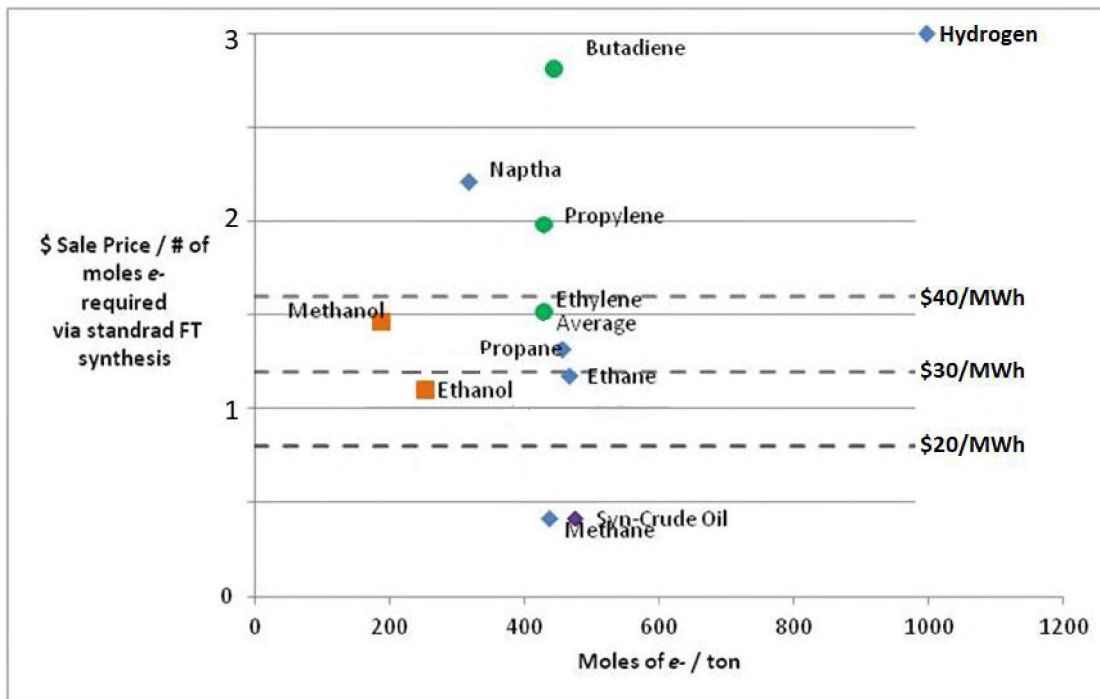


Figure 6.1 Electrochemical Production Of Chemicals Pricing. Prices Based On--March 2016 [64] [65] [66] [67]

prices of low-cost electricity have improved over the time frame between these economic cases. A more recent case using ERCOT real time pricing data from 2018 provides insight into the availability of cheap wholesale electricity [63].

Recently the production of olefins has significantly increased. The increase in production has decreased much of the profit potential that was part of the original motivation for this work. A case study of sample catalysts shows that for various market conditions, one before the oil price crashes, and one after-- hydrogen is the most consistently able to be produced at a profit.

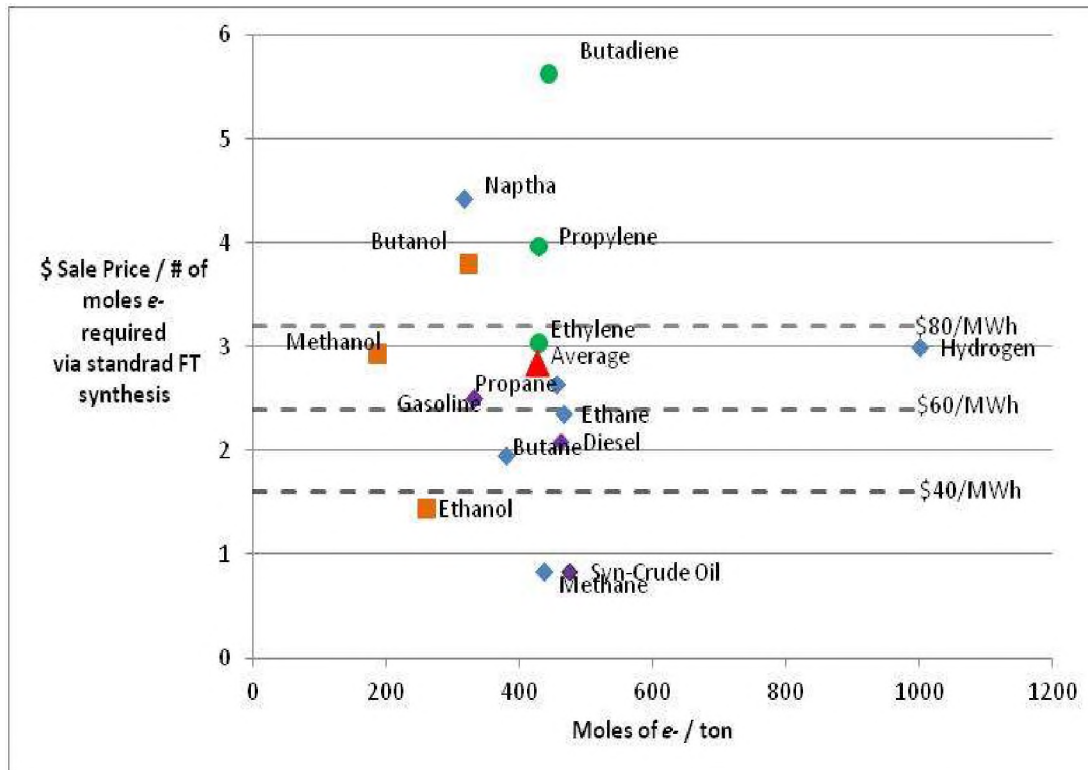


Figure 6.2 Electrochemical Production Of Chemicals Pricing. Prices Based On June 2020 [67] [68]

6.2. MARKETS

The petrochemical products market is substantially different from the hydrogen market. There is an estimated \$100 billion of hydrogen production consumed worldwide every year [69]. By comparison, the petrochemical market is approximately four times larger at an estimated \$450 billion in 2020[70]. Most major markets for hydrogen are contracted and dedicated purpose production. By comparison, most petrochemical products have a robust openly traded market price. This makes the exact evaluation of SOEC produced hydrogen's profitability more difficult than that of petrochemicals. Often, hydrogen will be able to set its price in negotiations with a buyer.

The chief competition for electrolytic hydrogen is fossil fuel reforming. The typical market price for a large-scale steam methane reforming plant is around \$1/kg [71] [72]. At smaller scales the price of hydrogen goes up significantly. For the near future, in the absence of any carbon taxes or other climate change oriented policies, green hydrogen will not be cost competitive for the most large scale hydrogen production plants. However, for small distributed systems, current electrolyzer costs are already at or near cost-parity with fossil-based hydrogen.

The difficulty in competing with large centralized users is further compounded by the difficulty in delivering hydrogen long distances. The extra costs of long-distance transport to potential market further locks hydrogen into sale to dedicated end-users and co-location of the hydrogen production near that end-user. Hydrogen can cost several \$/kg to transport a thousand miles. The costs of compression, specialized tube trailers, and the low density of the product contribute heavily to these costs. Pipelines are also costly. Estimates ultimately put a hydrogen pipeline in the same approximate cost as a natural gas pipeline [73]. Although pipeline transport can be effective, the leakage rate can represent a significant cost compared to a similar leakage rate of natural gas. This is due to the inherent value of hydrogen being much higher per unit volume, combined with a roughly 4x higher leakage rate compared to natural gas.

In comparison to hydrogen, the market for petrochemicals is much more uncertain. The market price can fluctuate wildly even within the course of a single year. This presents a different set of difficulties in evaluating the economics of a multi-decade capital project. The uncertainty drives the production of non-fossil fuel-based petrochemicals to be a very risky proposition. While higher market prices can produce a

very lucrative product, downturns can cause for the plant to shutdown and lead to costly losses.

While the direct market competitiveness of petrochemicals is lower than hydrogen, they have a much lower cost of transportation. This allows these products to compete in an open market and have a much wider access to geographic locations for production--unconstrained by needing to be near an end-user facility. Methanol and benzene are liquids at ambient conditions. Specialized tube trailers for cryogenic transport of ethylene are readily available. Hydrocarbon gas liquid pipelines are also accessible for a large amount of the country. Particularly, there are lots of hydrocarbon gas liquid pipeline access in parts of the country that have good wind energy resources.

The broad comparison between hydrogen and other petrochemicals can be summed up as hydrogen is more cost competitive and able to negotiate prices. However, due to transport costs for hydrogen, it requires being in close geographic proximity to the end user. In contrast, petrochemicals compete in a commodity market, but are able to be located freely geographically while having a much larger market access.

The breakeven pricing depends on the market price for the olefins. Olefin production competes in a commodity marketplace. This is both a benefit and a challenge. In comparison to a typical SOEC, the hydrogen produced does not have a large commodity market. Most hydrogen is produced and used on site by the end-user. The main users are ammonia production, methanol production, and petrochemical production. The necessity of co-location of hydrogen production and consumptions makes establishing a market for the hydrogen difficult. In contrast, olefins are frequently traded on the open market. Polymer manufacturers are often sited next to refineries to lower

distribution costs, but are more often separate entities. Additionally, the petrochemical market has been affected by the recent shale gas boom. The shale gas boom has altered the product distribution for the typical refinery [74]. There is a relative abundance of ethane compared to propane. The reduction in cracking units has led to the need for more on purpose olefins productions rather than production as byproducts. These have come on line in the recent years are partially responsible for the significant drop in ethylene prices. It is reasonable to expect that any significant reduction in shale gas will create a reverse market shift. This is a significant market opportunity for technology that can both displace fossil fuel inputs, and provide load leveling capabilities.

6.2.1. Paraffins. Alkanes and other paraffins form a large part of the products of a barrel of oil. These products are generally lower value and sold mostly for their energy content or for use as lubricants. While these are often the starting point for a lot of technology evaluations, based on their low value relative to energy input, this work considers them to be an uneconomical starting point for synthetic petrochemical technologies. In the future, if synthetic petrochemical technologies come down in price and fossil fuel based petrochemicals have environmental penalties attached to them then substitute fuels can potentially be an economical product.

6.2.2. Oxygenates. The oxygenate class of products present an opportunity if the selectivity of the catalyst can be refined to a narrow chain length. The production of C1 oxygenates is valuable and provides an entry point for a wide variety of chemical pathways (Figure 6.3). Methanol currently represents about \$40 billion per year in revenue worldwide. Changing pathways for other petrochemicals to be produced via methanol could increase that market substantially. C4+ oxygenates also provide a high

value product. With butanol being a drop-in substitute for gasoline in most engines, it also provides a large market opportunity for producing as much butanol as desired. The issue is that in order to be viable as drop-in replacement, the cost will have to go down to the point where it is cost competitive with gasoline, which thereby reduces the profit margin on the butanol

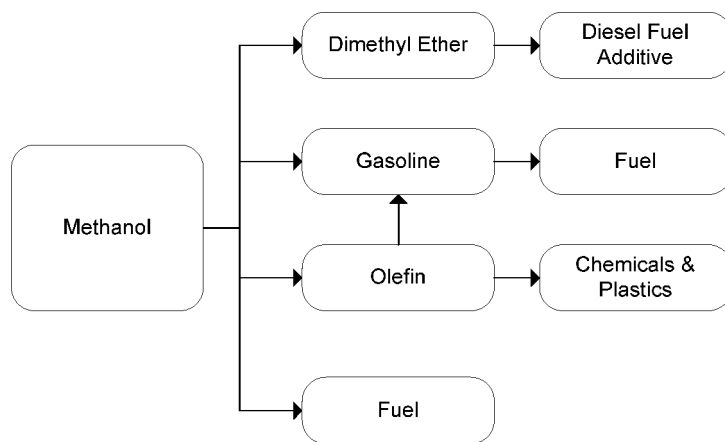


Figure 6.3 Chemicals And Fuel Use Pathways Of Methanol

production. Currently most catalysts produce a large amount of ethanol and propanol. Both of these compounds are very low value relative to alternatives. A catalyst that is highly selective towards methanol or butanol at the combined synfuel-SOEC operating temperatures would make these attractive target chemicals.

6.2.3. Olefins. Olefins are high value feedstock chemicals and form one of the basic building blocks for much of the petrochemical industry's finished products (Figure 6.4). The majority of ethylene goes into polyethylene production. Similar production between other olefins and their corresponding polymers is also common. This provides a benefit to the overall system as byproduct ethane and propane have the ability to feed into

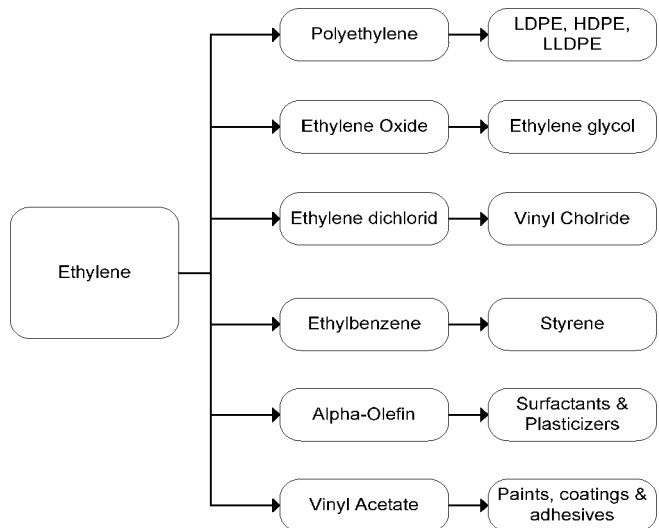


Figure 6.4 Major Chemical Products Derived From Ethylene [75] [76]

the existing crackers. The byproduct, light alkanes, can be used as feedstock for further olefin production using existing systems.

A survey of ethylene production from 2014 shows that the majority of ethylene production from steam crackers is located in Texas. [77] The map of ethane crackers (Figure 6.5) shows production of the olefins to be tied to the oil and gas industry, with the majority located near the gulf coast. Therefore, when market power prices are used in the economic analysis, it will be using power prices from the Texas region. Similarly, stand-alone wind data will also be used from that region.

As can be seen from the market prices of ethylene and propylene and their polymers, the market trends are similar for all the products [68]. Since simple plastics are near substitutes for each other they are not able to sustain a significant price differential relative to each other without the market following. Although a poly-olefin plant would

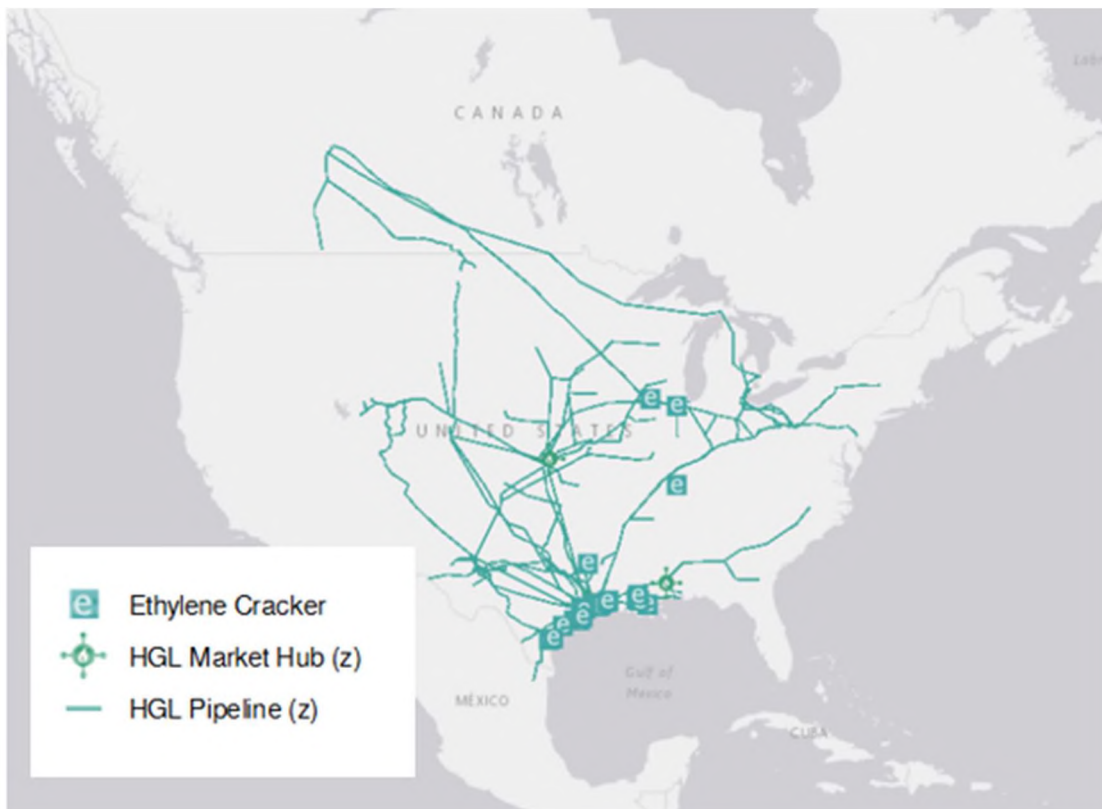


Figure 6.5 Hydrocarbon Gas Liquid Pipelines And Ethylene Cracker Map [78]

add value and reduce the transportation costs, analyzing poly-olefin manufacturing is beyond the scope of this work and is a potential subject for analysis in a future hybrid energy system.

6.2.4. Benzene, Toulene, Xylene. Another class of chemicals that is attractive for being widely used, easily transported, and high value per input energy are the benzene, toluene, xylene (BTX) chemicals. There are a number of derivative products that are of key importance to the economy that are produced from BTX chemicals (Figure 6.6).

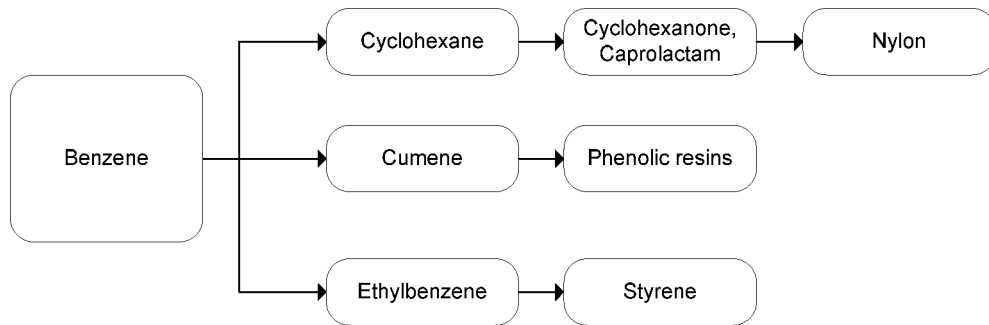


Figure 6.6 Benzene Product Pathways

6.2.5. Ammonia. The traditional operating temperature for Haber-Bosch and similar ammonia synthesis reactions are 400-600 °C and 200-300 Bar (Figure 6.7). The FT catalyst candidate Ru is also an ammonia synthesis catalyst. An ammonia focused system does gain the benefit of no coking challenges. However, the pressures involved are much higher. The integrated production of ammonia in the system is of interest, however, with the high pressures involved, but with an integrated ammonia synthesis reactor test is beyond the scope of this work.

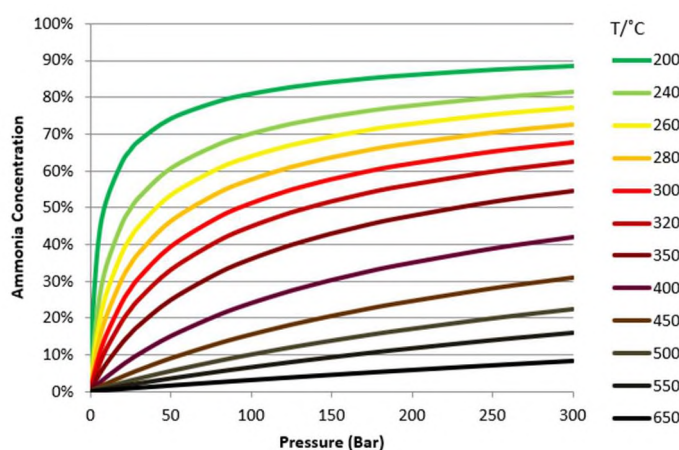


Figure 6.7 Equilibrium Ammonia Concentration As A Function Of Temperature And Pressure

7. INTERMEDIATE TEMPERATURE ALKALINE ELECTROLYZER SYSTEM

Concurrent with SOEC work, a second electrolyzer system was proposed and tested as part of this work. Theoretical integration of this electrolyzer is discussed below. The motivation for this work was started from reading the effects of temperature on alkaline electrolysis activity [79]. In recent years, there has been a growing interest in high-temperature alkaline electrolysis systems. This work is one of several that independently has been working on that approach [80] [81].

This work shows that endothermic operation of alkaline electrolysis is possible in a temperature range of 200-300 °C. This correlates well with the optimal temperature of FT reactions. A high-temperature, pressurized alkaline electrolysis systems was designed, built, and tested. These operating temperatures open up a host of proven catalysts for olefin and other FT-synthesis products [82].

7.1. INTEGRATED ALKALINE AND FT SYSTEM ANALYSIS

Endothermic operation at 1.3-1.4V water electrolysis with significant current density is feasible. Operating at this voltage gives an endothermic load of 40 kJ/kg. Feeding that system to a FT results in a heat release of 100 kJ/kg. In order to closely thermally couple the two units, a small reaction space is proposed to reside in the bipolar plate of the high-temperature alkaline electrolyzer. The design is physically similar to a micro-channel heat exchanger. The operations performed are functionally equivalent to a micro-channel heat exchanger, a micro-channel reactor, and an alkaline electrolyzer all in one package. Based upon a current density of (0.5 A/cm²) and a GHSV of 6000/hr, then

the appropriate thickness of this internal reactor is 4mm. This is only nominally different than a typical bipolar plate by a factor of 2.

7.2. EXPERIMENT

The intermediate temperature alkaline electrolysis system was operated at the vapor pressure of the system. At a series of different temperatures, various current sweeps were performed, as well as EIS measurements. These measurements characterize the cell as operating in line with expectations from the reviewed literature. In comparison with traditional alkaline, PEM, and SOEC, the system behaves with a comparable current to SOEC despite operating at a much lower temperature. A peak current of 256 mA/cm^2 at 1.4 V is excellent electrochemical performance for water splitting Figure 7.1.

Under these conditions the cell is 100% energy efficient. The only losses to the system were from heat losses through the insulation. As this was a proof-of-concept device, no effort was made to quantify heat losses to the surroundings. This level of efficiency is a significant achievement for water electrolysis. The electrochemical characterization of the system shows a consistent improvement based on increasing temperature. The Nyquist plot shows the very low ohmic and polarization losses for the system (Figure 7.2). At 246 °C the ASR is approximately 0.92 ohm-cm^2 .

The challenges associated with the technology are the complicated pressurized separation of the produced gases from the electrolyte. This requires a large volume of pressurized hot electrolyte, or a recuperating electrolyte cooler to recover the heat while cooling the electrolyte to a much less aggressive temperature. Very few materials have

long stable lifetimes at the operating conditions of the cell. Teflon and PEEK coatings are expected to be needed on most of the high temperature wetted parts.

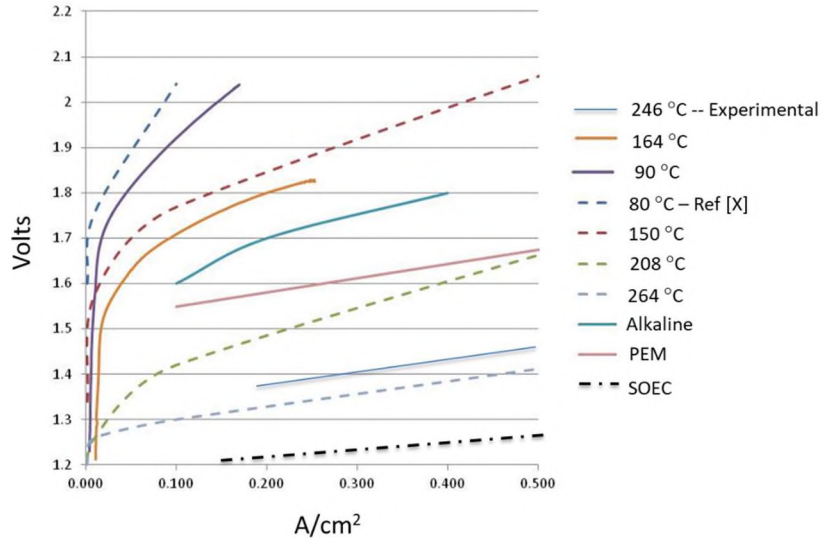


Figure 7.1 I-V Curves Of High Temperature Alkaline Electrolysis Compared With Previous Literature Experiments And Traditional Technologies [83]

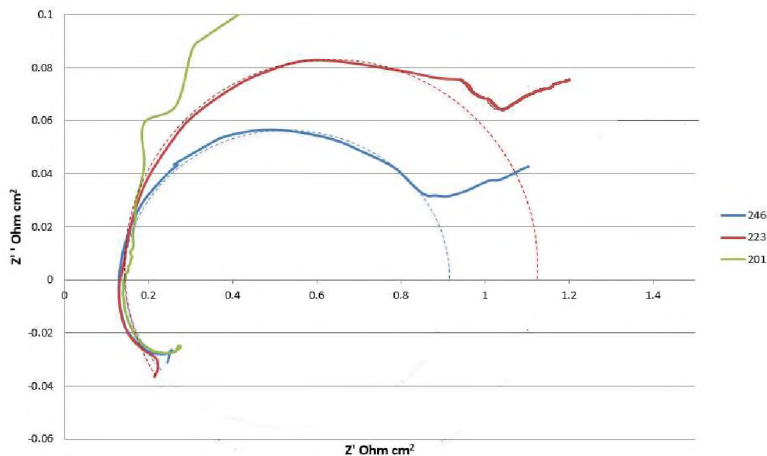


Figure 7.2 Nyquist Plot Of High Temperature Alkaline Electrolyzer

7.3. ECONOMICS

The initial estimates of the economics for the intermediate temperature alkaline electrolysis route to fuels are nearly identical to the standard route of SOEC followed by FT. The operating energy requirement and the reactor conditions are all nearly the same. The only significant difference is the lack of energy required for steam production. Also, due the immaturity of the technology, no thorough analysis or estimate of full-scale production system costs is available. An estimated cost of being similar to full-scale alkaline or SOEC is a reasonable starting point, but the uncertainty in the final cost of the system is still a large variable. Due to these difficulties in estimating the system cost, a preliminary estimate based-off of the separate unit SOEC and FT economic analysis will be made in the results of the economic evaluation section.

8. INTEGRATED FUEL SYNTHESIS AND SOLID OXIDE ELECTROLYSIS

8.1. METHODS

The system uses commercially available parts where possible. The test setup is designed for 1" nominal diameter circular button cells. The test furnaces are temperature controlled. The gas flows were measured by calibrated rotameters. Steam was added via a temperature-controlled humidifier. Gas samples are taken via aluminized mylar sample bags. The gas composition is analyzed via an Inficon micro GC or a Bruker FID system. Electrochemical measurements were taken by a Gamry potentiostat and EIS machine. Long duration current and voltage holds were performed by an Arbin electrochemical measurement and charging system.

8.1.1. Catalyst Preparation. The olefin production catalyst was prepared by combining HZSM-5 with molybdenum oxide at 5% wt molybdenum oxide. The compound was then calcined at 500 °C for 5 hours. The calcined catalyst was then screen between 60 and 40 mesh screens. The catalyst was then loaded into the system and reaction bonded with the cell at 500 °C for 2 hours. The catalyst was activated by flowing syngas over the cell at 650 °C for 12 hours. This is done in order to form the Mo₂C phase that is the active site for the reaction. After 12 hours, the system was put under a 50/50 mix of CO₂ and H₂. This purge condition was continued for 1 hour. The images of fresh catalyst compared to used catalyst clearly show the change of chemical composition of the catalyst Figure 8.1. The degree to which the color change is a result of the formation of the Mo₂C or coking is unknown. Both carbon desposition and Mo₂C would give the observed grey coloring.



Figure 8.1 Fresh And Spent Mo HZSM5 Catalyst

8.1.2. Cell Description. The cells are a YSZ electrolyte supported cells with either the custom applied electrode or a nickel cermet electrode. The oxygen side of the system has a lanthanum cobalt ferrite electrode (LSCF) which has been shown to have long service life with low degradation for electrolysis mode. The electrolyte is ~150 micron thick. Both of the electrodes are ~30 microns thick. The electrodes are both 2 cm² in active area. The electrodes are square on a 1-inch round cell. The cobalt cell was fabricated using the same techniques as the standard nickel cell, with cobalt oxide replacing nickel oxide on a 1:1 basis. Given the similar density of cobalt to both metallic nickel and nickel oxide, direct substitution of nickel with cobalt provided a simple starting point for an initial cobalt-based cell. The ink was prepared using a 3-roll mill and then screen printed onto the electrolyte substrate.

8.2. TEST STAND

The cells were glass sealed to the top of a 12" long zirconia tube. Platinum mesh current collectors and leads were fixed from the test cell to cold connections for the

power supply and EIS equipment. A rubber stopper is connected to the tube outside of the hot zone. The stopper has two tubes, one for inlet and one for outlet flows. The experimental setup was modified for this work, and a valve was added to the test stand to change flow direction from a gas-sampling bag and a vent line is on the outlet side. The inlet side is connected to the bubbler and has a valve to connect to a sampling line Figure 8.2.

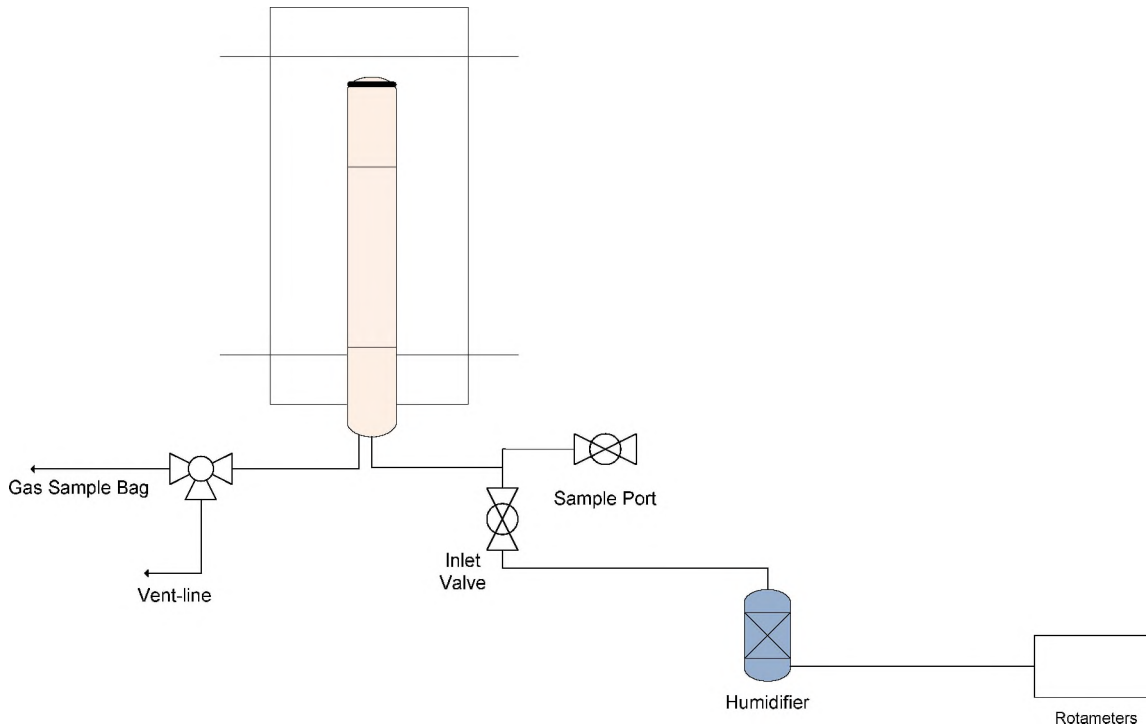


Figure 8.2 Test Stand Diagram for High Temperature FT-SOEC

8.2.1. Test Stand Operating Constraints. Given the fully oxidized incoming stream composed of water and carbon dioxide, the current necessary to fully electrolyze the stream can be found as a function of flow rate. This is calculated by taking the molar

Table 8.1 Current Needed For Full Reduction Of Incoming Steam And Carbon Dioxide Stream For A Given Gas Flow Rate

Flowrate (SCCM)	1	2	3	4	5	6	7	8	9	10
Current (A)	0.58	1.15	1.73	2.31	2.88	3.46	4.04	4.61	5.19	5.77

oxygen flow rate in the feed and the number of electrons needed to remove all of the incoming oxygen.

The results in Table 8.1 show that the current and flow rates needed are not compatible with the test stand capabilities. At higher temperatures, the current increases to a noticeable fraction of the needed current at low flow rates. However, even in this case, the current is not sufficient by itself to achieve sufficient electrochemical reduction of the incoming gases to the extent required by non-OCM and FT synthesis. These limitations on current and flow rates shifted the experimental design to having an already partially reduced incoming gas system instead of a totally oxidized inlet flow. This is achieved by having a lower inlet steam concentration, a higher incoming hydrogen fraction, and in the case of the high temperature reaction, methane in the feed is included as well. Based on the lower temperature Sabatier reaction steps and shifts, a high conversion to methane with high percent oxygen removal is a reasonable approximation of a higher current to flowrate ratio system. These experimental changes also correspond directly to a full system that would require a recycle stream to recover methane in order to improve the overall selectivity towards C₂+ hydrocarbons.

8.2.2. Sampling Method. Samples were taken both from the collected gas bag, and from the sample line on the inlet side. Samples were compared between the two sample points to see if a significant difference between the two sample locations was

observed. The sampling method was tested with known gas compositions and showed no detectable variation deviation between the two sample points. After this verification, samples for post-electrolysis reaction measurements were taken from the gas sample bag. Inlet samples were taken with flowing gas in order to validate the inlet composition to the reactor and an open valve to the feed line. The baseline samples sometimes included small amounts of nitrogen. Based on observations of sampling directly from a gas stream, the contaminating nitrogen appears to be from the sample draw and injection method. Samples concentrations reported are adjusted on the basis of the total non-nitrogen volume.

8.3. TEST PROCEDURE

The tests were carried out with the following three different types of cells: a baseline nickel cell, a screen printed cobalt-based cell, and the nickel cell with the addition of Mo/HZSM-5 catalyst loaded and bonded to the surface. All cells were mounted via a sealing glass to the tubes. Electrical connections were made with platinum mesh and wires. The cells were checked for leaks via a flammable gas detector. Leak checking at temperature was checked again via a static open circuit voltage (OCV) measurement for a non-flowing, closed volume tube. Cells that showed significant drop in OCV over the course of 5 minutes were cooled, re-examined, and re-sealed before further testing.

8.3.1. Baseline Nickel Cell. The tests were performed with a variation of CO₂/H₂O feed ratio. The steam content was controlled by adjusting the temperature of the humidifier. The during IV curve generation voltage was swept at a rate of 10 mV/s. EIS

showed the overall system performance. Nyquist plots were produced at a voltage of 1.1 V, and gas samples were taken at various intervals. The system was then allowed to run at steady state at 1.1 V for 12 hours. After which a new polarization plot and Nyquist plot were obtained.

8.3.2. Cobalt Electrolysis Cell. Tests were performed with the custom cobalt electrode which was then reduced under hydrogen for 30 minutes before running the system with the same parameters as the first test. Due to the low-overall current density, the cell was the run in sealed-batch mode for 12 hours.

8.3.3. Nickel Cell with Mo-HZSM5 Layer. Operation of the nickel cell at 650 °C with the Mo-HZSM5 catalyst was performed. The cell operated at a current of approximately 90 mA and was allowed to remain stable at that production rate for 1 hour before gas sampling. The inlet flows were 1 SCCM CO₂ and 1 SCCM H₂. These were measured by calibrated rotameters and confirmed with a water displacement method. This gas composition was flowed through a room temperature humidifier (30 °C). At higher temperature, the gas flows were raised to 30 SCCM and methane was introduced as the main component. The gas composition was 97% methane and the remainder CO₂ and H₂O to simulate high conversion. It was expected that methane reforming reactions would occur in order to provide the expected overall ratios of CO and H₂ as well.

8.4. RESULTS

The results from the experimental testing show consistent confirmation of the targeted production of C₂+ hydrocarbons. While the overall production rates are low and the total percentage of C₂ hydrocarbons is low, the measurement is consistent and well

within the sensitivity of the GC detection. For the low-temperature reactions, the possibility of another source contaminating the sample is very low.

8.4.1. Electrochemical Performance. The electrochemical performance of the cells at all temperatures were well within the normal expected values for electrolyte supported SOEC cells. While there was substantial variation between cells, it is within the typical variation for small scale button cell testing. The number of defects in processing and installation can cause this substantial variation. Most of the variation is typically due to the attaching of current collectors and leads and not from the cell itself. The overall variation in the area specific resistance (ASR) between the cells tested is fairly large but within previously observed variations of cell performance. The ASR varied between as low as 0.6 ohm cm^2 and as high as 1.2 ohm cm^2 .

8.4.1.1. Baseline nickel cell. The baseline nickel cell performed as expected. This validates the cell batch and method. When accounting for the difference in water electrolysis vs steam electrolysis, the cell operated at an electrical efficiency of 106% at a current density of 330mA/cm^2 . This represents the endothermic operating mode (Figure 8.3, Figure 8.4). The total system energy is supplied by the test stand heater and the heaters for the gas-humidification system. The overall system efficiency is not measured by the button cell testing equipment.

The overall ohmic resistance is slightly higher than is otherwise expected, but it within the variation observed in other cells produced.

8.4.1.2. Cobalt cell. The cobalt-based cell performed similarly to the nickel-based cells. At $800 \text{ }^\circ\text{C}$ the ASR was 0.95 ohm-cm^2 . The performance at $600 \text{ }^\circ\text{C}$ is shown from the Nyquist plot in Figure 8.5 Cobalt Cell Nyquist Plot At $600 \text{ }^\circ\text{C}$. There was a significant

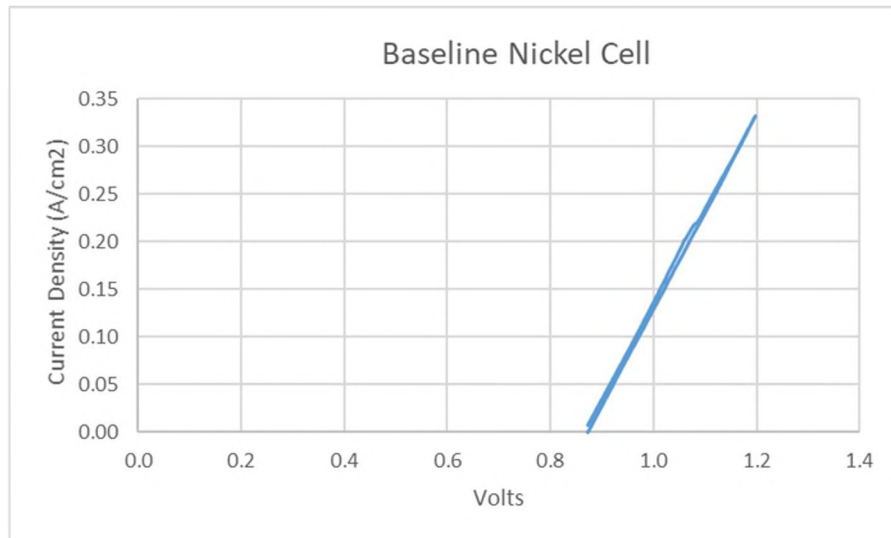


Figure 8.3 Baseline Nickel Cell IV Curve At A Temperature Of 800 °C

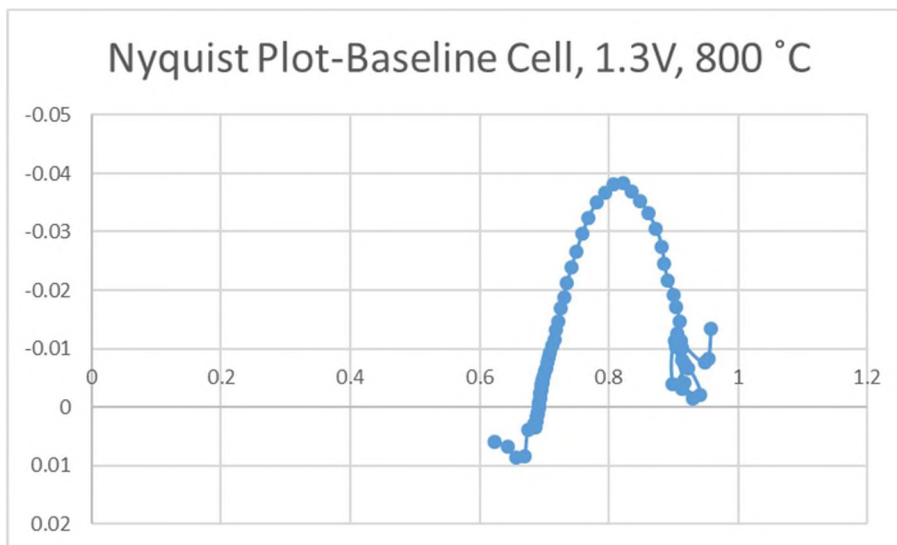


Figure 8.4 Baseline Nickel Cell Nyquist Plot At 800 °C

decrease in total current over the course of the cell testing. The initial cell current was 80 mA. This degraded to 19 mA over the course of 12 hours. After the completion of testing, heavy coking was observed on this cell. This is the most likely cause of the significant degradation of the cell.

8.4.2. Nickel Cell With Mo-HZSM5 Layer. The serial resistance of the cell is approximately 0.48 ohm-cm² (Figure 8.6 Figure 8.7). This correlates with the expected value of YSZ at 800 °C of .03 S/cm. This is a good indication that the leads were well attached to the cell and provided good electrical conductivity. The highly reducing conditions of the methane non-OCM shift operation may have positively changed the overall performance of the cell. Similar behavior was observed by Skafte et al. [59]. The decreased overall resistance of the cell is potentially attributed to the increasing mixed ionic/electronic conduction of the ceria-based fuel electrode.

The Nyquist plots show very typical electrochemical behavior for the cell. There is no noticeable difference between operation under these conditions and operation under typical steam electrolysis conditions. An ohmic resistance of 0.5 ohm-cm² and total resistance of 0.6 ohm-cm² is still within typical range of an electrolyte supported cell operating at 800 °C. However, since it is on the low end of the range, this another

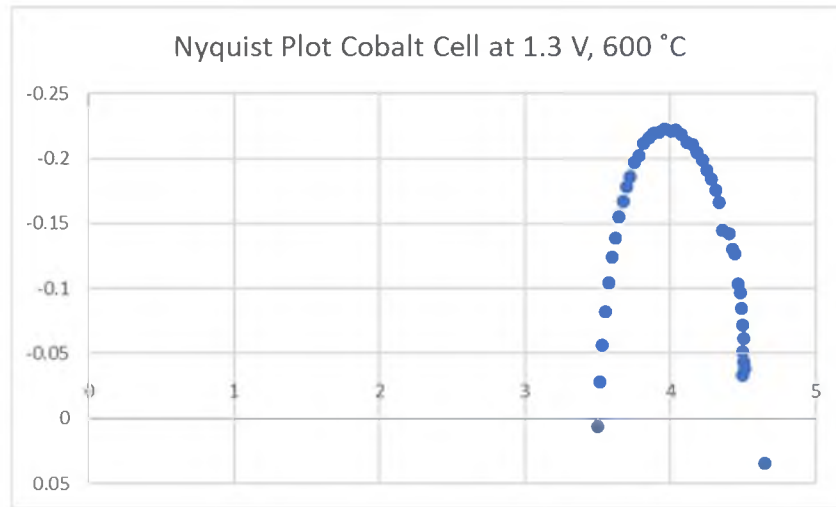


Figure 8.5 Cobalt Cell Nyquist Plot At 600 °C

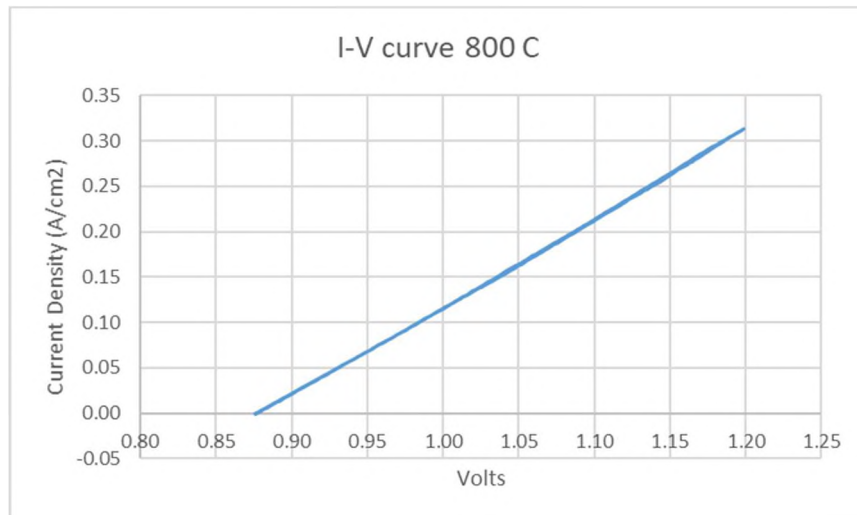


Figure 8.6 Voltage-Current Curve For Nickel Cell At 800 C

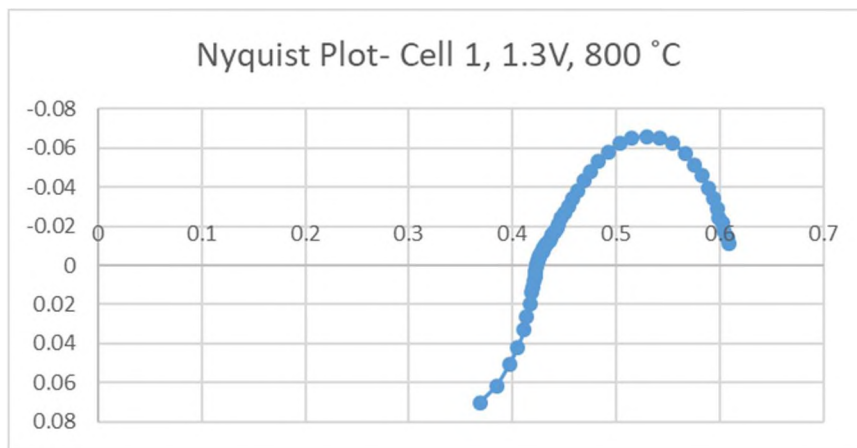


Figure 8.7 Nyquist Plots Of Cell At 800 °C

possible indication of the increased electrode activity due to the higher activation energy provided by change in ceria structure.

8.4.3. Chemical Products. The products of the system overall agree very strongly with the thermodynamics. The nickel and cobalt cells both coked at the low-temperature operating conditions in an attempt to produce methane. Some methane was detected but

for both the nickel and cobalt cells no detection of C₂ hydrocarbons to the detection limits of the system. The high temperature operation of the nickel cell with Mo-HZSM5 showed significant change in C₂ and the product was near the thermodynamic limits of the gas composition.

8.4.3.1. Cobalt cell products. The overnight products showed a small amount of methane. The overall composition on a dry basis is shown below in Table 8.2

Table 8.2 Cobalt Cell Products At 600 °C (Mole Percent)

	H ₂	CH ₄	CO	CO ₂
Measured	17.0	0.1	7.5	75.4
Theory	12.5	0.1	13.4	74.0

After failing to observe any products when operated under electrolysis conditions, syngas was fed to the cell at the same temperature. When operated with a syn-gas feed to simulate high electrochemical conversion of the incoming feed, the product distribution again came very close to the predicted equilibrium composition. The syngas composition is approximately 2:1 H₂:CO. The results of syngas feed to the cell can be seen in Table 8.3.

Table 8.3 Cobalt Cell with Syn-Gas Feed (Mole Percent)

	H ₂	CH ₄	CO	CO ₂	C ₂ H ₄	C ₂ H ₆
Measured	47.8	15.2	19.0	18.0	0.01	0.03
Theoretical	52.5	11.6	17.5	18.4	0.00	0.00

It is worth noting the trace amount of ethylene and ethane that is above the theoretical predictions for the composition. The very low production suggests that for this route to be successful as a FT-SOEC system, the electrochemical activity would have to improve significantly in order to have sufficient current to drive the reaction. Significant coking was also observed on the cell. This is the probable cause of cell electrochemical activity decreasing over the operating time.

8.4.3.2. Low temperature products. The results of these test conditions show that at low flow rate the composition is significantly different than equilibrium. A small amount of non-equilibrium ethane and ethylene are formed. A significant amount of excess hydrogen and unreacted CO₂ are also present. This validates the catalytic ability of the system to produce higher hydrocarbons even when the bulk composition is thermodynamically unfavorable. Some potential causes for the non-equilibrium composition are surface adsorption composition, diffusivity limitations to reaction sites, flow-bypassing the catalyst bed, and kinetic limitations.

The approximate total inlet gas flowrate of 2 SCCM meant that it took 15 minutes for a sample of sufficient volume to be available for GC injection. The system was allowed to run for 45 minutes between samples. The gas sampling bag was changed between samples. These lower flow rates and longer sample collection times increase the overall uncertainty in these measurements.

The nickel with Mo/HZSM5 cell was operated in constant voltage mode. A small change in the overall composition due to the relatively small change in current was observed. The total composition on a CHO basis is shown in Figure 8.8. It can be seen there is an overall trend of increasing total hydrogen content. The oxygen content

decreases proportionally to the hydrogen. There is also a small decrease in carbon in the exit composition. This suggests that carbon deposition was occurring and being shifted towards increasing carbon deposition under these conditions. The shift in composition validates the theoretical approach of using electrolysis for the removal of oxygen from the system through the electrolyte membrane to shift the equilibrium towards the target composition.

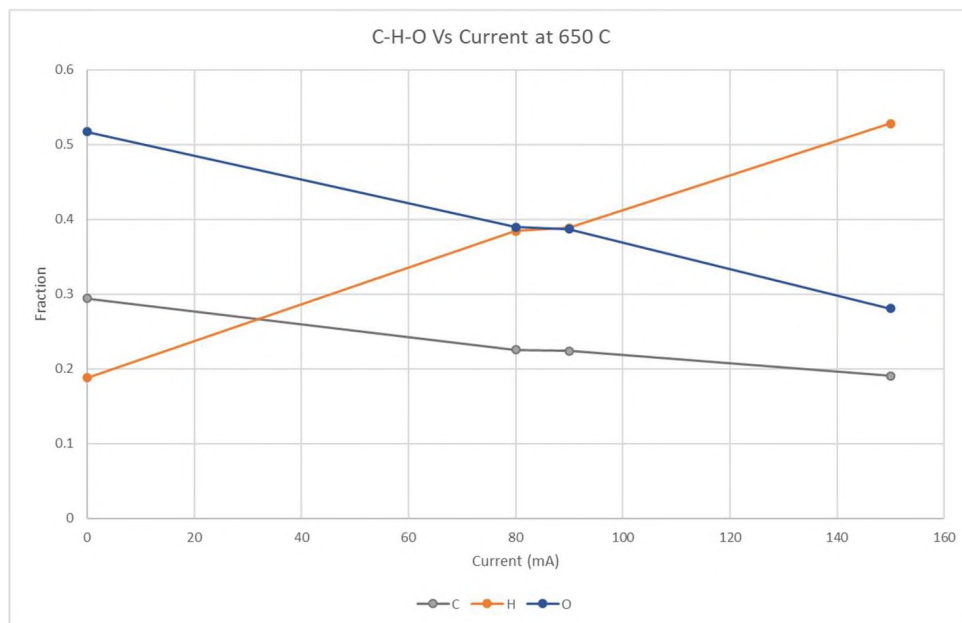


Figure 8.8 Ultimate Composition Of Outlet Vs Current

The chemical composition of the outlet vs current is shown in Figure 8.9 Mole Percent Of Products Vs Current. Again, hydrocarbon products increase, while oxygenated species decrease with increasing current. The presence of C_2 species is in line with the thermodynamic prediction. The presence of high CO_2 while simultaneous

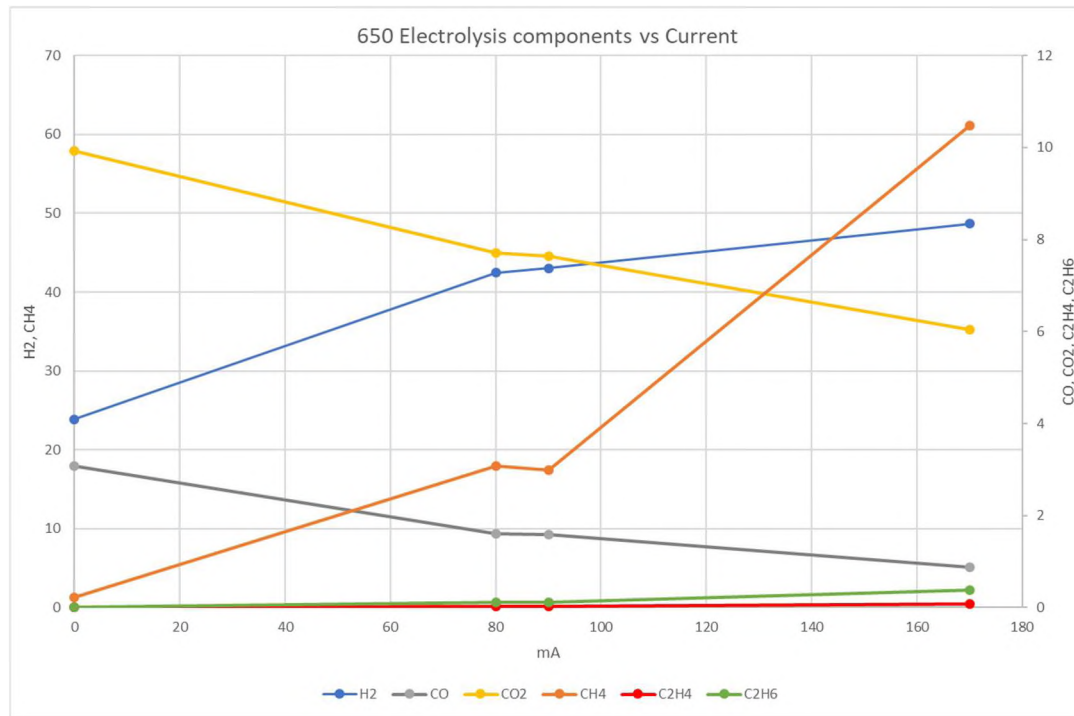


Figure 8.9 Mole Percent Of Products Vs Current

production of methane is unexpected under these conditions. A shift-reaction occurring during the exit stream cooling seems to be the most likely cause. The total amount of C₂ hydrocarbons is small, but indicates that the catalyst is active for the production of C₂ hydrocarbons.

These results give a high level of confidence that it is technically achievable under the right conditions to produce C₂ hydrocarbons directly in a SOEC system. The overall Faradaic efficiency towards C₂ products is very low. While this inhibits the economic viability of the process, it represents a similar overall current towards non-hydrogen products as the surveyed non-syngas, low-temperature CO₂ electroreduction reactors discussed in the introduction.

8.4.3.3. High temperature products. At 650 °C, the results from the nickel cell w/ Mo/HZSM5 show the potential for production of C₂ hydrocarbons in a SOEC cell. The higher current density of a cell at higher temperature is of interest in order to increase the potential for significant production rates. However, at 800 °C, methane is not a thermodynamic product at ambient pressure. The production of ethylene is only a relatively weak function of pressure, whereas methane formation is strongly favored by increasing pressure. The test is not capable of pressurized operation, and a pressurized operation with external heating and a hot wall vessel is not feasible at this stage of the work. Therefore, in order to simulate the effects of the electrolysis shift of equilibrium, methane was fed into the reactor to simulate the high-pressure conversion of the electrolysis products to methane. This high-methane inlet composition also approximates the incremental conversion over a cell at much higher total current to flow ratios, and the expected composition for a full-scale plant with separation and recycle. Observing the shift in the composition under these conditions, can provide an approximation of the intermediate conversion within the proposed integrated synfuel and SOEC system.

In Figure 8.11 the trend shows that electrolysis shifted the products further towards the olefin and higher hydrocarbon content. Using the Bruker 450 FID, no aromatic compounds were observed. The lack of benzene is uncommon for the product composition of Mo/HZSM5 catalyst. Based on the literature, the steaming of the zeolite may lead to the loss of acid sites via dealuminification. It has been shown that boron-based Mo/ZSM5 produces ethylene instead of benzene [84]. It is suggested that the high steam concentration reduced the acidity of the sites to the point that ethylene was the favored product of the reaction.

Given the thermodynamic composition of the overall products, it is probable that there is some ethylene in the reaction effluent is produced from the cracking of ethane to

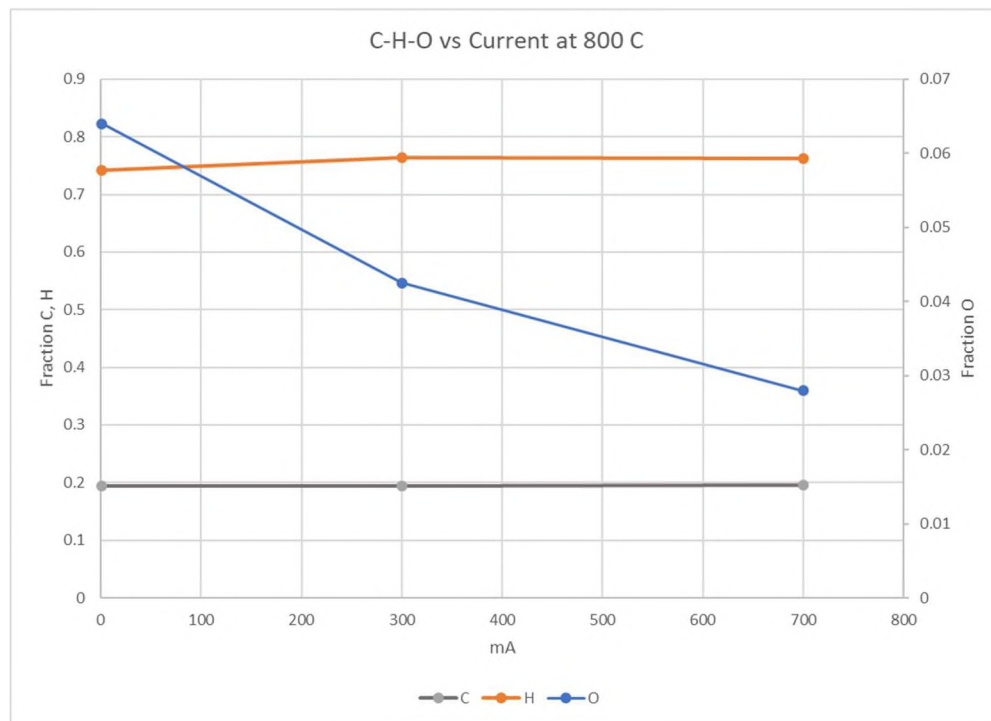


Figure 8.10 Ultimate Composition At Exit At 800 °C

ethylene and not from the coupling of methane. However, the natural gas feed used to produce the high methane concentration in the feed also had a lower total C₂ count than the reactor composition. The explanation for residual CO₂ and H₂O in the exit stream is uncertain. It can also be seen that there are some non-proportional shifts in outlet composition for several species. This may be due to the water-gas shift reaction being catalytically active during the exit of the reaction. Overall, the system does show consistent increasing removal of oxygen proportional to increasing current. Calculations done in HSC chemistry on the basis of the theoretical composition observed at high

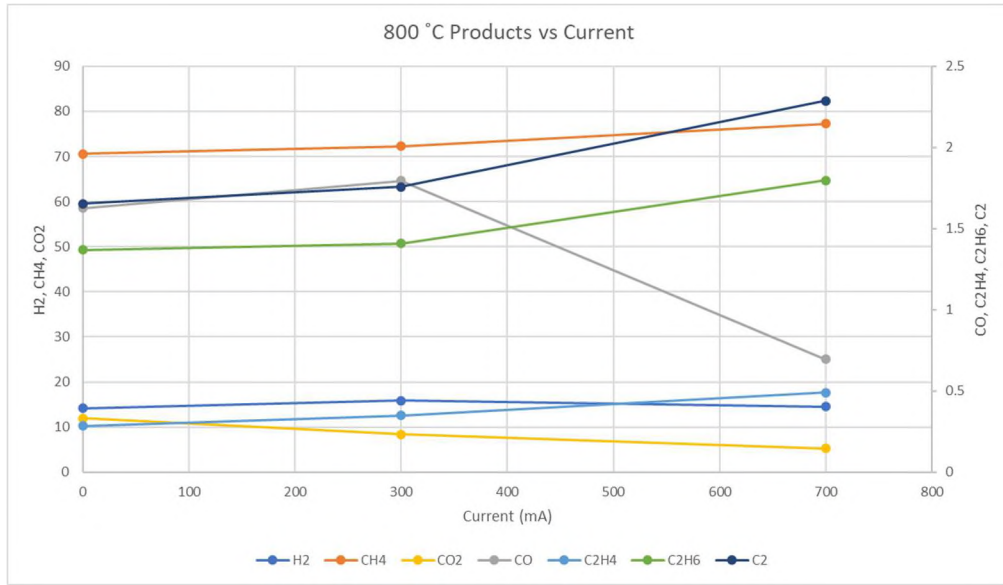


Figure 8.11 Mole Percent Composition At Exit At 800 °C. Minor Products C₂H₄, C₂H₆, CO Are Plotted On The Secondary Axis

temperature were shifted to lower temperatures. The most plausible explanation is the shift reactions were frozen at some point during the cool down of the product gas stream.

A consistent change in the composition of the products on a C-H-O basis indicates that the products are shifting based on the removal of oxygen Figure 8.10. The overall carbon content of the exit composition is constant. While carbon deposition may be occurring, the rate of carbon deposition is not affected by the amount of oxygen removal. The products show a slight change that is not in line with the changes in current and oxygen content. This indicates there may be substantial potential for variability in the catalyst products due to time on stream and slight variations in feed and outlet composition.

The overall trend is towards increasing C₂ hydrocarbons in the exit composition. The total exit C₂ hydrocarbon concentrations are increasing with increasing current and

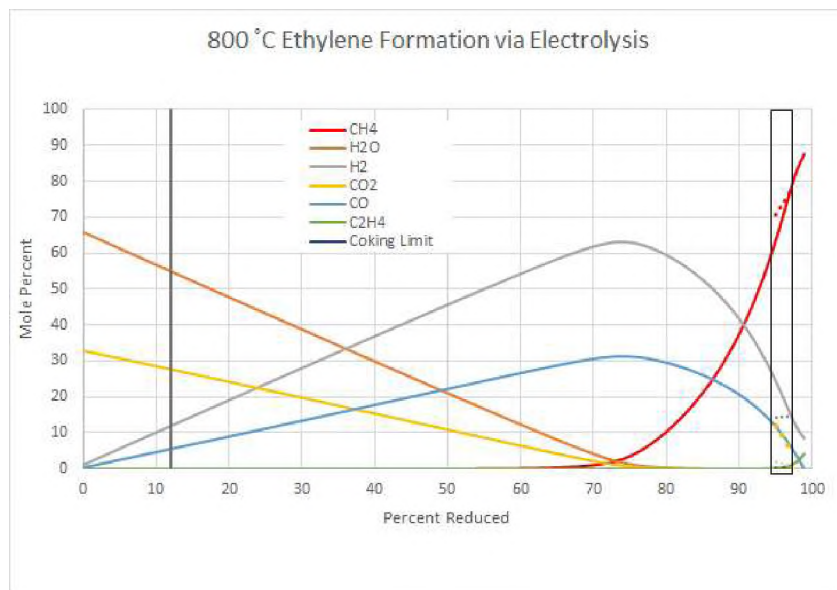


Figure 8.12 Products Compared To Theoretical. Experimental Results Are Dotted Lines Of The Same Color As The Theoretical Prediction

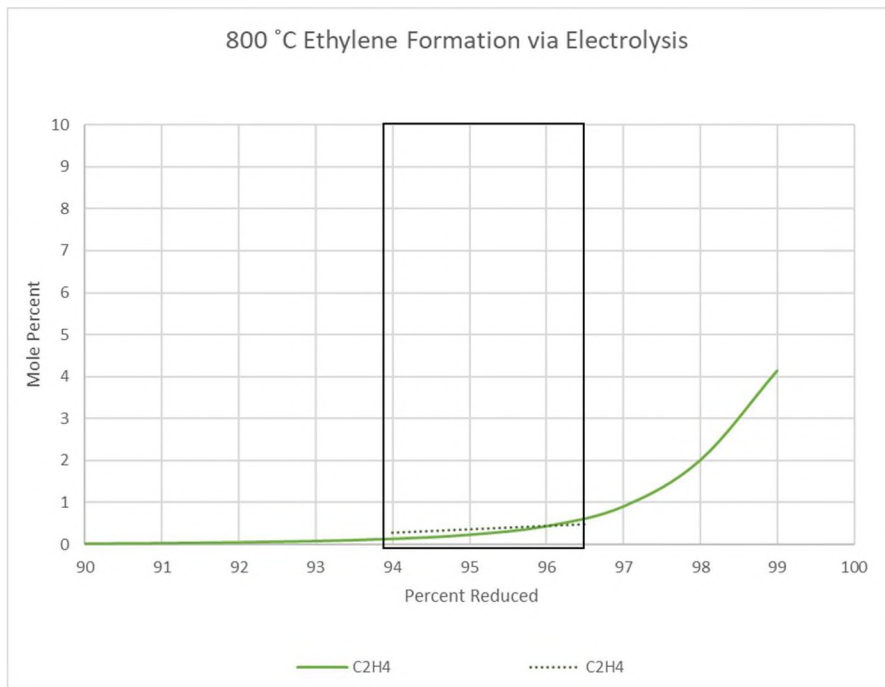


Figure 8.13 Ethylene Measurement Vs Theoretical

greater than the inlet C₂ hydrocarbon composition. The formation of ethylene could have been a potential ethane cracking reaction, but with the total exit C₂ count being greater than the total inlet C₂ precludes the possibility that all of the C₂ content was initially in the stream (Figure 8.12, Figure 8.13). However, if the outlet composition is viewed as having been quenched at a temperature between 400 and 500 °C, then the overall composition is once again in agreement with what would be theoretically expected. A somewhat higher than expected composition of CO₂ relative to CO was also observed in the work of Fujiwara et al. [36]. This adds another set of data suggesting that a reaction shift is likely occurring as the products exit the system and that the reactions are quenched upon cooling.

8.4.4. Experimental Uncertainty. All results reported in this work are obtained using calibrated instruments and methods. These methods are intended to reduce the possibility of sample contamination affecting the result. Possibilities remain for flow conditions and reactions that could impact the interpretation of the results. There are no direct operational measurements to control for these types of sources of error. Separate effects testing of the catalysts, electrolysis, and measurement system are intended to reduce the possibilities of these types of effects being significant sources of error. With these considerations in mind, the duration of sampling needed in order to produce a sample of sufficient size to inject into the GC allows for a variation in catalyst and electrolysis performance. Drift in the performance of both the catalyst and electrolysis over time can introduce noise into the accuracy of the data. Electrical voltage and current measurements were taken at the beginning and end of the sample run. The timing of these measurements means that average current over a run may have a minor difference

compared with the initial run. For most runs with significant interest, the current remained close to constant over the duration of a sample. Catalyst time on stream would also affect the results, as the duration needed for most sample collections was greater than 20 minutes.

9. ECONOMIC EVALUATION

An economic evaluation of the candidate system is presented based on the experimental results. The proposed system is also evaluated in context of the state-of-the-art production pathway. Further modifications are explored to examine their impact on the economic viability of the technology. These modifications provide direction and suggestions for future work.

The economic cases are the following: hydrogen from grid, grid-connected wind-only hydrogen, conventional syngas to FT, integrated non-OCM-SOEC for ethylene, integrated non-OCM-SOEC for benzene. The non-OCM-SOEC systems are based on an optimized full-scale system based off of the proof-of-concept work shown in the experimental section. The breakeven prices will be compared to market prices to determine the appropriate CO₂ costs needed to make the systems economically competitive.

The economic evaluation will use the default H2Analysis tool's SOEC Future case as the template for the economic analysis. The inputs will be altered based on the change in chemical output, as well as updated market electricity prices, and capital costs. The inputs that will be altered are electricity costs, capital costs, system availability, and energy required for a unit product. Explanations and justifications for these changes will be discussed and the cases evaluated.

9.1. INTEGRATED ELECTROLYSIS AND SYNTHESIS REACTOR COSTS

An estimate of the system costs is made by comparison to the typical FT and SOEC costs. The validity of the assumptions is reviewed both from engineering calculations and from literature review. Discussion of whether the system lifetime is substantially affected by the modified system is a major point of focus in validating the assumptions of the economic model.

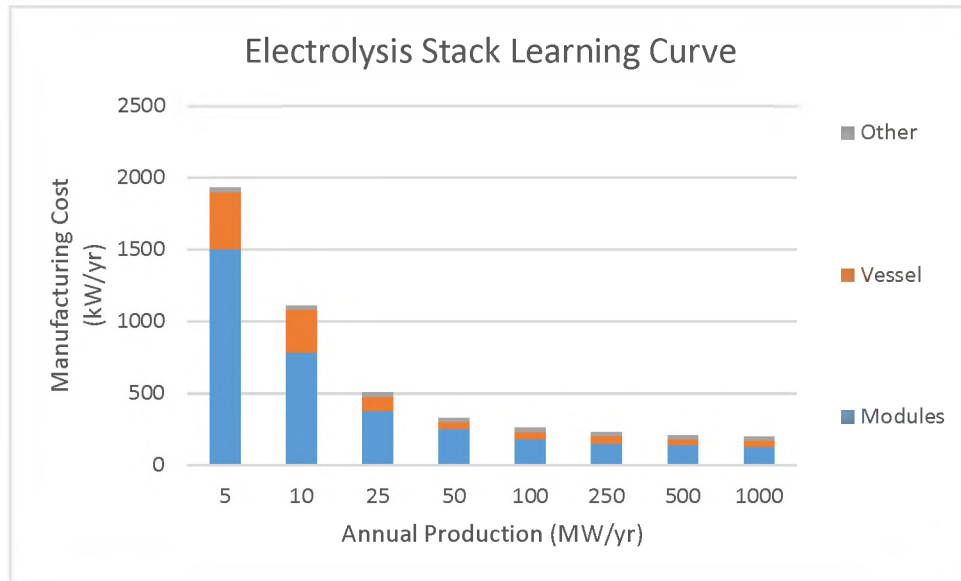


Figure 9.1 Electrolysis Stack Learning Curve Based On A Single Production Site

9.1.1. System Costs. For a preliminary estimate, typical SOFC production is similar to the procedure for producing the non-OCM-SOEC. The key parameter of determining economic viability will be production scale. At low scale production, the costs will be high. At large scale production, the costs will be much lower. Several reports show that production levels of 10 MW/year per facility are enough to lower SOFC costs down to \$500/kW [85] [86]. The cost of a similar electrolyzer is equivalent

to \$250/kW (Figure 9.1). The production of SOEC systems is very similar to SOFC systems on a technical basis. The electrolyte and electrode being produced in a similar manner as for a standard SOFC system, makes the prediction that producing this system have similar costs to SOFC valid. The key difference in this cost estimate is that the nominal power of an SOFC system is roughly half that of an equivalent area SOEC system. This is due to the power density of an electrolyzer being approximately double the power density of a fuel cell. This leads to an estimated cost of full-production SOEC being cost competitive with other electrolyzer technologies.

The main variation between SOEC subtypes is the composition and cost of the electrode layer, as well as the advanced techniques to produce a thinner electrolyte. Overall, it is expected that the initial cost of an electrode supported SOEC will be the same or less than an electrolyte supported SOEC.

9.1.2. System Lifetime. The lifetime of the system is a key metric in determining the economic value of the system. The main challenges with the new system are the catalyst lifetime, the thin electrolyte, and the operating voltage.

Much work has been done over the past decade to improve the reliability and lifetime of solid oxide electrolyte systems. SOFC lifetimes have improved from 7000 hours to 40000 hours. These improvements carry over to solid oxide electrolysis systems. The modeling has assumed a system lifetime of 40,000 hours. It is believed this is a reasonable target for a fully developed SOEC system, and the catalytic and electrolyte behavior of the system are similar enough for the non-OCM-SOEC that this is a reasonable expectation. [13]

9.1.3. Catalyst. The modeled synthesis catalyst lifetime is considered to be the useful life of the SOEC stack. The main method of deactivation at this temperature will likely be coking. In SOEC systems typical coking allows for steam or hydrogen regeneration of the catalyst. Catalyst coking with a constant steam feed should be reduced compared to other similar catalysts, such as oxidative coupling of methane. If the coking is severe, it is expected that the system can be regenerated to provide fresh catalyst activity. Changes to operating conditions to minimize the thermodynamic region of coking have already been examined. The next mechanism for catalyst deactivation is sintering. The catalyst however, will be operating at temperatures much higher than a typical olefin synthesis catalyst.

9.2. ELECTRICITY COSTS

The most impactful variables in the final cost of electrolysis-based hydrogen is electricity price and availability. The energy input cost of electricity under normal circumstances far exceeds the cost of any other input. Due to increasing availability of cheap green electricity, this factor is becoming less of a concern. Along with the increasingly low price, the increasing availability of non-dispatchable green energy increases the overall availability of clean electricity for hydrogen production. In analyzing ERCOT pricing data, estimates of the time-based carbon intensity of the grid will also be examined.

9.2.1. ERCOT Pricing Data. Wholesale electricity prices and generation data were obtained from the ERCOT website for the year 2018. These data provide the framework for analyzing the availability of cheap electricity for electrolyzer power

requirements. While the data from ERCOT is easily accessible, a review of other regions shows that similar costs are often available. For instance, a normal primary voltage user in most of XCEL energy territory can reach an effective price of \$35/MWh without participating in any demand response or other auxiliary service markets. This compares favorably with the \$40/MWh for the 96th percentile pricing for ERCOT (Figure 9.2).

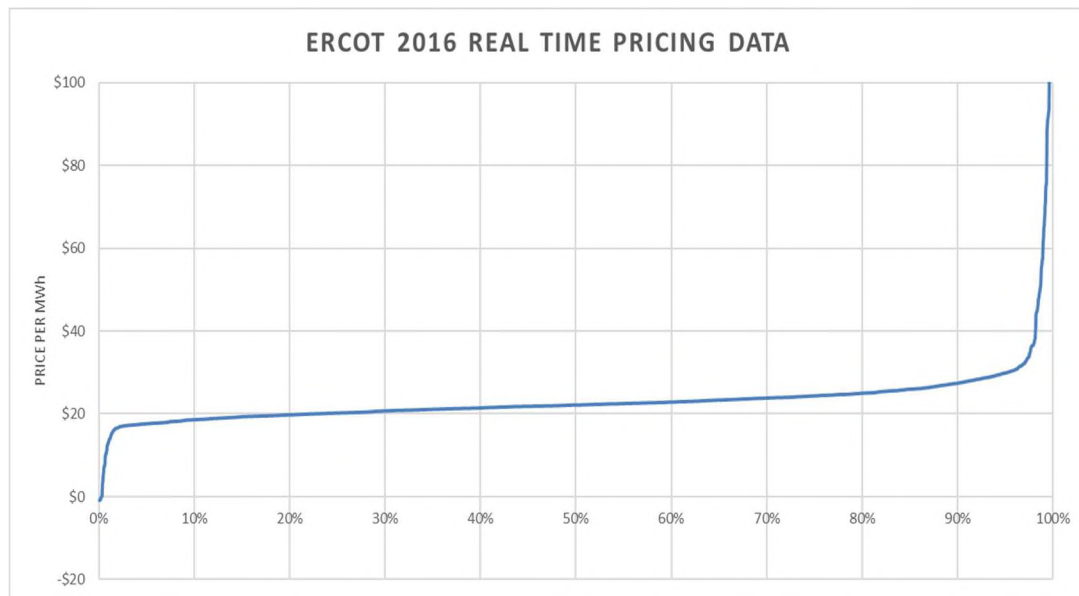


Figure 9.2 Real Time ERCOT Pricing Data Fraction Of Hours In A Year [63]

Using the ERCOT real time pricing data from 2018, it can be seen that the 50th percentile price is \$22.14/MWh, while the \$40/MWh price point is at the 96th percentile. Electricity at wholesale prices provides a large percentage of time that the system can operate economical if the electricity can be obtained at wholesale prices. The average price for the 96th percentile is \$20/MWh. That provides a reasonable input of \$20/MWh for the integrated synfuel SOEC system.

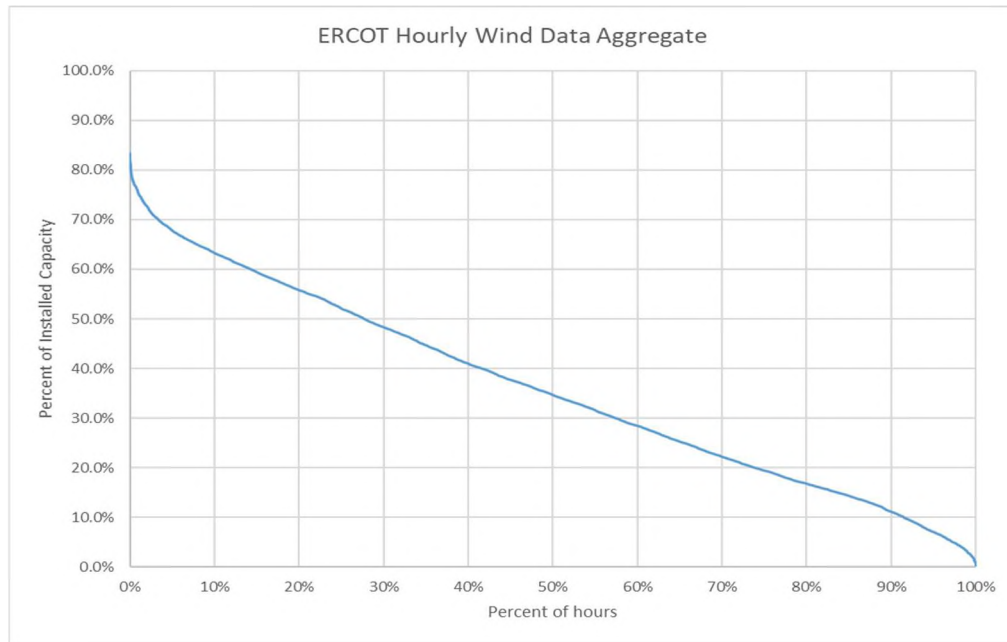


Figure 9.3 ERCOT 2018 Wind Production Capacity Factor As A Fraction Of The Year
[87]

If an electrolysis system is designed to run only on wind power, the fraction of the time that the system can run at a given power level is able to be determined by Figure 9.3. For example, a system running with an uptime of 50 percent of the year would be able to operate at a capacity of 30% of the nameplate capacity of the wind generation and average power up to 50% of the rated power of the wind turbines Figure 9.4.

The remainder of the power can be sold. This arrangement would require an electrolyzer system sized to meet the generation availability expected. A simple linear approximation of the system, allows for an electrolyzer to run 80% of the time with the electrolyzer to be rated at 18% of the installed wind turbine nameplate capacity.

The most important factor in determining the final sale cost for products of the SOEC system is the expected cost of electricity. The plot ERCOT grid data shows seen that the cost of wholesale electricity is very insensitive to the number of hours per year

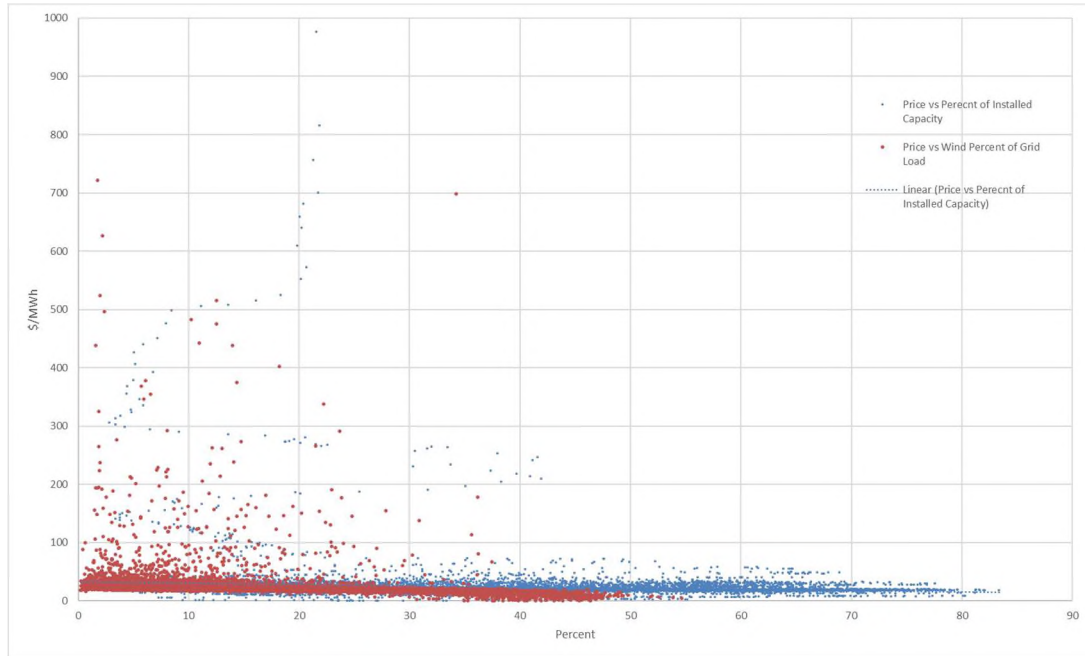


Figure 9.4 Wind Capacity Vs Pricing And Wind Percent Of Load Vs Pricing For ERCOT 2018

over a very wide range. The price only varies from \$17/MWh at the 3rd percentile to \$40/MWh at the 96th percentile. In the context of a grid-connected system, the assumption that the electricity price and integrated synfuel-SOEC capacity factor are uncoupled is a good assumption.

9.2.2. Hybrid Energy System Analysis. The impacts of the various uses and operating units on the electricity cost of the hybrid energy system are examined. In this approach to the hybrid energy system. The coal plant internally sells its CO₂ to the synfuel system at the cost of capture. This leaves the electricity products as market priced commodities, and each unit is independently optimizing its own production towards the higher bidder. The wind-farm, nuclear power plant, and the coal plant are all effectively using the SOEC system as a price floor mechanism.

9.2.2.1. Nuclear co-generation. Having a variable load is advantageous for nuclear power plants [88]. With increasing renewable generation market penetration, the load following capabilities of nuclear plants is often exceeded. With most of the cost of generating nuclear power being fixed costs, this makes operating a nuclear power plant increasingly uneconomical. Hydrogen production has been suggested as an alternative use to utilize nuclear power. The market availability provided by olefins and other chemicals provides a better option for a commodity product from the nuclear hybrid system.

9.2.2.2. Wind turbine. The case for a wind turbine to have a behind the meter connection to the SOEC, and the associated costs is discussed. In the case studies without grid connected emissions, a wind-turbine is assumed to produce a significant portion of the SOEC system's electrical needs. The modeling input for this is the capital cost of the wind turbines needed to provide the electricity for the SOEC system. The assumed capital cost for the wind turbines installed is \$1500/kW [89]. Any electricity production above the needs is sold as a byproduct. The SOEC can buy electricity at market price when the wind-turbine does not meet the SOEC production demands, or the SOEC can be curtailed. It is assumed in the model, that the SOEC will not purchase electricity over the price of \$40/MWh.

9.3. ECONOMIC CASES

The economic cases discussed are:

1. A baseline hydrogen-only production via SOEC
2. An SOEC system that feeds a FT reactor

3. Non-OCM-SOEC targeting ethylene
4. Non-OCM-SOEC targeting benzene

These cases and the differences between the individual case assumptions and the baseline discussion are examined. The results of each case are discussed and compared.

9.3.1. Hydrogen Production. Using the default inputs for grid-hydrogen production from SOEC, we can see that the electricity price sensitivity is by far the dominant factor in produced hydrogen pricing. The key factor driving the system is electricity price. Other key economic parameters are the price of electricity, system lifetime, and market prices.

The hydrogen production system should often accept reduced operating time for reduced system operating capacity factor. By modifying the electricity price to what can be seen as available in wholesale electricity markets, and including the potential for ancillary services provided by the system, the average electricity price for a grid-connected electrolyzer can be reduced even further Figure 9.5. By changing the system from a grid-connected system, to a wind-connected system, the operating expenses change from utility consumption, to increased CAPEX.

The capital investment for a wind-farm is modeled in the system costs. The model then compares wind production vs the max power of the system. By choosing to keep the electrolyzer powered, an opportunity cost for electricity production is incurred. By looking at the ERCOT wholesale market data, a behind-the-meter connection of an electrolyzer system to a wind-farm can provide a very low opportunity cost compared to the production of hydrogen. This configuration can give an effective electricity cost of \$20/MWh and very high availability.

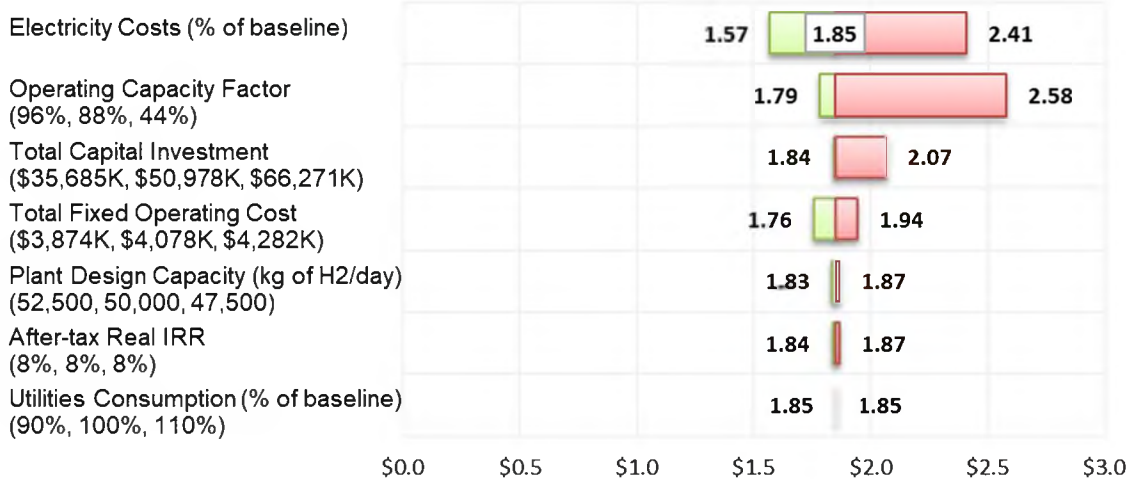


Figure 9.5 ERCOT Wholesale Grid Priced Electricity To Hydrogen

9.3.2. Fischer-Tropsch and Solid Oxide. By examining the traditional system with discrete operating units, a baseline is established for comparison with FT-SOEC. By increasing the capital cost for the system with the cost of a FT reactor and changing the required energy input to the system, the baseline case is modified for the sale price of traditional FT pathways.

The reactor price used is \$15,000/bpd of plant capacity. Much of the typical \$80,000/bpd of plant capacity is due to the steam methane reforming for syngas production and the related syngas clean-up. This system replaces those components with an SOEC system and primarily needs just the FT reactor and a few other supporting pieces of equipment. The traditional FT reactor route uses the wind case for electricity sourcing, and an input CO₂ cost of \$40/ton. The energy input per unit mass is modeled on C₁₀ alkane for the basis. This results in an approximate cost in \$/ton of ethylene. Additional processing steps for the system are necessary in order to have a fully saleable

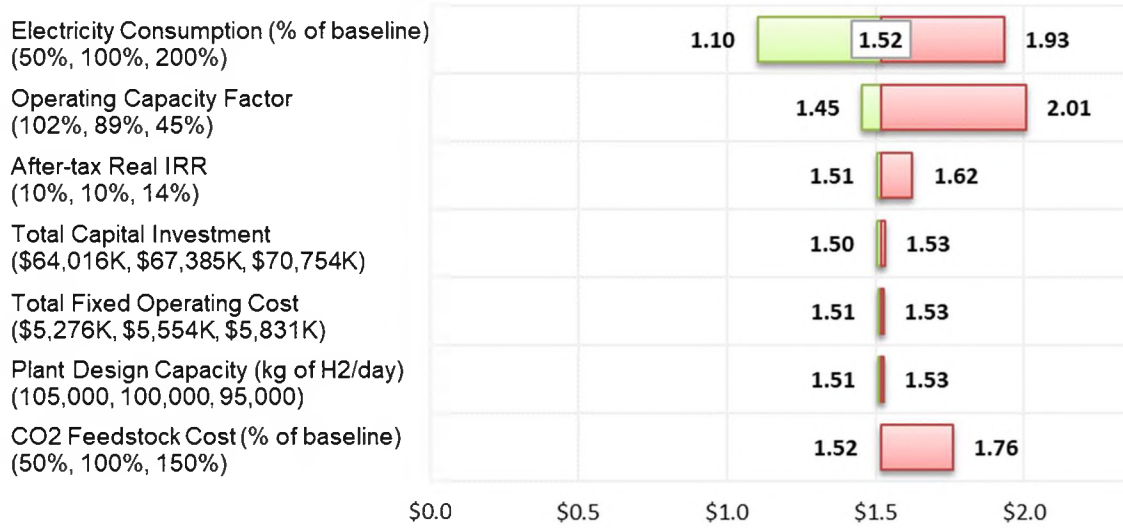


Figure 9.6 Fischer-Tropsch And SOEC Cost For Olefin Production

product, but the remainder of the costs are minor compared to the expected variation within the analysis (Figure 9.6).

After the initial analysis, due to the broad uncertainties of the alkaline system inputs, the FT and intermediate alkaline case is functionally identical to the FT-SOEC case. The resulting cost per ton for both cases is \$1520/ton olefin. The lower selectivity of the FT catalyst results in more separations and products. The average sale price averaged over the products is the result produced.

9.3.3. Non-OCM-SOEC Ethylene. This section evaluates the economic potential of a non-OCM-SOEC system based on the preliminary experimental data Figure 9.7. Following the same procedure as the combined FT-SOEC case, various changes to the inputs to the H2Analysis case of Future SOEC production were made. The modified case uses the reduced electricity input required for the non-OCM-SOEC, the reduced electricity prices from a wind-farm, and a modified SOEC capital cost. The increased

SOEC capital costs reflect the additional complexities associated with the production of a non-OCM-SOEC system. Additionally, the SOEC system lifetime is also reduced to reflect the consequences of the more extreme conditions of the system. The final modifications to the system are preliminary estimate for a separation loop and a thermal energy cost to drive that separation system. This system, like the traditional FT system, uses a CO₂ cost of \$40/ton for the carbon input.

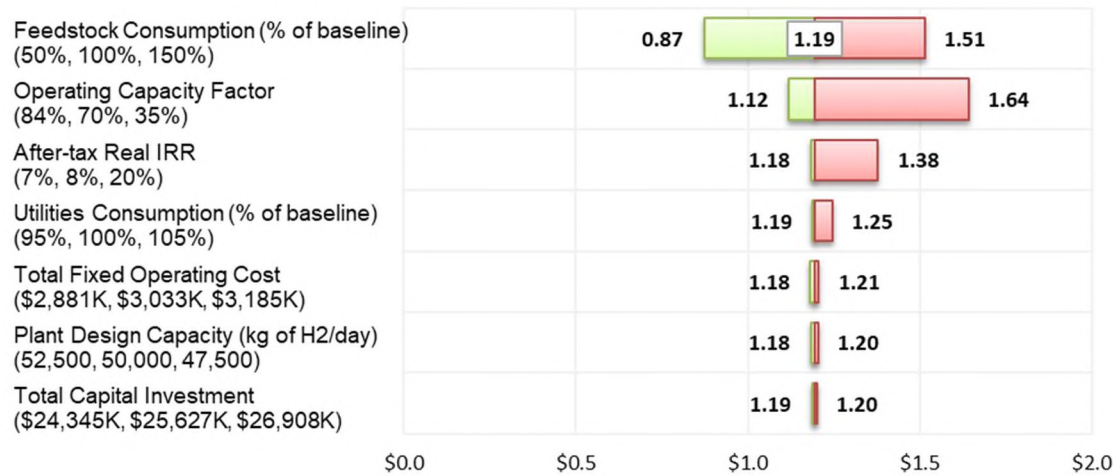


Figure 9.7 Tornado Chart For FT-SOEC Production Of Ethylene (\$/Kg)

Due to the relative complexity of the separations for ethylene production compared to the other cases, further examination and comparison with other economic evaluations in literature are discussed. By comparing the cost of a non-oxidative coupling of methane system with the cost of in stack high methane production replacing market natural gas, an approximate cost of the system can be compared to the modified H2Analysis tools result.

A significant discussion of the economics of direct non-oxidative coupling of methane by Huang et al. gives a breakeven price for ethylene at \$1,227/MT [90]. The

basis for the result includes a methane feedstock cost of \$2.85/Mcf of natural gas [91].

By rescaling the rest of the capital costs and non-natural gas costs of the system, a capital cost and operating cost for the modified H2Analysis can be used. With these changes to the H2Analysis tool inputs, the breakeven ethylene pricing moves from \$1190/MT to \$1410/MT. This is \$100/ton less than the baseline separate FT and SOEC pathway.

9.3.4. Non-OCM-SOEC Benzene. The last economic case to be evaluated is the FT-SOEC with a target product of benzene. The overall conversion of the system to benzene is more favorable thermodynamically. The separation of the methane and benzene for the recycle stream is also much simpler. This reduces the operating energy requirement and capital costs for the separation compared to the FT-SOEC ethylene case. Other than these changes, and the appropriate changes to the energy input per unit mass, the inputs are the same as the FT-SOEC Ethylene case Figure 9.8. The changes overall per pass conversion and easier separation result in a benzene price of \$1100/MT.

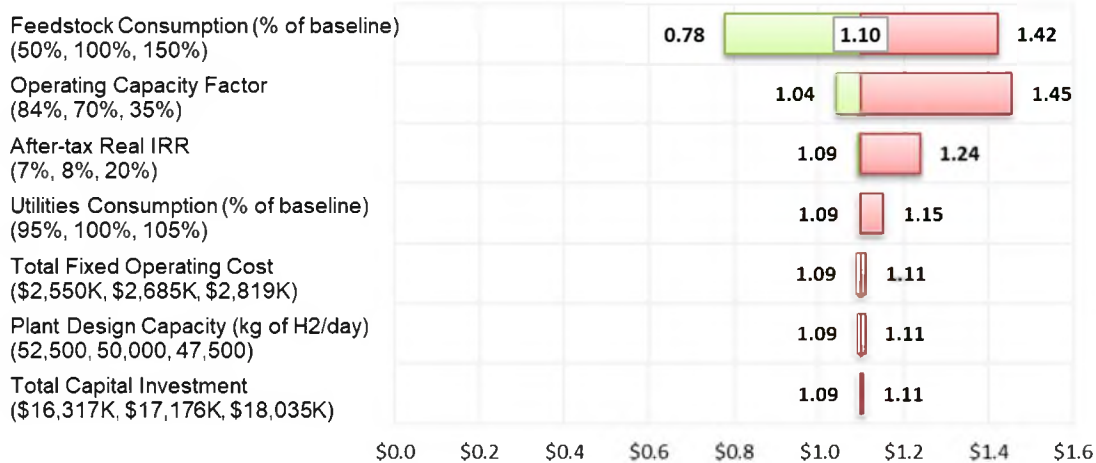


Figure 9.8 Tornado Chart For FT-SOEC Production Of Benzene (\$/kg)

9.4. CARBON PRICING

The breakeven CO₂ is calculated based on the results of the individual breakeven prices. The baseline CO₂ emissions for the products are shown in Table 9.1.

Table 9.1 Carbon Emissions of Studied Chemicals By Pathway [92]

Kg of CO ₂ /Kg of Product		Chemical		
		H ₂	C ₂ H ₄	C ₆ H ₆
Source	Fossil Fuel	9-14	1.4	2.4
	Grid	12.6	7.1	2.6
	Low-Carbon	0.3	0.2	0.1

For the grid connected cases, carbon emissions are expected to be approximately 300g CO₂/kWh for ERCOT in 2020. With that carbon intensity, grid-electrolysis produced hydrogen will have approximately 12.6 kg CO₂/kg H₂ of carbon emissions. This corresponds to the mid to high emissions range for steam methane reforming.

Changing the product output to olefins reduces the carbon output to 7.1 kg CO₂/kg C₂H₄. In contrast, making polyolefins from primary oil results in emissions of 1.4kg CO₂/kg C₂H₄. It can be seen that with the current carbon intensity of the ERCOT grid, that the electrolysis-based system is higher carbon than the fossil-based alternatives. For benzene the result is much closer. The grid-based electrolysis route is 2.6 kg CO₂/kg benzene.

The alternative to a grid-connected case would be to simply build wind turbines to directly feed the electrolyzer, and sell the excess to the grid or store it. Further analysis of

a wind driven case is evaluated here. This represents a better case to attempt to quantify the economic benefit of the hybrid system for chemical production with environmental externalities included. The grid-connected case would face additional costs with the carbon pricing added to the production costs. Because the carbon emissions are higher with grid connected carbon, we calculated what the breakeven grid-carbon intensity would be to have equivalent carbon emissions from the fossil-fuel based process and the SOEC pathway.

9.5. ECONOMIC SUMMARY

The results of the carbon intensity and economic costs are combined to produce a breakeven cost of carbon. Since the grid-connected cases are higher carbon than the fossil-fuel-based alternatives, they are not included in this section. A wind turbine connected system is used along with the current and historical market prices. The results of this analysis is shown in Table 9.2.

Table 9.2 Chemical Costs Via Different Pathways. Breakeven CO₂ Costs In Current And Historical Markets

\$/ton	Chemical	H ₂	C ₂ H ₄	C ₆ H ₆
	Clean Route	\$ 1,340	\$ 1,410	\$ 1,100
	Current Market	\$ 1,000	\$ 330	\$ 500
	CO₂ Price	\$ 27	\$ 923	\$ 259
	Historical Market		\$ 1,000	\$ 1,000
	CO₂ Price		\$ 350	\$ 43

In terms of carbon abatement costs, all pathways other than hydrogen production are significantly higher than typical carbon prices. Historical prices of these chemicals present a better case. With the historical pricing, benzene may be a target chemical of interest for a low-carbon pathway.

9.6. SCALING AND APPLICABILITY

After examining the results and the theoretical thermodynamic limits of the system, while there is a small technically achievable amount of direct olefin production, the present economic argument for such a system is poor. While the production of hydrocarbons has merit, economically the profitability of such a system depends on relatively high oil prices. Given recent market trends and instability, the decision to construct a plant with a 20-year lifetime is a high-risk proposition. At this time, an integrated fuel synthesis reactor and solid oxide electrolyzer is to be unable to compete with a traditional coupled electrolysis and FT reactor in separate operational units. The thermodynamic and kinetic limitations of the systems would require a breakthrough in catalyst, solid oxide electrolyzer operating temperature, or both.

10. CONCLUSIONS

10.1. DISSERTATION SUMMARY

Research into the integrated production of C₂ hydrocarbons within a single combined SOEC and synthesis unit has been performed. The experimental results support the conclusion that production of C₂ hydrocarbons are achievable in a highly reduced gas stream. The C₂ products are produced at near the thermodynamic limit. System stability over 18 hours shows no signs of catastrophic failure or excessive degradation.

Economic evaluation of the proposed system suggests that like most synthetic fuel production systems, the economic viability is highly dependent on market conditions. The fluctuations of the petrochemical market can change the economics from highly valuable to extremely poor. In order for the system to be justifiable, CO₂ emissions costs need to be between \$43-\$923/ton in order to be competitive with fossil fuel-based sources. The wide range is dependent on market price volatility, and whether the target chemical is benzene or ethylene. Ethylene has breakeven carbon cost range of \$350-\$923/ton CO₂, while benzene has a range of \$43-259/ton CO₂. By comparison, low-carbon hydrogen can be cost competitive with fossil-based hydrogen for as little as \$27/ton carbon.

Intermediate temperature alkaline electrolysis has also been demonstrated. The technical demonstration of the ability to operate electrolysis endothermically at or below traditional FT temperatures provides a case for thermal integration of the two systems. The relative immaturity of intermediate temperature alkaline electrolysis make full

economic comparison difficult. The preliminary economic comparison is favorable with the other baseline technologies.

10.2. RESEARCH CONTRIBUTIONS

A novel and new approach to integrated fuel and chemical synthesis in a solid oxide electrolysis unit is the prime contribution of this work. The production of C₂ via electrolysis at high temperatures on a SOEC has never been reported before. Use of catalysts and electrolytes at the limit of their reasonable operating conditions and combining them is new work. Specifically, the targeting of olefins via FT synthesis in-situ in the same unit as the SOEC is a new method developed by this work. The analysis of the thermodynamic operating space and economically profitable outputs are also unique and new contributions. Previous to this work, no analysis of endothermic low-temperature electrolysis coupled to Fischer Tropsch synthesis has been performed. The analysis of the integrated production of C₂ hydrocarbons in a combined single high temperature electrolysis and synthesis reactor has also never been performed previous to this work. Proof-of-concept testing of the reaction scheme has been confirmed experimentally. Further examination of potential for improved catalysts and electrolyte behavior for the system are also significant contributions. The combination of a catalyst and operational conditions in a single unit was one of the main objectives of this work.

10.3. LIMITATIONS

The experimental work is preliminary work done with the intent of being proof-of-concept. Further work can be used to establish long-term performance and degradation.

10.4. FUTURE WORK

Further work would focus primarily on an increased area cell, and pressurized operating conditions. This would allow for further shifting of the oxygen content in a single pass. These improvements would enable the examination of anti-coking materials and additives in order to shift the equilibrium yield from a syngas formation and mechanism to a surface hydrogenation mechanism. Additional optimization of catalyst performance, electrolyte, operating conditions, and process separations would be necessary to produce an economical device and system.

APPENDIX

1. INSTRUMENTATION

1.1. POTENTIOSTAT/ELECTROCHEMICAL IMPEDANCE SPECTROSCOPY

Gamry Reference 3000 Model

1.2. GAS CHOMATOGRAPH

Inficon 3000:

Channel A: Molecular Sieve, Argon.

Channel B: Molecular Sieve, Helium.

Channel C: Plot U, Helium.

Channel D: OV-1, Helium, not used.

Bruker:

Scion 456-GC

CP-Al₂O₃/KCL 50m, 0.32 MM ID, 5um df.



Figure A.1 Equipment Test Stand

BIBLIOGRAPHY

- [1] K. Buchheit, "Process design, dynamics, and techno-economic analysis of a sustainable coal, wind, and small modular nuclearreactor hybrid energy system," *Doctoral Dissertations*, vol. 2439, 2015.
- [2] K. Buchheit and J. Smith, "Production Possibilities of a Sustainable Coal, Wind, and Small Modular Reactor Hybrid Energy System," *Energy & Fuels*, vol. 32, no. 10, pp. 10864-10878, 2018.
- [3] J. Smith, K. Buchheit, H. Zhang, H. Golpour, J. Hartvigsen and H. Al-Ruby, *Hybrid Energy Systems*, Taylor & Francis, 2016.
- [4] C. McMillan, R. Boardman, M. McKellar, P. Sabharwall, M. Ruth and S. Bragg-Sitton, "Generation and Use of Thermal Energy in the U.S. Industrial Sector and Opportunities to Reduce its Carbon Emissions," NREL, Golden, CO, 2016.
- [5] K. L. Buchheit, J. D. Smith, U. Guntupalli and C. Chen, "Techno-economic analysis of a sustainable coal, wind, and nuclear hybrid energy system," *Energy & Fuels*, vol. 30, no. 12, pp. 10721-10729, 2016.
- [6] Creative Commons License Wuppidu, DE, *Fuel Cell*, thenounproject.com.
- [7] S. Budinis, S. Krevor, N. Mac Dowell, N. Brandon and A. Hawkes, "An assessment of CCS costs, barriers and potential," *Energy Strategy Reviews*, vol. 22, pp. 61-81, 2018.
- [8] J. S. Herring, J. E. O'Brien, C. M. Stoots, G. L. Hawkes, J. J. Hartvigsen and M. Shahnam, "Progress in high-temperature electrolysis for hydrogen production using planar SOFC technology," *International Journal of Hydrogen Energy*, vol. 32, no. 4, pp. 440-450, 2007.
- [9] J. E. O'Brien, C. M. Stoots and J. J. Hartvigsen, "Performance of Planar High-Temperature Electrolysis Stacks for Hydrogen Production from Nuclear Energy," *Nuclear Technology*, vol. 158, 2007.
- [10] M. A. Laguna-Bercero, "Laguna-Bercero, M. A. (2012). Recent advances in high temperature electrolysis using solid oxide fuel cells: A review," *Journal of Power Sources*, vol. 203, pp. 4-16, 2012.
- [11] Y. Zheng, J. Wang, B. Yu, W. Zhang, J. Chen, J. Qiao and J. Zhang, "A review of high temperature co-electrolysis of H₂O and CO₂ to produce sustainable fuels using solid oxide electrolysis cells (SOECs): advancedmaterials and technology," *Chem Soc Rev*, vol. 46, p. 1427, 2017.

- [12] C. Graves, S. D. Ebbesen, . S. H. Jensen, . S. B. Simonsen and M. B. Mogensen, "Eliminating degradation in solid oxide electrochemical cells by reversible operation," *Nature Materials*, vol. 14, pp. 239-244, 2015.
- [13] Y. Tao, S. D. Ebbesen and M. B. Mogensen, "Degradation of solid oxide cells during co-electrolysis of steam and carbon dioxide at high current densities," *Journal of Power Sources*, vol. 328, pp. 452-462, 2016.
- [14] N. Minh, J. Mizusaki and S. C. Singhal, "Advances in Solid Oxide Fuel Cells: Review of Progress through Three Decades of the International Symposia on Solid Oxide Fuel Cells," *ECS Transactions*, vol. 78, no. 1, pp. 63-73, 2017.
- [15] J. E. O'Brien, M. G. McKellar, C. M. Stoops, J. S. Herring and G. L. Hawkes, "Parametric study of large-scale production of syngas via high-temperature co-electrolysis," *International Journal of Hydrogen Energy*, vol. 34, no. 9, pp. 4216-4226, 2009.
- [16] K. McSpadden, "Audi Just Invented Fuel Made From CO₂ and Water," Time, 28 April 2015. [Online]. Available: <https://time.com/3837814/audi-environmental-protection-green-energy-climate-change-cars/>. [Accessed 13 October 2020].
- [17] R. E. Barbara Fisher, "Electrocatalytic Reduction of Carbon Dioxide by Using macrocycles of nickel and cobalt," *J. Am. Chem. SO*, no. 102, pp. 7361-7362, 1980.
- [18] N. G. A. C. M. Gattrell, "A review of the aqueous electrochemical reduction of CO₂ to hydrocarbons at copper," *Journal of Electroanalytical Chemistry*, p. 1-19, (2006).
- [19] K. Malik, S. Singh, S. Basu and A. Verma, "Electrochemical reduction of CO₂ for synthesis of green fuel," *Wiley Interdisciplinary Reviews: Energy and Environment*, vol. 6, no. 4, 2017.
- [20] C. M. Stoops, J. E. O'Brien and J. J. Hartvigsen, "Results of recent high temperature coelectrolysis studies at the Idaho National Laboratory," *International Journal of Hydrogen Energy*, vol. 34, no. 9, pp. 4208-4215, 2009.
- [21] C. M. Stoops, J. E. O'Brien, K. G. Condie and J. J. Hartvigsen, "High-temperature electrolysis for large-scale hydrogen production from nuclear energy – Experimental investigations," *International Journal of Hydrogen Energy*, vol. 35, no. 10, pp. 4861-4870, 2010.
- [22] D. T. W. a. P. J. A. Kenis, "Prospects of CO₂ Utilization via Direct Heterogeneous Electrochemical Reduction," *The Journal of Physical Chemistry Letters*, vol. 1, no. 24, pp. 3451-3458, 2010.
- [23] M. R. a. J.-M. S. Cyrille Costentin, "Catalysis of the electrochemical reduction of carbon," *Chem Soc Rev*, vol. 42, p. 2423, 2013.

- [24] Y. Fang and J. C. Flake, "Electrochemical Reduction of CO₂ at Functionalized Au Electrodes," *Journal of the American Chemical Society*, vol. 139, no. 9, pp. 3399-3405, 2017.
- [25] C. S. Chen, A. D. Handoko, J. H. Wan, L. Ma, D. Ren and B. S. Yeo, "Stable and selective electrochemical reduction of carbon dioxide to ethylene on copper mesocrystals," *Catalysis Science & Technology*, vol. 5, no. 1, pp. 161-168, 2015.
- [26] F. S. Roberts, F. P. Kuhl and A. Nilsson, "High Selectivity for Ethylene from Carbon Dioxide Reduction over Copper Nanocube Electrocatalysts," *Angewandte Chemie*, vol. 127, no. 17, pp. 5268-5271, 2015.
- [27] F. Zhou, S. Liu, B. Yang, P. Wang, A. S. Alshammary and Y. Deng, "Highly selective *electrocatalytic* reduction of carbon dioxide to carbon monoxide on silver electrode with aqueous ionic liquids," *Electrochemistry Communications*, vol. 46, pp. 103-106, 2014.
- [28] J. L. DiMeglio and J. Rosenthal, "Selective Conversion of CO₂ to CO with High Efficiency Using an Inexpensive Bismuth-Based Electrocatalyst," *Journal of the American Chemical Society*, vol. 135, no. 24, pp. 8798-8801, 2013.
- [29] M. R. Gonçalves, A. Gomes, J. Condeço, R. Fernandes, T. Pardal, C. A. C. Sequeira and J. B. Branco, "elective electrochemical conversion of CO₂ to C₂ hydrocarbons," *Energy Conversion and Management*, vol. 51, no. 1, pp. 30-32, 2010.
- [30] J. Qu, X. Zhang, Y. Wang and C. Xie, "Electrochemical reduction of CO₂ on RuO₂/TiO₂ nanotubes composite modified Pt electrode," *Electrochimica Acta*, vol. 50, no. 16-17, pp. 3576-3580, 2005.
- [31] J. Choi, M. J. Kim, S. H. Ahn, I. Choi, J. H. Jang, Y. S. Ham, J. J. Kim and S.-K. Kim, "Electrochemical CO₂ reduction to CO on dendritic Ag–Cu electrocatalysts prepared by *electrodeposition*," *Chemical Engineering Journal*, vol. 299, pp. 37-44, 2016.
- [32] R. Kortleve, I. Peters, S. Koper and M. T. Koper, "Electrochemical CO₂ Reduction to Formic Acid at Low Overpotential and with High Faradaic Efficiency on Carbon-Supported Bimetallic Pd–Pt Nanoparticles," *ACS Catalysis*, vol. 5, no. 7, pp. 3916-3923, 2015.
- [33] M. Le, M. Ren, Z. Zhang, P. T. Sprunger, R. L. Kurts and J. C. Flake, "Electrochemical Reduction of CO₂ to CH₃OH at Copper Oxide Surfaces," *Journal of the Electrochemical Society*, vol. 158, no. 5, pp. E45-E49, 2011.
- [34] S. Rasul, D. H. Anjum, A. Jedidi, Y. Minenkov, L. Cavallo and K. Takanabe, "A Highly Selective Copper–Indium Bimetallic Electrocatalyst for the Electrochemical Reduction of Aqueous CO₂ to CO[†]," *Angewandte Chemie International Edition*, vol. 54, no. 7, 2014.

- [35] B. Kumar, J. P. Brian, V. Atla, S. Kumari, K. A. Bertram, R. T. White and J. M. Spurgeon, "New trends in the development of heterogeneous catalysts for electrochemical CO₂ reduction," *Catalysis Today*, vol. 270, pp. 19-30, 2016.
- [36] N. Fujiwara, R. Kikuchi, A. Takagaki, T. Sugawara and S. T. Oyama, "Investigation of Solid Oxide Electrolysis Cell Electrodes for Methane Synthesis," *ECS Transactions*, vol. 78, p. 3247, 2017.
- [37] W. Li, H. Wang, Y. Shi and N. Cai, "Performance and methane production characteristics of H₂O-CO₂ co-electrolysis in solid oxide electrolysis cells," *International Journal of Hydrogen Energy*, vol. 38, pp. 11104-11109, 2013.
- [38] G. L. Hawkes, J. E. O'Brien, C. M. Stoots, J. S. Herring and M. Shahnam, "Computational Fluid Dynamics Model of a Planar Solid-Oxide Electrolysis Cell for Hydrogen Production from Nuclear Energy," *Nuclear Technology*, vol. 158, no. 2, pp. 132-144, 2007.
- [39] X. Sun, M. Chen, S. H. Jensen, S. D. Ebbesen, C. Graves and M. Mogensen, "Thermodynamic analysis of synthetic hydrocarbon fuel production in pressurized solid oxide electrolysis cells," *International Journal of Hydrogen Energy*, vol. 37, no. 22, pp. 17101-17110, 2012.
- [40] F. Jiao, J. Li, X. Pan, J. Xiao, H. Li, H. Ma, M. Wei, Y. Pan, Z. Zhou, M. Li, S. Miao, J. Li, Y. Zhu, D. Xiao, T. He, J. Yang, F. Qi, Q. Fu and X. Bao, "Selective conversion of syngas to light olefins," *Science*, vol. 351, no. 6277, pp. 1065-1068, 2016.
- [41] H. M. T. G. a. K. P. d. Jong, "Catalysts for Production of Lower Olefins from Synthesis Gas: A," *ACS Catalysis*, vol. 3, pp. 2130-2149, 2013.
- [42] S. L. Soled, E. Iglesia, S. Miseo, B. A. DeRites and R. A. Fiato, "Selective synthesis of α -olefins on Fe-Zn Fischer-Tropsch catalysts," *Topics in Catalysis*, vol. 2, no. 1-4, pp. 193-205, 1995.
- [43] J. G. Speight, "Gasification processes for synthetic liquid fuel production," in *Gasification for Synthetic Fuel Production*, Woodhead Publishing, 2015, pp. 103-198.
- [44] E. W. Kuipers, H. Oosterbeek and I. H. Vinkenburg, "Chain Length Dependence of α -Olefin Readsorption in Fischer-Tropsch Synthesis," *Journal of Catalysis*, vol. 152, no. 1, pp. 137-146, 1995.
- [45] J. Cheng, P. Hu, P. Ellis, S. French, G. Kelly and C. M. Lok, "A DFT study of the chain growth probability in Fischer-Tropsch synthesis," *Journal of Catalysis*, pp. 221-228, 2008.
- [46] I. A. Filot, B. Zijlstra, R. J. Broos, W. Chen, R. Pestman and E. J. Hensen, "Kinetic aspects of chain growth in Fischer-Tropsch synthesis," *Faraday Discussions*, vol. 197, 2017.

- [47] E. Igleisa, "Design, synthesis, and use of cobalt-based Fischer-Tropsch synthesis catalysts," *Applied Catalysis A: General*, vol. 161, no. 1-2, pp. 59-78, 1997.
- [48] F. K. J. N. a. J. R. v. O. David Vervloet, "Fischer–Tropsch reaction–diffusion in a cobalt catalyst particle: aspects," *Catalysis*, vol. 2, pp. 1221-1233, 2012.
- [49] I. A. W. Filot, B. Zijlstra, R. J. P. Broos, W. Chen, R. Pestman and E. J. M. Hensen, "Kinetic *aspects* of chain growth in Fischer–Tropsch synthesis," *Faraday Discussions*, vol. 197, 2017.
- [50] J. Lu, L. Yang, B. Xu, Q. Wu, D. Zhang, S. Yuan, Y. Zhai, X. Wang, Y. Fan and Z. Hu, "Promotion Effects of Nitrogen Doping into Carbon Nanotubes on Supported Iron Fischer–Tropsch Catalysts for Lower Olefins," *ACS Catalysis*, vol. 4, no. 2, pp. 613-621, 2014.
- [51] T. T. Lari, A. A. Mirzaei and A. Hossein, "Influence of Fabrication Temperature and Time on Light Olefin Selectivity of Iron–Cobalt–Cerium Mixed Oxide Nanocatalyst for CO Hydrogenation," *Ind. Eng. Chem. Res.*, vol. 55, no. 51, pp. 12991-13007, 2016.
- [52] K. Sonal and S. Upadhyayula, "Detailed kinetics of Fischer Tropsch synthesis over Fe-Co *bimetallic* catalyst considering chain length dependent olefin desorption," *Fuel*, vol. 236, pp. 1263-1272, 2019.
- [53] Y. Cheng, J. Lin, K. Xu, H. Wang, X. Yao, Y. Pei, S. Yan, M. Qiao and B. Zong, "Fischer–Tropsch Synthesis to Lower Olefins over Potassium-Promoted Reduced Graphene Oxide Supported Iron Catalysts," *ACS Catalysis*, vol. 6, no. 1, pp. 389-399, 2016.
- [54] X. Wang, D. Wu, J. Zhang, X. Gao, Q. Ma, S. Fang and T.-S. Zhao, "Highly selective conversion of CO₂ to light olefins via Fischer-Tropsch synthesis over stable *layered* K–Fe–Ti catalysts," *Applied Catalysis A: General*, vol. 573, pp. 32-40, 2019.
- [55] d. Wang, X. Zhou, J. Ji, X. Duan, G. Qian, X. Zhou, D. Chen and W. Yuan, "Modified *carbon* nanotubes by KMnO₄ supported iron Fischer–Tropsch catalyst for the direct conversion of syngas to lower olefins," *Journal of Materials Chemistry A*, vol. 3, no. 8, pp. 4560-4567, 2015.
- [56] M. Oschatz, J. P. Hofmann, T. W. van Deelen, W. S. Lamme, N. A. Krans, E. J. M. Hensen and K. P. de Jong, "Effects of the Functionalization of the Ordered Mesoporous Carbon Support Surface on Iron Catalysts for the Fischer–Tropsch Synthesis of Lower Olefins," *ChemCatChem*, vol. 9, no. 4, 2016.
- [57] M. Oschatz, W. S. Lamme, J. Xie, A. I. Dugulan and K. P. de Jong, "Ordered Mesoporous Materials as Supports for Stable Iron Catalysts in the Fischer–Tropsch Synthesis of Lower Olefins," *ChemCatChem*, vol. 8, no. 17, 2016.

- [58] Z. R. Ismagilov, E. V. Matus and L. T. Tsikoza, "Direct conversion of methane on Mo/ZSM-5 catalysts to produce benzene and hydrogen: achievements and perspectives," *Energy Environmental Science*, vol. 1, pp. 526-541, 2008.
- [59] T. L. Skafte, Z. Guan, M. L. Machala, C. B. Gopal, M. Monti, L. Martinez, E. Stamate, S. Sanna, J. A. Garrido Torres, E. J. Crumlin, M. Garcia-Melchor, M. Bajdich, W. C. Chueh and C. Graves, "Selective high-temperature CO₂ electrolysis enabled by oxidized carbon intermediates," *Nature Energy*, vol. 4, pp. 846-855, 2019.
- [60] P. M. Mortensen and I. Dybkjaer, "Industrial scale experience on steam reforming of CO₂-rich gas," *Applied Catalysis A: General*, no. 495, pp. 141-151, 2015.
- [61] C. Milliken, S. Guruswamy and A. Khandkar, "Properties and Performance of Cation-Doped Ceria Electrolyte Materials in Solid Oxide Fuel Cell Applications," *Journal of the American Ceramic Society*, vol. 85, no. 10, pp. 2479-2486, 2005.
- [62] V. V. Kharton, F. M. B. Marques and A. Atkinson, "Transport properties of solid oxide electrolyte ceramics: a brief review," *Solid State Ionics*, vol. 174, no. 1-4, pp. 135-149, 2004.
- [63] ERCOT, "ERCOT Market info," [Online]. Available: <http://www.ercot.com/mktinfo/prices>. [Accessed 10 12 2019].
- [64] J. Yi, "Benzene spread stuck," *ICIS Chemical Business*, vol. 298, no. 13, pp. 10-11, 2016.
- [65] T. Dang, "US ethylene contracts settle lower for May," *ICIS Chemical Business*, vol. 298, no. 22, p. 15, 2016.
- [66] H. Finch, "August propylene to remain tight.,," *ICIS Chemical Business*, vol. 6, no. 14, p. 290, 2016.
- [67] US Energy Information Administration, "Short-Term Energy Outlook," 2020.
- [68] "ICIS News weekly price snapshot," *ICIS Chemical Business*, vol. 297, no. 24, 2020.
- [69] Grand View Research, Inc. , "Hydrogen Generation Market Size, Share & Trends Analysis Report By Application (Coal Gasification, Steam Methane Reforming), By Systems (Merchant, Captive), By Technology, And Segment Forecasts, 2020 - 2027," Grand View Research, San Francisco, 2020.
- [70] Grandview Research, Inc, "Petrochemicals Market Size, Share & Trends Analysis Report By Product (Ethylene, Propylene, Butadiene, Benzene, Xylene, Toluene, Methanol), By Region, And Segment Forecasts, 2020 - 2027," Grandview Research, San Francisco, 2020.

- [71] H. *Dagdougui*, R. Sacile, C. Bersani and A. Ouammi, "Hydrogen Production and Current Technologies," in *Hydrogen Infrastructure for Energy Applications*, Academic Press, 2018, pp. 7-21.
- [72] IRENA, "HYDROGEN:A RENEWABLE ENERGY PERSPECTIVE," International Renewable Energy Agency, Abu Dhabi, 2019.
- [73] J. R. *Fekete*, J. W. Sowards and R. L. Amaro, "Economic Impact of Applying High Strength Steels in Hydrogen Pipelines," *International Journal of Hydrogen Energy*, vol. 40, no. 33, pp. 10547-10558, 2015.
- [74] S. Kim, S. Jeong and E. Heo, "Effects of the shale boom on ethylene and propylene prices," *Energy Sources, Part B: Economics, Planning, and Policy*, vol. 14, no. 3, pp. 49-66, 2019.
- [75] *Energetics Inc.*, "Energy and Environmental Profile of the U.S. Chemical Industry," U.S. Department of Energy Office of Industrial Technologies, 2000.
- [76] M. J. Biddy, C. Scarlata and C. Kinchin, "Chemicals from Biomass: A Market Assessment of Bioproducts with Near-Term Potential," National Renewable Energy Laboratory, 2016.
- [77] L. *Koottungal*, "INTERNATIONAL SURVEY OF ETHYLENE FROM STEAM CRACKERS," 2014.
- [78] US Energy Information Administration, "US Energy Mapping System," US Energy Information Administration, [Online]. Available: <https://www.eia.gov/state/maps.php>. [Accessed 2 Oct 2020].
- [79] M. H. Miles, G. Kissel, P. W. T. Lu and S. Srinivasan, "Effect of Temperature on Electrode Kinetic Parameters for Hydrogen and Oxygen Evolution Reactions on Nickel *Electrodes* in Alkaline Solutions," *Jouranal of the Electrochemical Society*, vol. 123, no. 3, 1976.
- [80] F. Allebrod, C. Chatzichristodoulou and M. B. Mogensen, "Alkaline electrolysis cell at high temperature and pressure of 250 °C and 42 bar," *Journal of Power Sources*, vol. 229, no. 1, pp. 22-31, 2013.
- [81] C. Chatzichristodoulou, "Microstructural optimization of gas diffusion electrodes for high *temperature* and pressure alkaline electrolysis," in *2nd International Conference on Electrolysis 2019* , Loen, Norway, 2019.
- [82] Y. Dai, Y. Zhao, T. Lin, S. Li, F. Yu, Y. An, X. Wang, K. Xiao, F. Sun, Z. Jian, Y. Lu, H. Wang, L. Zhong and Y. Sun, "Particle Size Effects of Cobalt Carbide for Fischer–Tropsch to Olefins," *ACS Catalysis*, vol. 9, no. 2, pp. 798-809, 2019.
- [83] N. H. Behling, Fuel Cells: Current Technology Challenges and Future Research Needs, Elsevier, 2013.

- [84] H. Shen, E. P. Schreiner, W. Zheng and R. F. Lobo, "Non-oxidative Coupling of Methane to *Ethylene* Using Mo₂C/[B]ZSM-5," *ChemPhysChem*, vol. 19, no. 4, pp. 504-5011, 2017.
- [85] M. Weimar, L. Chick, D. Gotthold and G. Whyatt, "Cost Study for Manufacturing of Solid *Oxide* Fuel Cell Power Systems," US Department of Energy, 2013.
- [86] Battelle, "MANUFACTURING COST ANALYSIS OF 1KW AND 5KW SOLID OXIDE FUEL CELL(SOFC)FOR AUXILLIARY POWERAPPLICATIONS," Battelle Memorial Institute, Columbus OH, 2014.
- [87] ERCOT, "ERCOT Hourly AGGREGATED WIND OUTPUT," [Online]. Available: <http://mis.ercot.com/misapp/GetReports.do?reportTypeId=13424&reportTitle=Hourly%20Aggregated%20Wind%20Output&showHTMLView=&mimicKey>. [Accessed 3 July 2020].
- [88] J. S. Kim, R. D. Boardman and S. M. Bragg-Sitton, "Dynamic performance analysis of a high-*temperature* steam electrolysis plant integrated within nuclear-renewable hybrid energy systems," *Applied Energy*, vol. 228, pp. 2090-2110, 2018.
- [89] R. Wiser, M. Bolinger, B. Hoen, D. Millstein, J. Rand, G. Barbose, N. Darghouth, W. Gorman, S. Jeong, A. Mills and B. Paulos, "Wind Energy Technology Data Update: 2020 Edition," Lawrence Berkley National Laboratory, Berkley, 2020.
- [90] K. Huang, J. B. Miller, G. W. Huber, J. A. Dumesic and C. T. Maravelias, "A General *Framework* for the Evaluation of Direct Nonoxidative Methane Conversion Strategies," *Joule*, vol. 2, no. 2, pp. 349-365, 2018.
- [91] US Energy Information Administration, "United States Natural Gas Industrial Price (Dollars per Thousand Cubic Feet)," 30 September 2020. [Online]. Available: https://www.eia.gov/dnav/ng/hist_xls/N3035US3a.xls. [Accessed 12 October 2020].
- [92] Argonne National Lab, *GREET 2018 [Computer Software]*, 2018.
- [93] US Energy Information Administration, "Petroleum Supply Monthly," EIA, 2016.
- [94] M. F. Ruth, O. R. Zinaman, M. Antkowiak, R. D. Boardman, R. S. Cherry and M. D. Dzailian, "Nuclear-renewable hybrid energy systems: Opportunities, interconnections, and needs," *Energy Conversion and Management*, vol. 78, pp. 684-694, 2014.
- [95] B. Pivovar, "NREL," 4 April 2016. [Online]. Available: <https://www.nrel.gov/docs/fy16osti/66246.pdf>. [Accessed 13 4 2019].

- [96] H. Schulz and M. Claeys, "Reactions of α -olefins of different chain length added during Fischer–Tropsch synthesis on a cobalt catalyst in a slurry reactor," *Applied Catalysis A: General*, vol. 186, no. 1-2, pp. 71-90, 1999.
- [97] J. Barrault, C. Forquy and V. Perrichon, "Effects of manganese oxide and sulphate on olefin selectivity of iron supported catalysts in the Fischer-Tropsch reaction," *Applied Catalysis*, vol. 5, no. 1, pp. 119-125, 1983.
- [98] H. Schulz, "Major and Minor Reactions in Fischer–Tropsch Synthesis on Cobalt Catalysts," *Topics In Catalysis*, vol. 26, no. 1-4, pp. 73-85, 2003.
- [99] Z. Li, L. Zhong, F. Yu, Y. An, Y. Dai, Y. Yang, T. Lin, S. Li, H. Wang, P. Gao, Y. Sun and M. He, "Effects of Sodium on the Catalytic Performance of CoMn Catalysts for Fischer–Tropsch to Olefin Reactions," *ACS Catalysis*, vol. 7, no. 5, pp. 3622-3631, 2017.
- [100] C. Zhu, M. Zhang, C. Huang, L. Zhong and K. Fang, "Carbon-encapsulated highly dispersed FeMn nanoparticles for Fischer–Tropsch synthesis to light olefins," *New Journal of Chemistry*, vol. 42, no. 4, pp. 2413-2421, 2018.
- [101] L. Zhou, F. Yu, Y. An, Y. Zhao, Y. Sun, Z. Li, T. Lin, Y. Lin, X. Qi, Y. Dai, L. GU, J. Hu, S. Jin, Q. Shen and H. Wang, "Cobalt carbide nanoprisms for direct production of lower olefins from syngas," *Nature*, vol. 538, pp. 84-87, 2016.
- [102] W.-G. Zhou, J.-Y. Liu, X. Wu, J.-F. Chen and Y. Zhang, "An effective Co/MnO_x catalyst for forming light olefins via Fischer–Tropsch synthesis," *Catalysis Communications*, vol. 60, pp. 76-81, 2015.
- [103] E. Pedersen, I.-H. Svenum and E. Blekkan, "Mn promoted Co catalysts for Fischer-Tropsch production of light olefins – An experimental and theoretical study," *Journal of Catalysis*, vol. 361, pp. 23-32, 2018.
- [104] S. J. Jensen, C. Graves, M. Mogensen, C. Wendel, R. Braun, G. Hughes, Z. Gao and S. A. Barneet, "Large-scale electricity storage utilizing reversible solid oxide cells combined with underground storage of CO₂ and CH₄," *Energy & Environmental Science*, no. 8, 2015.

VITA

Jeremy Lee Hartvigsen earned a BS in Chemical Engineering from Brigham Young University in 2011, a MS in Chemical Engineering from Missouri University of Science and Technology in August 2020. He received his PhD in Chemical Engineering from Missouri University of Science and Technology in December 2020.